Katarzyna Szymczak-Kulus

LUDZKA α-1,4-GALAKTOZYLOTRANSFERAZA JAKO ENZYM REGULUJĄCY WIĄZANIE TOKSYN SHIGA

Promotor:
prof. dr hab. Marcin Czerwiński

Praca doktorska

wykonana w Laboratorium Glikobiologii

Instytutu Immunologii i Terapii Doświadczalnej im. Ludwika Hirszfelda

Polskiej Akademii Nauk

Wrocław 2021

Katarzyna Szymczak-Kulus

HUMAN α-1,4-GALACTOSYLTRANSFERASE AS AN ENZYME REGULATING SHIGA TOXIN BINDING

Supervisor:
prof. dr hab. Marcin Czerwiński

This doctoral dissertation is based on experimental work performed

in Laboratory of Glycobiology,

Hirszfeld Institute of Immunology and Experimental Therapy,

Polish Academy of Sciences

Wrocław 2021

Acknowledgements

Results of this thesis were included in the following publications:

Kaczmarek R., Szymczak-Kulus K., Bereźnicka A., Mikołajczyk K., Duk M., Majorczyk E., Krop-Watorek A., Klausa E., Skowrońska J., Michalewska B., Brojer E., Czerwinski M. Single nucleotide polymorphisms in A4GALT spur extra products of the human Gb3/CD77 synthase and underlie the P1PK blood group system. PLoS One. 2018 Apr 30;13(4):e0196627. doi: 10.1371/journal.pone.0196627.

Szymczak-Kulus K., Weidler S., Bereznicka A., Mikolajczyk K., Kaczmarek R., Bednarz B., Zhang T., Urbaniak A., Olczak M., Park E. Y., Majorczyk E., Kapczynska K., Lukasiewicz J., Wuhrer M., Unverzagt C., Czerwinski M. Human Gb3/CD77 synthase produces P1 glycotope-capped N-glycans, which mediate Shiga toxin 1 but not Shiga toxin 2 cell entry. J Biol Chem. 2021 Jan 15:100299. doi: 10.1016/j.jbc.2021.100299.

Table of contents

1. Streszczenie

Ludzka α-1,4-galaktozylotransferaza, kodowana przez gen *A4GALT*, charakteryzuje się wysoką rozwiązłością enzymatyczną. Jest odpowiedzialna za syntezę końcowej struktury Galα1→4Gal swojego głównego produktu, antygenu P^k (globotriaozyloceramidu, Gb3, CD77), oraz dodatkowo antygenu P1. Te glikosfingolipidowe antygeny należą do układu grupowego krwi P1PK. Podstawienie pojedynczej reszty aminokwasowej w pozycji 211 łańcucha polipeptydowego enzymu (p.Q211E) powoduje dalsze pogłębienie jego rozwiązłości akceptorowej, skutkiem czego jest przyłączanie reszt galaktozy również do *N*-acetylogalaktozaminy i synteza rzadkiego antygenu NOR (występującego w formach NOR1 i NOR2). Antygen P^k (Gb3) powszechnie występuje na powierzchni erytrocytów, natomiast obecność lub brak antygenu P1 uwarunkowuje zróżnicowanie fenotypowe krwi, odpowiednio na grupę P_1 lub P_2. Podłoże genetyczne tego zróżnicowania długo pozostawało niewyjaśnione, ale wyniki niniejszej pracy sugerują, że polimorfizm pojedynczego nukleotydu w obrebie intronu 1 genu *A4GALT* rs5751348 wykazuje najwyższą korelację z fenotypem P_1/P_2. Ponadto, antygen P^k jest głównym receptorem dla toksyn Shiga produkowanych przez enterokrwotoczne szczepy *Escherichia coli*, natomiast rola antygenu P1 w kontekście wiązania toksyn Shiga nigdy przedtem nie była przedmiotem badań. W pracy wykazano, że ludzka α-1,4-galaktozylotransferaza, uważana dotychczas za enzym swoisty wyłącznie wobec glikosfingolipidów, może przyłączać reszty galaktozy do glikoproteinowych akceptorów. Zarówno konsensowa α-1,4-galaktozylotransferaza, jak i enzym z podstawieniem p.Q211E, syntezują końcowe struktury Galα1→4Galβ1→4GlcNAc złożonych N-glikanów. Wykazano też, że N-glikoproteiny zawierające łańcuchy zakończone tymi strukturami są rozpoznawane przez podjednostkę B toksyny Shiga, oraz służą jako funkcjonalne receptory dla toksyny Shiga 1, ale nie dla toksyny Shiga 2. Tak więc toksyna Shiga 1 może wiązać i wykorzystywać jako receptory glikosfingolipidy oraz glikoproteiny, w przeciwieństwie do toksyny Shiga 2, która oddziałuje jedynie z glikosfingolipidami.

2. Abstract

The human α-1,4-galactosyltransferase, encoded by the *A4GALT* gene, is an unusually promiscuous glycosyltransferase. It synthesizes the terminal Galα1→4Gal structure of the P^k and P1 antigens. These glycosphingolipid antigens belong to the P1PK histo-blood group system. A single amino acid substitution (p.Q211E) enhances the promiscuity of the enzyme, rendering it able to attach Gal both to another Gal residue but also to GalNAc, giving rise to NOR1 and NOR2 glycosphingolipids. The P^k antigen (Gb3) is present on erythrocytes of most individuals, whereas presence of P1 antigen underlies two main phenotypes: P_1, if the P1 antigen is present, and P_2, if P1 is absent. The genetic background of P_1/P_2 polymorphism has eluded clarification for years, and the results of this study show that rs5751348 offers the best predictive value for the P_1/P_2 phenotypic polymorphism. Significantly, the P^k antigen is the major receptor for Shiga toxins produced by enterohemorrhagic *Escherichia coli*, but the role of P1 antigen in Shiga toxin binding has never been examined. Results of this study contributed to the elucidation of P_1/P_2 polymorphism background. The human α-1,4-galactosyltransferase has been long believed to transfer Gal only to glycosphingolipid acceptors, but the data presented in this thesis demonstrate that the enzyme is able to add galactose also to glycoprotein acceptors. The consensus α-1,4-galactosyltransferase, as well as p.Q211E mutein, can synthesize the P1 glycotope (terminal Galα1→4Galβ1→4GlcNAc) on complex type N-glycans, with the mutein exhibiting an elevated level of activity. To date, glycosphingolipids were considered the only receptors for Shiga toxins. However, results of this study revealed that N-glycoproteins carrying P1 glycotopes are recognized by Shiga toxin 1 but not Shiga toxin 2 B subunits. Furthermore, such glycoproteins may act as functional receptors for Shiga toxin 1, but not for Shiga toxin 2. Thus, Shiga toxin 1 can recognize and use P1-terminated N-glycoproteins in addition to its canonical glycosphingolipid receptors to enter and kill the cells, while Shiga toxin 2 can use glycosphingolipids only. Since the interaction with Shiga toxins is a consequence of human α-1,4-galactosyltransferase activity, the enzyme may be considered a regulator of Shiga toxin binding.

3. Abbreviations

αMEM	Minimum Essential Medium – α modification
A4GalT	recombinant, soluble catalytic domain of human α-1,4-galactosyltransferase
A4GalT p.Q211E	recombinant, soluble catalytic domain of human α-1,4-galactosyltransferase with p.Q211E substitution
aa	amino acid
ABC	antibody binding capacity
Asp	aspartic acid
BCIP	5-bromo-4-chloro-3-indolyl phosphate
BSA	bovine serum albumine
CAZy	Carbohydrate-Active enZYmes database
CBB	Coomassie Brilliant Blue
CMP-Neu5Ac	cytidine monophosphate N-acetylneuraminic acid
DMEM	Dulbecco's Modified Eagle's Medium
DNA	deoxyribonucleic acid
dNTP	deoxyribonucleotide triphosphate
EDTA	ethylenediaminetetraacetic acid
EGR1	early growth response 1 transcription factor
ELISA	enzyme-linked immunosorbent assay
ER	endoplasmic reticulum
ESI-MS	electrospray ionization mass spectrometry
ESI-TOF	electrospray ionization-time of flight
FBS	fetal bovine serum
FITC	fluorescein isothiocyanate
Gal	galactose
GalCer	galactosylceramide
GalNAc	N-acetylgalactosamine
GDP-Man	guanidine diphosphate mannose
Genz-123346	N-[(1R,2R)-1-(2,3-dihydro-1,4-benzodioxin-6-yl)-1-hydroxy-3-pyrrolidin-1-ylpropan-2-yl]nonanamide
Glc	glucose
GlcCer	glucosylceramide
GlcNAc	N-acetylglucosamine
GSL	glycosphingolipid
GSL I B4	*Griffonia simplicifolia* lectin I isolectin B4
HPTLC	high-performance thin layer chromatography
HR-MS	high resolution mass spectrometry
HUS	hemolytic uremic syndrome
IPTG	isopropyl β-D-1-thiogalactopyranoside
ISBT	International Society of Blood Transfusion
LC-MS	liquid chromatography mass spectrometry
MALDI-TOF	matrix-assisted laser desorption/ionization–time of flight

Man	mannose
MOI	multiplicity of infection
MS	mass spectrometry
NBT	nitro blue tetrazolium
Ni-NTA	nickel-nitrilotriacetic acid
NMR	nuclear magnetic resonance
OD	optical density
ORF	open reading frame
PCR	polymerase chain reaction
PNGase F	peptide-N-glycosidase F
RBC	red blood cell
RP-HPLC	reversed phase high-performance liquid chromatography
RNA	ribonucleic acid
RUNX1	Runt-related transcription factor 1
SapD	saposin D
SapD9	saposin D glycoform with nonasaccharide N-glycan chain
SapD11	saposin D glycoform with undecasaccharide N-glycan chain
SDS-PAGE	sodium dodecyl sulfate–polyacrylamide gel electrophoresis
SNP	single nucleotide polymorphism
SPR	surface plasmon resonance
SLT	Shiga-like toxin
STEC	Shiga toxin producing *Escherichia coli*
Stx	Shiga toxin
Stx1B	B subunit of Shiga toxin 1
Stx2B	B subunit of Shiga toxin 2
UDP-Gal	uridine diphosphate galactose
UDP-Glc	uridine diphosphate glucose
UHPLC	ultrahigh-performance chromatography
UV	ultraviolet
VT	verotoxin
X-Gal	5-bromo-4-chloro-3-indolyl β-D-galactopyranoside

4. Introduction

Glycosyltransferases (GTs) attach sugar residues to other carbohydrates, as well as polypeptides, lipids, small organic molecules and DNA. Products of these enzymes constitute endothelial glycocalyx, which modulates cell adhesion, maintain vascular homeostasis and transmits mechanical forces to the cytoskeleton of endothelial cells. Furthermore, glycans can serve as receptors or coreceptors for diverse microorganisms, parasites, and viruses. Among products of glycosyltransferases, histo-blood group antigens are of a particular interest, because they can serve as a model how glycosylation influences response of the immune system. In addition, studying of role played by GTs in synthesis of histo-blood group antigens can increase our knowledge about interaction between surface antigens and pathogens.

4.1 Glycosyltransferases

Glycosyltransferases are enzymes which transfer activated sugar moieties to a wide range of acceptors with the synthesis of *O*-, NH-, S- or C-glycosidic bond (Mestrom *et al.*, 2019). The most common class of donor substrates are sugar nucleotides (i.e. UDP-Glc, GDP-Man, CMP-Neu5Ac); however, some glycosyltransferases use sugars linked to the phosphorylated lipids (*i.e.* dolichol-P-glucose, undecaprenyl-pyrophosphoryl-*N*-acetylmuramic acid-pentapeptide-*N*-acetylglucosamine) (Varki *et al.*, 2009). Sugar nucleotides and enzymes which utilize them are called Leloir donors and Leloir glycosyltransferases, respectively, in honor of Luis Federico Leloir awarded with Nobel prize in 1970 for discovery of the UDP-Glc (Cardini *et al.*, 1950).

Currently, the Carbohydrate-Active enZYmes database (CAZy, http://www.cazy.org) comprises over 790 000 glycosyltransferases, majority of which are classified in 112 families based on the amino acid sequence similarity (Coutinho *et al.*, 2003; Lombard *et al.*, 2014). Analysis of completely sequenced genomes indicates the number of genes encoding glycosyltransferases constitute 1-2% of all genes of archaeal, bacterial and eukaryotic organisms (Lairson *et al.*, 2008).

4.1.1 Structure

Glycosyltransferases are predominantly type II transmembrane proteins with short N-terminal cytoplasmic tail, single transmembrane domain, disordered stem region and C-terminal catalytic domain in the lumen of endoplasmic reticulum or Golgi apparatus. A so-called CTS domain, encompassing cytoplasmic, transmembrane and stem regions, determines localization of Golgi-resident glycosyltransferases (Welch and Munro, 2019). The transmembrane and stem region can participate in enzyme homo- and heterooligomerization.

Most glycosyltransferases represent one of five structural folds: GT-A, GT-B, GT-C, GT-D, GT-E (Fig. 1). Structures of GT-A and GT-B enzymes are characterized by two β/α/β-Rossmann-like domains involved in nucleotide sugar binding, abutting (in the case of GT-A) or facing (regarding to the GT-B) each other (Breton, Fournel-Gigleux and Palcic, 2012). Glycosyltransferases displaying GT-A fold often contain DXD motif (Asp-Xaa-Asp) involved in coordination binding of divalent metal ion (usually Mn^{2+} or Mg^{2+}) interacting with Leloir donors (Breton *et al.*, 2006). GT-B glycosyltransferases are generally considered as divalent cation-independent (Albesa-Jové *et al.*, 2014). Enzymes belonging to the GT-C superfamily are non-Leloir glycosyltransferases which use polyisoprenol-linked donor substrates and follow inverting catalytic mechanism. They consist of 7 to 13 transmembrane domains and share low sequence homology (Albuquerque-Wendt *et al.*, 2019). Besides GT-A and GT-B, also the GT-D superfamily comprises Leloir glycosyltransferases, transferring glucose to hexasaccharide O-glycans of bacterial adhesins (Zhang *et al.*, 2014). Although they have Rossmann-like domain, their structure and sequence do not reveal any identity with GT-A or GT-B type glycosyltransferases. Furthermore, GT-D enzymes contain conserved DXE motif (instead of DXD, characteristic for GT-A superfamily) which is essential for their activity though it does not directly bind a divalent cation (Zhang *et al.*, 2014). The recently resolved structure of TagA glycosyltransferase from *Thermoanaerobacter italicus* involved in wall teichoic acid synthesis revealed substantially distinct topology than four above described folds and it has been designated GT-E. TagA and its homologs display Rossmann-like domain but lack DXD or DXE motif and do not depend on divalent cation binding (Kattke *et al.*, 2019).
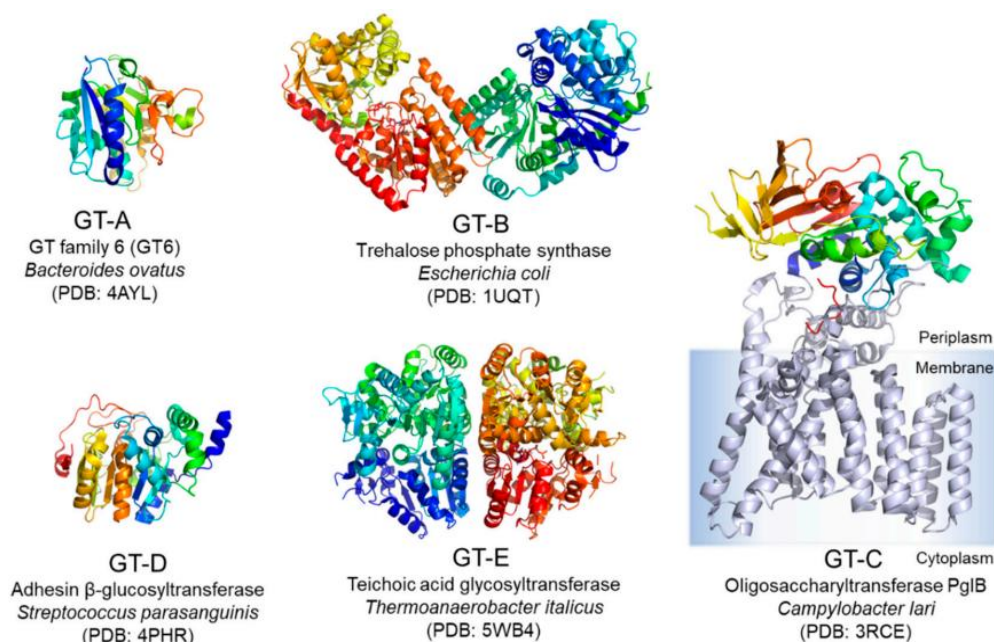
Fig. 1. Structures of glycosyltransferases representing different superfamilies: GT-A, GT-B, GT-C, GT-D, GT-E (Mestrom *et al.*, 2019).

4.1.2 Mechanism of action

Catalytic mechanism of glycosyltransferases involves creating ternary complex of enzyme and substrates after non-covalent binding of the donor substrate to the active site followed by recruitment of the acceptor. Enzyme activation occurs upon binding of the acceptor substrate and conformational change to prevent hydrolysis of the activated monosaccharide (Ardèvol and Rovira, 2015). Stereochemically, reaction catalyzed by glycosyltransferase can result in inversion or retention of the attached sugar configuration (Breton, Fournel-Gigleux and Palcic, 2012). Inverting enzymes operate via single displacement S_N2 mechanism with acceptor hydroxyl group as a nucleophile attacking anomeric carbon of the donor sugar (Fig. 2A). Usually during this substitution the side chain of aspartic or glutamic acid residue deprotonates hydroxyl group of the acceptor increasing its nucleophility (Ardèvol and Rovira, 2015).

For the reactions occurring with the retention of anomeric configuration, two main modes of action are usually considered. The firstly proposed double-displacement mechanism involves nucleophilic attack of aspartate or glutamate side chain on the anomeric carbon of the sugar donor with formation of covalent glycosyl-enzyme intermediate (Fig. 2B). Then, the donor carbon atom is attacked by acceptor nucleophile (Albesa-Jové and Guerin, 2016). The second model of reaction with retention of configuration is S_Ni-like, displaying attack of the acceptor nucleophile from the same side of sugar donor as the departure of the leaving group. This so called front-face reaction occurs usually when the enzyme active site lacks amino acid residue which can act as a nucleophile. The S_Ni-like mechanism is often presented as a fully concerted reaction (Fig. 2C); however, most probably it occurs rather step-wise, involving formation of short lived intermediate (Fig. 2D) (Albesa-Jové *et al.*, 2017).

(a) **Inverting GTs** – Single displacement
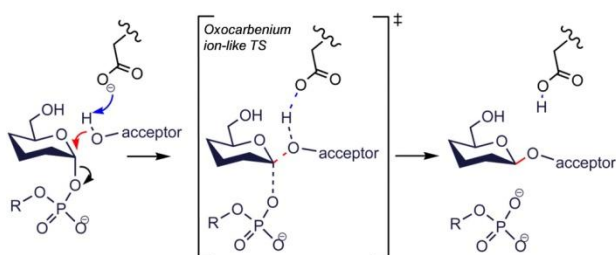
(b) **Retaining GTs** – Double displacement
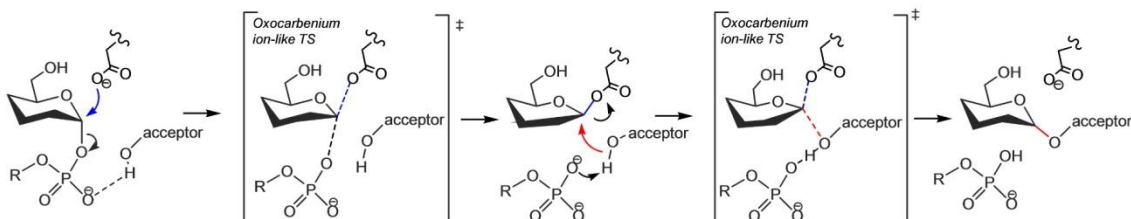
(c) **Retaining GTs** – Concerted front-face
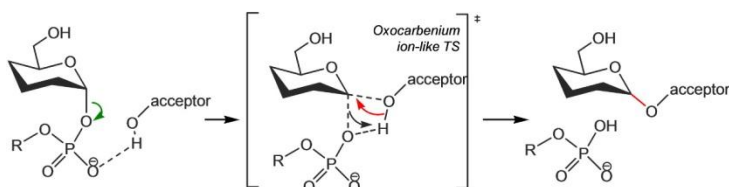
(d) **Retaining GTs** – Stepwise front-face
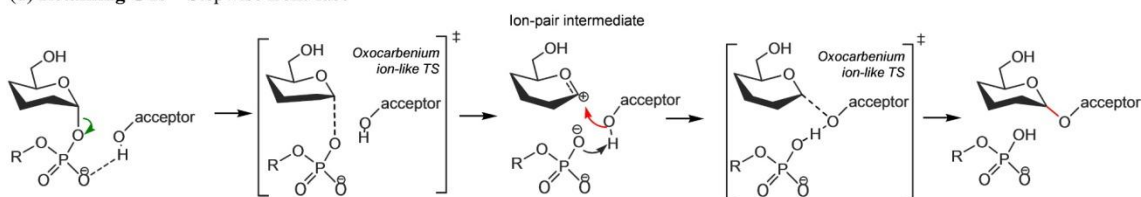
Fig. 2. Reaction mechanisms of inverting (A) and retaining (B-D) glycosyltransferases. A) S_N2 single displacement mechanism; B) double displacement mechanism; C) concerted S_Ni-like front face reaction; D) stepwise S_Ni-like front face reaction (Ardèvol and Rovira, 2015).

4.1.3 Specificity

Glycosyltransferases exhibit usually high regio- and stereo-substrate specificity, but current understanding of glycobiology is far from the "one enzyme, one linkage" early hypothesis (Hagopian and Eylar, 1968), because a specific glycosidic linkage may be the product of one of several structurally and genetically related enzymes. Moreover, some glycosyltransferases can form two different glycosidic bonds, and the acceptor specificity of an enzyme can be altered by another protein. The classic example is α-lactalbumin, which switches the acceptor specificity of β-1,4-galactosyltransferase from GlcNAc to Glc, allowing lactose synthesis during milk formation. Moreover, some of the enzymes can catalyze two

stepwise glycosyltransferase reactions (e.g., the copolymerases that synthesize the backbones of glycosaminoglycan chains) (Varki *et al.*, 2009).

Donor and acceptor specificities of glycosyltransferases appear to be precisely tuned. Mutation of one critical amino acid residue can result not merely in abolishing the enzyme activity, but instead lead to alteration of its donor or acceptor preferences. Multiple reports about a shift or broadening of the donor preferences by substitution of a single amino acid residue have been published (Ouzzine *et al.*, 2002; Ramakrishnan and Qasba, 2002, 2007; Meech *et al.*, 2012; Nair *et al.*, 2015; Chen and Li, 2017). Some of such substitutions may be useful in glycosyltransferase engineering for carbohydrate synthesis (McArthur and Chen, 2016). The flagship examples of differences in donor selectivity conferred by mutation of a single codon are human blood group A and B transferases. These enzymes are encoded by the same *ABO* locus and differ only by four amino acid residues, of which codons 266 and 268 are critical for donor substrate specificity. The A transferase with L266, G268 and the B transferase with M266, A268 catalyze the transfer of GalNAcα1→3 or Galα1→3, respectively, to the same precursor, creating A or B blood group antigens. Substitution of the A transferase L266 for M (from the B transferase), as well as for D, I, N, Q or W (and G268A mutation), generates enzyme that can use both UDP-GalNAc and UDP-Gal as donor substrates; however, substitution for F, H or Y shifts donor specificity to UDP-Gal. And *vice versa*, substitution of the B transferase M266 for L (from the A transferase), A, C, G, N, S, T or V (and A268G mutation), leads to the enzyme dual donor specificity, and mutation for P changes enzyme selectivity to UDP-GalNAc (Yamamoto *et al.*, 2015). On the other hand, Q211E substitution of human α-1,4-galactosyltransferase extends enzyme specificity from glycosphingolipids terminated only with Gal residue to both Gal- and GalNAc-terminated (section 4.2.2) (Suchanowska *et al.*, 2012; Kaczmarek, Duk, *et al.*, 2016). So far, it is the sole example of alteration of glycosyltransferase acceptor selectivity upon mutation of the single codon.

Several mammalian glycosyltransferases display extended acceptor specificity attaching sugar residues to both glycosphingolipids and glycoproteins. The well-studied example are human A and B transferases, which can synthesize A and B blood group antigens on N-, O-glycans as well as on glycosphingolipids (Cooling *et al.*, 2005). Moreover, at least five human β-galactosyltrasferases, three α-1,3-fucosyltransferases, human and mouse sialyltransferases use glycosphingolipids and glycoproteins as acceptor substrates (Taniguchi *et al.*, 2014).

4.2 Glycosphingolipids and their biosynthesis

Glycosphingolipids (GSLs) are synthesized by attaching sugar residues to a ceramide, which consists of sphingoid base linked to a fatty acid by an amide bond (Fig. 3). Ceramide synthesis occurs on the cytoplasmic face of the ER. After flipping to the lumenal leaflet, ceramide can be galactosylated to form galactosylceramide (GalCer), which then moves to the Golgi (Varki *et al.*, 2009). Glucosylceramide (GlcCer) synthesis takes place on the cytoplasmic face of the ER or early Golgi. The GlcCer is then translocated into lumenal leaflet of the Golgi membrane, where it can be elongated by Golgi-resident glycosyltransferases into complex GSLs (D'Angelo *et al.*, 2013). The majority of GSLs are classified on the basis of tetrasaccharide neutral sugar core sequences into seven series: ganglio, lacto, neolacto, globo, isoglobo, mollu, arthro (Fig. 4).
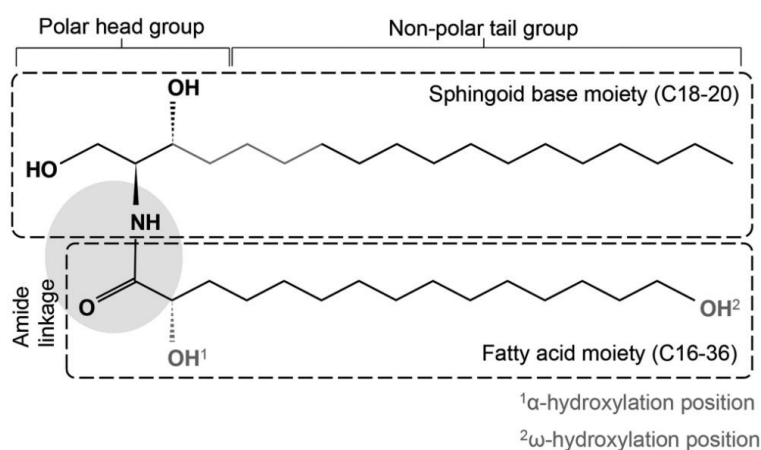
Fig. 3. Structure of ceramide, composed of sphingoid base linked to a fatty acid by an amide bond (CHA *et al.*, 2016).
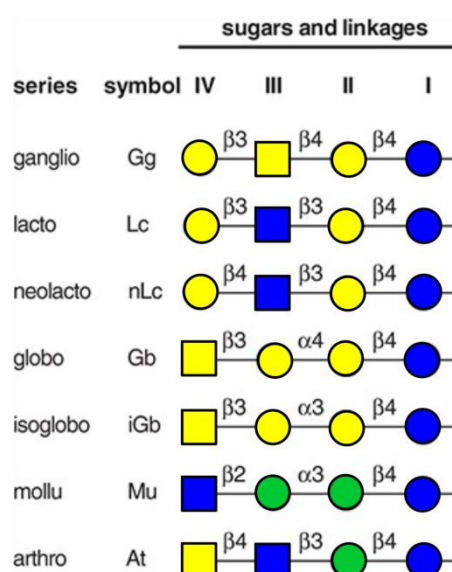
Fig. 4. Neutral sugar core sequences of GSLs belonging to the following series: ganglio, lacto, neolacto, globo, isoglobo, mollu, arthro (Varki *et al.*, 2009). Yellow circle – Gal; blue circle – Glc; green circle – Man; yellow square – GalNAc; blue square – GlcNAc).

4.2.1 Human α-1,4-galactosyltransferase

The human α-1,4-galactosyltransferase (P1/P^k synthase, Gb3/CD77 synthase, UDP-galactose: β-D-galactosyl-β1-R 4-α-D-galactosyltransferase) is encoded by the *A4GALT* gene located on the 22 chromosome. The gene consists of three exons, the third of which encodes the whole open reading frame (ORF). The enzyme is responsible for biosynthesis of glycosphingolipid antigens belonging to the P1PK histo-blood group system (International Society of Blood Transfusion no. 003, (Daniels, 2013)). The consensus enzyme encoded by the high-frequency *A4GALT* gene variant (GenBank NG_007495.2) catalyzes transfer of galactose residue to lactosylceramide and paragloboside, thereby creating antigens with Galα1→4Galβ1 terminal structure: P^k (globotriaosylceramide, Gb3, CD77) and P1, respectively (Fig. 5). However, α-1,4-galactosyltransferase with p.Q211E substitution caused by c.631C>G mutation in *A4GALT* (rs397514502) exhibits broader acceptor specificity and attaches galactose residue also to the GSL acceptors with terminal *N*-acetylgalactosamine (Suchanowska *et al.*, 2012; Kaczmarek, Duk, *et al.*, 2016).
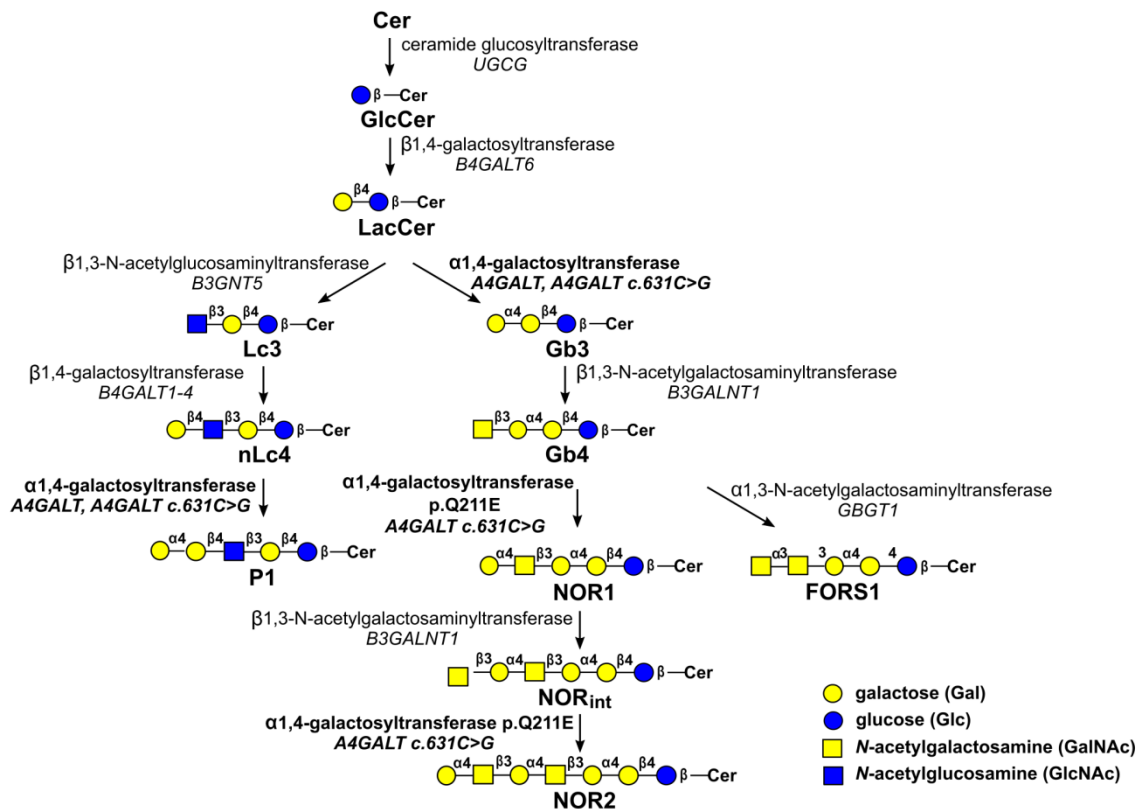
Fig. 5. Schematic representation of the biosynthesis of the P1PK and related antigens.

Classified under the Enzyme Commission number EC 2.4.1.228, human α-1,4-galactosyltransferase belongs to the 32nd family of glycosyltransferases (CAZy, http://www.cazy.org). It is a 353 amino acid-long protein with calculated molecular weight

40 499 Da and pI 9.16. Although crystal structure of α-1,4-galactosyltransferase has not been resolved yet, it is predicted type II transmembrane protein residing in Golgi apparatus membrane. The enzyme was shown to be localized in the Golgi by confocal microscopy imaging (Yamaji *et al.*, 2019). It was found that α-1,4-galactosyltransferase interacts with lysosomal protein transmembrane 4α (LAPTM4A), which is essential for its activity, and transmembrane 9 superfamily 2 protein (TM9SF2), which is responsible for the enzyme subcellular localization (Tian *et al.*, 2018; Yamaji *et al.*, 2019). Recently, it was shown that Golgi phosphoprotein 3 (GOLPH3) support retention of α-1,4-galactosyltransferase in the Golgi by binding to the LXXR motif (LLLR, 7-10 aa) of the enzyme N-terminal cytoplasmic tail (Rizzo *et al.*, 2021).

α-1,4-galactosyltransferase contains the DXD motif (DTD, 192-194 aa, UniProtKB - Q9NPC4 (A4GAT_HUMAN)) and two putative N-glycosylation sites (N121 and N203). We demonstrated previously that recombinant catalytic domain of α-1,4-galactosyltransferase obtained in insect cells become inactive after PNGase F treatment, suggesting that N-glycans play an important role in enzyme activity (Szymczak *et al.*, 2016). Recently, the activity of α-1,4-galactosyltransferase variants with destroyed N-glycosylation sites was evaluated (p.S123A, p.T205A and p.S123A / p.T205A). The variants differed by molecular mass, indicating that the consensus enzyme is N-glycosylated at both N121 and N203 sites. Strikingly, the p.S123A variant showed an increased activity in comparison to consensus α-1,4-galactosyltransferase, while p.T205A and p.S123A / p.T205A are less active (Mikolajczyk *et al.*, 2021).

4.2.2   P1PK histo-blood group system

The human P1PK histo-blood group system is classified under the International Society of Blood Transfusion (ISBT) number 003, among 38 distinguished systems (www.isbtweb.org). Since its discovery in 1927 by Landsteiner and Levine (Landsteiner and Levine, 1927), the P1PK system underwent several nomenclature changes. Currently it comprises three antigens: P^k (globotriaosylceraamide, Gb3, CD77), P1 and NOR (Kaczmarek *et al.*, 2014). The structures of P1PK blood group antigens are shown in Table 1.

Table 1. Structures of P1PK blood group antigens.

Antigen	Structure	Series
P^k (Gb3/CD77)	Galα1→4Galβ1→4Glc-Cer	Globo
P1	Galα1→4Galβ1→4GlcNAcβ1→3Galβ1→4Glc-Cer	Neolacto
NOR1	Galα1→4GalNAcβ1→3Galα1→4Galβ1→4Glc-Cer	Globo
NOR_{int}	GalNAcβ1→3Galα1→4GalNAcβ1→3Galα1→4Galβ1→4Glc-Cer	Globo
NOR2	Galα1→4GalNAcβ1→3Galα1→4GalNAcβ1→3Galα1→4Galβ1→ →4Glc-Cer	Globo

The P^k antigen (Gb3) is expressed on erythrocytes of most individuals (except of the null phenotype, denoted p), whereas P1 presence varies in different populations: from 30% in Japanese to 80% in Caucasians, to 94% in Blacks, thus underlying two common phenotypes: P_1, if the P1 antigen is present, and P_2, if P1 is absent (Table 2). The rare p phenotype results from mutations in *A4GALT* ORF, including missense, nonsense and frameshift mutations (Hellberg *et al.*, 2003).

Table 2. Phenotypes of P1PK histo-blood group system and *A4GALT* genotypes (ψψ does not encode any functional protein).

Phenotype	Genotype	Antigens
P_1	P^1P^1	P1, P^k
	P^1P^2	
P_2	P^2P^2	P^k
p	ψψ	-
P_1NOR	$P^{1NOR}P^1$	P1, P^k, NOR1, NOR2, NOR_{int}
	$P^{1NOR}P^2$	

The genetic background of the P_1/P_2 phenotypic polymorphism remained ambiguous for years, because it does not result from mutations in *A4GALT* coding region (Steffensen *et al.*, 2000). *A4GALT* transcript level was found to be higher in P_1 individuals and it was generally accepted that the P_1/P_2 status derives from varied *A4GALT* transcript levels (Iwamura *et al.*, 2003; Thuresson, Westman and Olsson, 2011). Several single nucleotide polymorphisms (SNPs) upstream from the coding region were suggested to underlie the P_1/P_2 difference (Iwamura

et al., 2003; Thuresson, Westman and Olsson, 2011; Lai *et al.*, 2014). Two mutations of the promoter region present in one allele, c.-551_-550insC (rs5845556) and c.-160G>A (rs28910285), were found to correlate with P_2 phenotype (Iwamura *et al.*, 2003). Although analyzed by Iwamura and coworkers P_2 individuals were homozygous for this allele, and P_1 were heterozygous, a study conducted on a bigger group revealed over 25% of P1 individuals appeared to be also homozygous (Tilley, Green and Daniels, 2006).

Further analysis of *A4GALT* gene characterized a novel transcript containing the noncoding exon 1 and a short fragment of intron 1, termed exon 2a (Thuresson, Westman and Olsson, 2011). At position 42 of this exon was found SNP C/T (rs8138197; Fig. 6) correlated with P_1/P_2 polymorphism, which introduces a potential start codon in P^2 allele initiating new ORF encoding 28 aa peptide. The authors suggested the peptide could act as an *A4GALT* expression modulator, but they were unable to support this hypothesis on experimental way. Later, in a larger scale analysis, another SNPs (rs2143918, rs2143919 and rs5751348; Fig. 6) in *A4GALT* intron 1 were proposed as important for P_1/P_2 polymorphism (Lai *et al.*, 2014). However, at that point it was still unclear, how important are these SNPs (rs8138197, rs2143918, rs2143919, rs5751348) in general and in relation to each other. Part of the results of this thesis contributed to elucidation of their significance and indicated that rs5751348 was the most reliable (Kaczmarek *et al.*, 2018). Eventually, it was found that the rs5751348G region in intron 2 appears to be preferentially bound by transcription factor early growth response 1 (EGR1) and Runt-related transcription factor 1 (RUNX1) (Westman *et al.*, 2018; Yeh *et al.*, 2018).
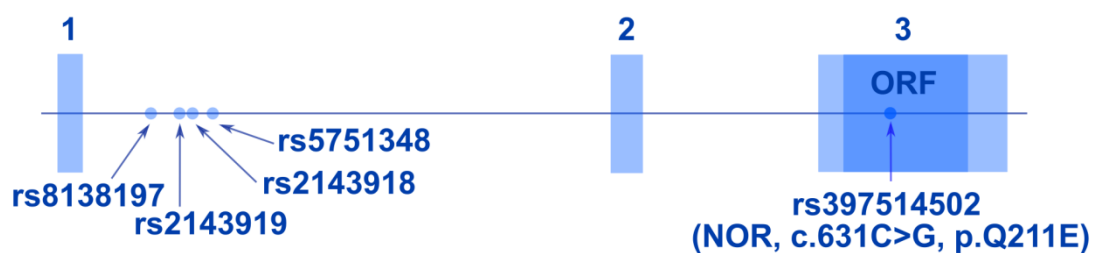
Fig. 6. Schematic representation of *A4GALT* gene. Blue rectangles depict the three exons.

Besides red blood cells (RBCs), the P^k antigen (Gb3) is present in human lymphocytes, kidney, heart, lung, smooth muscle and epithelium of gastrointestinal tract (Cooling, 2015). Moreover, elevated levels of P^k (Gb3) have been reported in colorectal (Kovbasnjuk *et al.*, 2005), gastric (Geyer *et al.*, 2016) and ovarian cancer (Johansson *et al.*, 2009). In the case of

ovarian cancer, a decrease of α-1,4-galactosyltransferase expression and lower level of P^k (Gb3) was shown to be associated with epithelial to mesenchymal transition (Jacob *et al.*, 2018). In addition, accumulation of P^k (Gb3) is the hallmark of Fabry disease, caused by α-galactosidase deficiency (Miller, Kanack and Dahms, 2019). On the other hand, the P1 expression seems to be limited to the erythroid lineage (Cooling, 2015) and outside of RBCs it has only been detected on ovarian cancer cells, where it was termed a cancer-associated antigen (Jacob *et al.*, 2014).

The third antigen of P1PK system is NOR, which exists in two forms: NOR1 and NOR2, and is synthesized by α-1,4-galactosyltransferase with p.Q211E substitution (Fig. 5) (Suchanowska *et al.*, 2012). The variant enzyme shows a broader acceptor specificity and in addition to P^k (Gb3) and P1 with Galα1→4Galβ1 terminal structure it catalyzes the synthesis of NOR with Galα1→4GalNAcβ1 terminal structure, never before found in mammals (Kaczmarek, Duk, *et al.*, 2016). NOR1 is synthesized from globoside (globotetraosylceramide, Gb4, P antigen, GalNAcβ1→3Galα1→4Galβ1→4Glc-Cer) and NOR2 arises as a result of NOR1 extension by β-1,3-*N*-acetylgalactosaminyltransferase and α-1,4-galactosyltransferase p.Q211E (Fig. 5). The structure of NOR antigens was established earlier in our laboratory (Duk *et al.*, 2001). The presence of NOR antigens on the surface of red blood cells causes rare inheritable NOR polyagglutination syndrome. The NOR erythrocytes are agglutinated by most ABO blood group–matched human sera which contain antibodies recognizing terminal Galα1→4GalNAcβ1 moiety in NOR1 and NOR2. At present, only two families with NOR-positive individuals are known, one in the USA, and one in Poland.

It was generally believed that human α-1,4-galactosyltransferase can add terminal Gal residue only to GSL acceptors. However, it was shown recently that glycoproteins of P^1P^1 and some of P^1P^2 RBCs carry P1 glycotopes, but the authors used only western blotting with anti-P1 antibodies (Stenfelt *et al.*, 2019). A comprehensive analysis of α-1,4-galactosyltransferase activity toward glycoprotein acceptors is necessary to elucidate whether such structures are produced by this enzyme.

P^k (Gb3) and P1 antigens can serve as receptors for PapG adhesin from P-fimbriated uropathogenic *Escherichia coli*, while P^k (Gb3) may act as receptor for SadP adhesin from *Streptococcus suis* (Ferrando *et al.*, 2017) and vacuolating cytotoxin VacA from *Helicobacter pylori* (Roche *et al.*, 2007). Furthermore, it is generally accepted that P^k (Gb3) is the main receptor for Shiga toxins (Stxs), the most formidable virulence factors produced by *Shigella dysenteriae* of serotype 1 and enterohemorrhagic *E. coli* (Bruyand *et al.*, 2018; Lee and Tesh, 2019).

4.3 Shiga toxins

Stxs derive their name from Japanese microbiologist Kiyoshi Shiga, who in 1897 discovered the bacterial origin of dysentery caused by *Shigella dysenteriae* and toxins produced by this organism (Shiga, 1898). In 1977, Konowalchuk described a cytotoxin produced by *E. coli*, which was toxic to Vero cells (line initiated from the kidney of a normal adult African green monkey), and hence termed it "verotoxin (VT)" (Konowalchuk, Speirs and Stavric, 1977). Later it was revealed that some *E. coli* isolates produce toxins related to Shiga toxin from *S. dysenteriae*, and these factors were referred to as "Shiga-like toxin (SLT)" (O'Brien et al. 1984). Further studies uncovered "verotoxins" and "Shiga-like toxins" are closely related to the prototypic Shiga toxin and they began to be called this way; however, many researchers still continue to use the term "verotoxins" (Scheutz *et al.*, 2012).

4.3.1 Classification

Stxs released by enterohemorrhagic Stx-producing *E. coli* (STEC) fall into two types: Stx1, which is nearly identical to the toxin secreted by *S. dysenteriae* of serotype 1 (differing by a single amino acid in A subunit of the toxin), and more genetically distinct Stx2 (Liu *et al.*, 2021). Stx2 shows higher virulence and is more frequently associated with severe course of STEC infection in comparison to Stx1 (Melton-Celsa, 2014). Stx1 and Stx2 variants are further cathegorized into subtypes based on similarity of nucleotide and amino acid sequences. Currently four Stx1 subtypes are known: Stx1a, Stx1c, Stx1d, Stx1e, and twelve Stx2 subtypes: Stx2a-l (Table 3) (Koutsoumanis *et al.*, 2020).

Table 3. Stx classification.

Toxin type	Toxin subtype	Reference
Stx1	Stx1a	(O'Brien *et al.*, 1984)
	Stx1c	(Zhang *et al.*, 2002)
	Stx1d	(Burk *et al.*, 2003)
	Stx1e[#]	(Probert, McQuaid and Schrader, 2014)
Stx2	Stx2a	(O'Brien *et al.*, 1984)
	Stx2b	(Paton *et al.*, 1992)
	Stx2c	(Russmann *et al.*, 1994)
	Stx2d	(Samuel *et al.*, 1990)
	Stx2e	(Gannon and Gyles, 1990)
	Stx2f	(Schmidt *et al.*, 2000)
	Stx2g	(Leung *et al.*, 2003)
	Stx2h*	(Bai *et al.*, 2018)
	Stx2i*	(Lacher *et al.*, 2016)
	Stx2j*	(Koutsoumanis *et al.*, 2020)
	Stx2k*	(Hughes *et al.*, 2019)
	Stx2l*	(Lacher *et al.*, 2016)

[#] found only in *Enterobacter cloacae*
* provisional designation

The presence of Stx-encoding genes in *E. coli* strains is thought to be a consequence of horizontal gene transfer from *Shigella*, mediated by lambdoid bacteriophages (Łoś and Węgrzyn, 2011; Pinto *et al.*, 2021). Other microorganisms (than *S. dysenteriae* and *E. coli*) producing Stx have been also reported, i.a. *Acinetobacter haemolyticus*, *Aeromonas sp.*, *Citrobacter freundii*, *Enterobacter cloacae* and *Escherichia albertii* (Schmidt *et al.*, 1993; Paton and Paton, 1996; Grotiuz *et al.*, 2006; Alperi and Figueras, 2010; Ooka *et al.*, 2012). However, transduction of these bacteria by Stx encoding phages seem to be rather unstable, with the exception of *Enterobacter cloacae* strain producing Stx1e subtype (Probert, McQuaid and Schrader, 2014).

4.3.2 Structure

Stxs belong to AB$_5$ class of toxins, similarly as cholera toxin, pertussis toxin, subtilase cytotoxin and heat labile enterotoxins. All members of this class consist of one catalytic A domain responsible for interrupting essential host functions, and pentamer of B subunits interacting with a cellular receptor (Beddoe *et al.*, 2010). Five Stx B subunits are arranged around the central pore in which the C-terminus of the A moiety is anchored (Fig. 7). Each B subunit is 69 amino acid long (for Stx/Stx1a, 71 aa for Stx2a) and encompasses up to three receptor binding sites. However, at least one of them is formed by residues from adjacent moieties (Johannes and Römer, 2010). Thus, the B pentamer can potentially interact with 15 receptor molecules providing high affinity binding (Liu *et al.*, 2021).
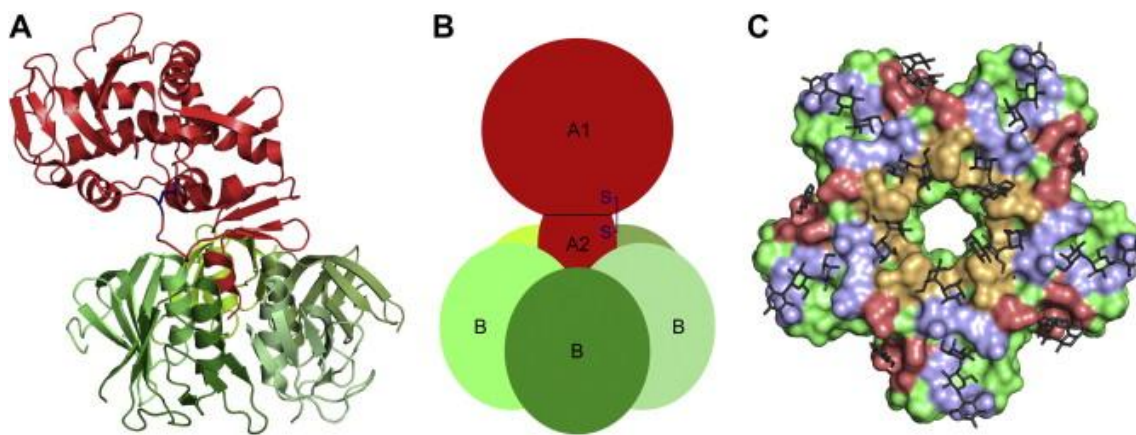
Fig. 7. A) The structure of Stx produced by *S. dysenteriae* determined by X-ray crystallography (PDB ID: 1DM0). B) Stx structure. C) The surface of the B pentamer indicating the location of the 15 potential receptor binding sites, based on the structure of Stx1 complexed to the Gb3 analog MCO-PK (PDB ID: 1BOS). The sugar moieties of MCO-PK are shown as black sticks (Bergan *et al.*, 2012).

The main Stx receptor is P^k antigen (Gb3); however, Gb4 and Forssman antigen (FORS1, GalNAcα1→3GalNAcβ1→3Galα1→4Galβ1→4Glc-Cer), synthesized downstream in the GSL globo series pathway (Fig. 5), are suggested additional receptors for Stx2e variant responsible for pig edema disease (DeGrandis *et al.*, 1989; Müthing *et al.*, 2012). Gb4 has been reported as a low-affinity receptor for a few Stx variants, but presented evidence is debatable and Gb4 role requires further elucidation (Okuda *et al.*, 2006; Zumbrun *et al.*, 2010; Gallegos *et al.*, 2012; Karve and Weiss, 2014).

The mature Stx A subunit consists of 293 aa (for Stx/Stx1a, 297 aa for Stx2a) and is enzymatically cleaved into an A1 subunit and A2 peptide held together by a disulfide bridge.

The enzymatic activity of the toxin resides within A1 while the A2 peptide anchors A1 to the B pentamer (Melton-Celsa, 2014).

4.3.3 Mechanism of action

After binding to P^k antigen (Gb3) and subsequent internalization, Stx is transported to the Golgi apparatus, then retrogradely to the ER, where A1 subunit is released and translocated to the cytosol. There the A1 binds and cleaves a critical adenine residue on 28S rRNA of 60S ribosomal subunit thus acting as a ribosome inactivating protein. Besides direct inhibition of protein synthesis, the A1 subunit induces pro-inflammatory cytokine expression and activates signaling cascades leading to apoptosis (Johannes and Römer, 2010; Kavaliauskiene *et al.*, 2017). Although protein synthesis inhibition itself may lead to cell death, ribotoxic and ER stress signalling are considered of greater importance (Lee and Tesh, 2019). Moreover, Stxs may display *N*-glycosidase activity also toward the nuclear DNA, causing its fragmentation, which induces the apoptosis (Brigotti *et al.*, 2007; Zoja, Buelli and Morigi, 2010).

4.3.4 Hemolytic uremic syndrome (HUS)

Worldwide, it is estimated that approximately 2.8 million of acute diseases annually are caused by Stx producing *Escherichia coli* (STEC) (Majowicz *et al.*, 2014). STEC infections induce heamorrhagic colitis, which can often progress into hemolytic uremic syndrome (HUS), a severe complication characterized by thrombocytopenia, anemia and acute kidney failure (Cody and Dixon, 2019). The risk of developing HUS reaches a peak in children under the age of 10 (up to 15% of STEC-diagnosed patients) (Tarr, Gordon and Chandler, 2005).

STEC are foodborne pathogens and the predominant sources of infection comprise contaminated food (raw meet and milk, vegetables and sprouts), water, and direct contact with animals. Person-to-person transmission have been also reported (Radosavljević, Finke and Belojević, 2016; Heredia and García, 2018; Schlager *et al.*, 2018). Ingested STEC secrete Shiga toxins, which then translocate through intestinal mucosa and reach the bloodstream, where they bind to circulating leukocytes, platelets and erythrocytes (Bitzan *et al.*, 1994; Karpman *et al.*, 2006; Brigotti *et al.*, 2008; Ståhl *et al.*, 2009; Arvidsson *et al.*, 2015). Stx promote their activation and shedding of pro-inflammatory and pro-thrombotic microvesicles, which also serve as toxin carriers (Karpman *et al.*, 2006; Ståhl *et al.*, 2009; Villysson, Tontanahal and Karpman, 2017; Brigotti *et al.*, 2018).

5. Aims of the study

Although several different SNPs upstream from the *A4GALT* coding region have been proposed to underlie the P_1/P_2 phenotype diversity, their significance at the time when the Ph.D. project began was not evaluated, because the role played by mutations in the *A4GALT* promoter region in modulation of transcriptional activity of the gene was a subject of controversy. The role of potential non-canonical Shiga toxin receptors, such as Gb4 and P1 antigen was also not fully evaluated. In addition, our preliminary data suggested that α-1,4-galactosyltransferase may be active not only toward glycosphingolipids, but also toward glycoproteins, what raised the question whether such glycoproteins may act as functional receptors for Shiga toxins.

Thus, the aims of the study were:

1. To evaluate the significance of alleged SNPs (rs8138197, rs2143918, rs2143919, rs5751348) in P_1/P_2 polymorphism, including the NOR-positive individuals.
2. To answer the question what is the activity of α-1,4-galactosyltransferase toward glycoproteins.
3. To explore the role of glycotopes other than P^k antigen produced by α-1,4-galactosyltransferase in binding and internalization of Shiga toxins.

Outline of the study is presented on Fig. 8.
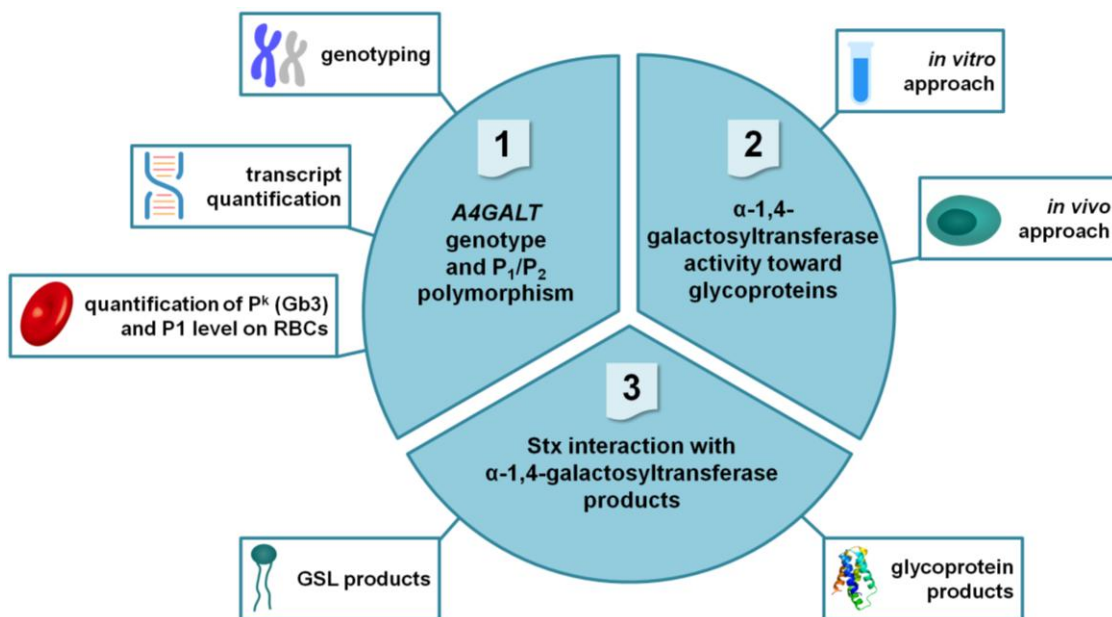
Fig. 8. General outline of the experiments performed in this study.

6. Materials and methods

6.1 Antibodies

Table 4. Monoclonal antibodies used in this study.

Antibody	Clone	Manufacturer/reference
anti-P1	P3NIL100	Immucor Inc
anti-P1	650	Ce-Immundiagnostika
anti-CD77	5B5	BioLegend
anti-NOR*	nor118	(Duk *et al.*, 2005)
anti-Gb4*	PA5	(Okuda, 2017)
anti-A4GALT*	5C7	(Mikolajczyk *et al.*, 2021)
anti-Stx1B, FITC conjugate	13C4	Merck
anti-6x-His Tag	HIS.H8	Thermo Fisher Scientific
anti-c-Myc*	9E10	ATCC

* used as a hybridoma culture supernatant

Table 5. Polyclonal antibodies used in this study

Antibody	Conjugate	Manufacturer
goat anti-human polyvalent immunoglobulins antibody	Biotin	Sigma-Aldrich
goat anti-mouse IgG/A/M (H/L) antibody	Biotin	Bio-Rad Laboratories
goat anti-human IgM antibody	FITC	Thermo Fisher Scientific
goat anti-mouse IgM antibody	FITC	Thermo Fisher Scientific
goat anti-mouse immunoglobulins antibody, F(ab')2 fragment	FITC	Agilent Technologies

6.2 SNPs at *A4GALT* locus and the genetic background of P_1/P_2 polymorphism

6.2.1 Blood collection and storage

Blood was collected from 109 healthy donors following an informed consent according to the Declaration of Helsinki. The study was approved by the Wroclaw Medical University Bioethics Committee, Consent 641/2014, December 14, 2014. For DNA isolation and flow cytometry analysis of RBCs, blood was collected on EDTA, whereas for RNA isolation on heparin. Flow cytometry analysis of RBCs was performed during 24 h after blood donation or washed RBCs were frozen in CellStab low-ionic strength preservative solution (DiaMed, Cressier, Switzerland) and used freshly after thawing.

6.2.2 Genomic DNA isolation

DNA isolation from whole blood was performed with the use of Quick Blood DNA Purification Kit (EURx, Gdansk, Poland) according to the manufacturer's instruction.

6.2.3 Analysis of single nucleotide polymorphisms in *A4GALT* gene

6.2.3.1 Polymerase chain reaction

Three DNA fragments encompassing the studied SNPs (rs8138197, rs2143918, rs2143919, rs5751348 and rs397514502) in *A4GALT* gene were amplified using polymerase chain reaction (PCR) with the use of MJ Mini Gradient Thermal Cycler (Bio-Rad, Hercules, CA, USA). Primers sequences are presented in Table 6. rs8138197sense and rs8138197anti primers were used to cover DNA fragment containing rs8138197. rsLaisense and rsLaianti primers were employed to the amplification of fragment encompassing rs2143918, rs2143919 and rs5751348. A4GTsense and A4GTanti primers were exploited to cover fragment containing rs397514502.

20 µl of the reaction mixture included:

- ✓ 200 ng of genomic DNA;
- ✓ 0.2 mM forward primer (Genomed, Warsaw, Poland);
- ✓ 0.2 mM reverse primer (Genomed);
- ✓ 0.2 mM dNTP mix (EURx, Gdansk, Poland);
- ✓ 1.5 mM $MgCl_2$ (EURx);
- ✓ reaction buffer containing KCl (EURx);
- ✓ 1 unit of Taq polymerase (EURx).

Table 6. Sequences of primers used for genotyping.

Name of primer	Sequence (5'→3')
rs8138197sense	TGAATTAACCGAAAGAAGTAGG
rs8138197anti	CATAGCAAAATGCAAGCA
rsLaisense	GCATTCCTCATCGCAGAC
rsLaianti	ATAAATGCAGCCAAGTCTC
A4GTsense	GGAGAGCCCAAGGAGAAAG
A4GTanti	CAAGTACATTTTCATGGCCTC

Table 7. PCR conditions used for amplification of *A4GALT* fragments encompassing the studied SNPs.

Reaction step	Reaction parameters		
	Temperature [°C]	Time [s]	Number of cycles
Initial denaturation	94	180	1
Denaturation	94	30	
Annealing	58	30	29
Extension	72	150	
Final extension	72	600	1

6.2.3.2 *DNA precipitation from the reaction mixture*

DNA was precipitated from the reaction mixture by the addition of 1 µl of 20 mg/ml glycogen (Sigma-Aldrich), 1/3 of reaction volume of 3 M sodium acetate, pH 4.5 (Avantor, Gliwice, Poland) and 3 volumes of 96% ethanol (Avantor, Gliwice, Poland). After 20 min incubation at -20˚C, the samples were centrifuged (30 min, 15800 x g, 4°C; Centrifuge 5424 R (Eppendorf, Hamburg, Germany)) and the pellet was washed with 1 ml of 70% ethanol (3 min, 15800 x g, 4°C). Then the pellet was dried with the use of SpeedVac vacuum concentrator (Thermo Fisher Scientific, Waltham, MA, USA) and solubilized in UltraPure DNase/RNase-Free Distilled Water (Carlsbad, CA, USA).

6.2.3.3 *DNA quantification*

DNA concentration was measured with the use of NanoDrop Lite Spectrophotometer (Thermo Fisher Scientific).

6.2.3.4 *DNA sequencing*

Sequencing of DNA fragments was ordered at Genomed sequencing laboratory (Warsaw, Poland).

6.2.3.5 *DNA electrophoresis*

DNA fragments were analyzed by electrophoresis in 1% agarose (Sigma-Aldrich, Saint Louis, MO, USA) gel containing Midori Green Advance DNA Stain (ABO, Gdansk, Poland). Beforehand the samples were mixed with DNA Gel Loading Dye (6x; Thermo Fisher Scientific). The electrophoresis was performed in TAE buffer at the voltage of 90 V at room temperature, with the use of Wide Mini-Sub Cell GT Horizontal Electrophoresis System (Bio-Rad, Hercules, CA, USA). The DNA bands were visualized on GBox (Syngene, Cambridge, UK) with UV transilluminator and compared with Lambda DNA/HindIII Marker (Thermo Fisher Scientific) or phiX174 DNA/BsuRI (HaeIII) Marker (Thermo Fisher Scientific).

6.2.4 RNA isolation

RNA isolation from the buffy coat of blood was performed using Human Blood RNA Purification Kit (EURx, Gdansk, Poland) according to the manufacturer's protocol.

6.2.5 Reverse transcription of mRNA

Complementary DNAs (cDNAs) synthesis was accomplished using 240 ng of RNA and SuperScript III First-Strand Synthesis kit (Life Technologies, Carlsbad, CA, USA) with oligo(dT) primers.

6.2.6 *A4GALT* transcript quantification in RBCs

For quantitative analysis of *A4GALT* transcript, 3 µl of cDNA was used as a template in PCR reaction with a predesigned TaqMan assay targeting exon 2–3 boundary (Hs00213726_m1; Life Technologies). The reaction was carried out in the volume of 20 µl, with the use of 7500 Fast Real-Time PCR System (Life Technologies). *A4GALT* transcript quantities were normalized to *ACTB* (β-actin) endogenous control (assay Hs99999903_m1). All samples were run in triplicates, and P^2P^2 samples served as the calibrator. Results were analyzed using Sequence Detection software Version 1.3.1 (Life Technologies). Quantitative PCR conditions are listed in Table 8.

Table 8. Quantitative PCR conditions used for *A4GALT* gene expression assays.

Thermal cycling conditions			
Parameter	Initial denaturation	PCR (42 cycles)	
		Denaturation	Annealing/ extension
Temperature [°C]	95	95	60
Time [s]	600	15	60

6.2.7 Agglutination

RBCs were washed three times with PBS (3 min, 400 x g, 4˚C; centrifuge 5424 R, Eppendorf). Then papain (a non-selective protease) digestion was performed in order to allow efficient recognition of glycosphingolipid epitopes. 20 µl of RBCs was mixed with papain solution 1:1 (v/v) and incubated in 37˚C for 40 min. After washing five times (all washes done with PBS), 20 µl of 2% RBCs suspension was mixed with 20 µl of anti-P1 (P3NIL100) or anti-NOR (nor118) monoclonal antibody on 96-well polystyrene round bottom plates (Thermo Fisher Scientific). Agglutination was analyzed after 30 min of incubation.

6.2.8 Quantitative flow cytometry analysis of RBCs

After papain treatment, 100 µl of 0.5% RBCs suspension was incubated for 40 min on ice with 100 µl of primary antibody (anti-P1, P3NIL100 1:400; anti-P1, 650 1:200; anti-NOR, nor118 1:20; all dilutions done with PBS). After two washes, RBCs were incubated for 40 min

on ice in dark with 100 µl of FITC-conjugated secondary antibody (accordingly: anti-human IgM, anti-mouse IgM, anti-mouse IgG, all diluted 1:100). Then the cells were washed twice and suspended in 750 µl of cold PBS. Flow cytometry analysis was performed on FACSCalibur (BD Biosciences, Franklin Lakes, NJ, USA). 10 000 of gated events were recorded and results were analyzed using Flowing Software (Perttu Terho, University of Turku, Turku, Finland).

For quantitative measurements, Quantum calibration microspheres (Bio-Rad, Hercules, CA, USA) were used. The beads were analyzed during each flow cytometry experiment, and fluorescence intensity of their five populations of defined FITC quantities were used to plot calibration curves (mean fluorescence intensity versus Molecules of Equivalent Soluble Fluorochrome units). Based on the calibration curves and fluorophore-to-protein molar ratios of FITC-conjugates, antibody binding capacity (ABC) per RBC was calculated. Two-tailed two-sample independent t-test, or Welch's test in the case of $P^{1NOR}P^2$ versus P^1P^2 and $P^{1NOR}P^1$ versus P^1P^1 anti-P1 (P3NIL100) ABCs, and $P^{1NOR}P^1$ versus P^1P^1 and P^1P^2 versus P^2P^2 anti-P1 (650) ABCs, because of unequal variances, was employed for intercohort ABC mean comparisons.

6.3 Testing of human α-1,4-galactosyltransferase activity toward glycoprotein acceptors *in vitro*

6.3.1 Cloning, expression and purification of recombinant soluble catalytic domain of human α-1,4-galactosyltransferase in insect cells

To obtain the catalytic domain (amino acid residues from 44 to 353) of human consensus α-1,4-galactosyltransferase and p.Q211E mutein, fragments of *A4GALT* or *A4GALT C631G* ORF, accordingly, spanning the nucleotides from 130 to 1059 were cloned in frame with sequence encoding 6x-His and c-Myc tags (at the C-terminus) into pGEM-T Easy vector (Promega, Madison, WI, USA) (vector map presented on Fig. A1). Then the vector was subjected to EcoRI and NotI (Fermentas) restriction enzymes digestion and the construct containing *A4GALT* fragment was inserted into pAcGP67C vector, which was used to the production of recombinant baculovirus (GenScript, Pistacaway Township, NJ, USA). Soluble catalytic domain of human α-1,4-galactosyltransferase was purified from High Five cell culture medium after infection of the cells with the baculovirus.

6.3.1.1 *Polymerase chain reaction*

Amplification of the *A4GALT* and *A4GALT C631G* ORF fragment was accomplished by polymerase chain reaction performed with the use of T100 Thermal Cycler (Bio-Rad, Hercules, CA, USA). pCAG vector encoding the full-length human α-1,4-galactosyltransferase, either consensus or p.Q211E mutein, obtained from Dr Anna Suchanowska served as a template.

Sequence recognized by EcoRI enzyme was introduced in forward primer, and nucleotides recognized by NotI, as well as sequence encoding 6x-His and c-Myc tags were introduced in reverse primer. 20 μl of the reaction mixture included:

- ✓ 20 ng of plasmid DNA;
- ✓ 0.2 mM forward primer (5'→3': CATGGGAATTCCGGAGAGCCCAAGGAGAAAG (Genomed);
- ✓ 0.2 mM reverse primer (5'→3': AAAAGCGGCCGCCTAATGATGATGATGATG ATGCAGATCCTCTTCTGAGATGAGTTTTTGTTCCAAGTACATTTTCATGGCCT) (Genomed);
- ✓ 0.2 mM dNTP mix (EURx);
- ✓ 1.5 mM MgCl$_2$ (EURx);
- ✓ reaction buffer containing KCl (EURx);
- ✓ 1 unit of Taq polymerase (1 U/μl) (EURx).

Table 9. PCR conditions used for amplification of *A4GALT* fragment.

Reaction step	Reaction parameters		
	Temperature [°C]	Time [s]	Number of cycles
Initial denaturation	94	180	1
Denaturation	94	30	
Annealing	55-60	30	29
Extension	72	120	
Final extension	72	600	1

6.3.1.2 Preparative DNA electrophoresis

DNA fragments were separated by preparative electrophoresis in 1% agarose (Sigma-Aldrich, Saint Louis, MO, USA) gel containing Midori Green Advance DNA Stain (ABO, Gdansk, Poland). The electrophoresis was performed with the use of Wide Mini-Sub Cell GT Horizontal Electrophoresis System (Bio-Rad, Hercules, CA, USA), in TAE buffer, at the voltage of 50 V at room temperature, and desired DNA band was cut out.

6.3.1.3 DNA isolation from the agarose gel

DNA was purified from the agarose gel with the use of Gel-Out kit (A&A Biotechnology, Gdynia, Poland), according to the manufacturer's instruction.

6.3.1.4 Ligation into pGEM-T Easy vector

Ligation of amplified *A4GALT* fragment into pGEM-T Easy vector (vector map presented on Fig. A1) was carried out at 4:1 insert to vector w/w ratio with the use of 200 ng of the insert and 1 unit of T4 DNA Ligase (Promega, Madison, WI, USA). The reaction was run for 1 h at

room temperature at the volume of 15 μl. Then the product was precipitated and utilized to the transformation of electrocompetent cells.

6.3.1.5 Ligation into pAcGP67C vector

A4GALT fragment was cut out from pGEM-T Easy vector with the use of EcoRI and NotI restriction enzymes and ligated into pAcGP67C vector (linearized and dephosphorylated). Vector map is presented on Fig. A2. Ligation was performed in 3:1 insert to vector molar ratio, with the use of 1 unit of T4 DNA Ligase. Reaction was carried out overnight at 15˚C.

6.3.1.6 Electrocompetent cell preparation

XL1-Blue *Escherichia coli* (Stratagene, San Diego, CA, USA) were seeded on the agar plates containing 10 μg/ml tetracycline (Polfa Tarchomin, Warsaw, Poland). One of the colonies was used to the inoculation of 10 ml of SB medium with 10 μg/ml tetracycline. Bacteria were grown overnight at 30˚C, 190 rpm with the use of New Brunswick Excella E24 Shaker (Eppendorf). Then the culture was transferred to 200 ml of SB medium with 10 μg/ml tetracycline and grown until OD_{600} reached 0.5. The culture was centrifuged (10 min, 6371 x g, 4˚C, Beckman J2-MC centrifuge; Beckman Coulter, Brea, CA, USA). Bacterial pellet was washed twice with 370 ml of water, once with 10 ml of 20% glycerol (Sigma-Aldrich) (10 min, 9780 x g, 4˚C) and suspended in 5 ml of 20% glycerol. Electrocompetent bacteria were portioned in microcentrifuge tubes, frozen in dry ice ethanol bath and maintained at -80˚C.

6.3.1.7 Electrocompetent cell transformation

Competent cells were transformed with the plasmid after ligation. 100 μl of cell suspension was thawed on ice, mixed with 10 μl of plasmid DNA and transferred to electroporation cuvette (2 mm wide gap; Bio-Rad). Then the mix was subjected to pulsed electric currents 2 kV/0.1 cm (50 μF, 1500 Ω) with the use of Gene Pulser Xcell Electroporation System (Bio-Rad). The cells were suspended in 1 ml of SOC medium (Sigma-Aldrich) immediately after electroporation and cultured for 1 h, 190 rpm at 37˚C in New Brunswick Excella E24 Shaker (Eppendorf). Then 10 μl and 100 μl of cell suspension were seeded on agar plates containing appropriate antibiotics.

6.3.1.8 Selection culture on IPTG/X-Gal plates

Selection culture of the bacteria transformed with pGEM-T Easy vector containing ligated insert was performed on agar plates containing 10 μg/ml carbenicillin (Polfa Tarchomin, Warsaw, Poland) and 10 μg/ml tetracycline. Before seeding of bacteria, the plates were covered with 5.88 μl of 1M IPTG (isopropyl β-D-1-thiogalactopyranoside; Sigma-Aldrich) and

40 µl of X-Gal (5-bromo-4-chloro-3-indolyl β-D-galactopyranoside; Sigma-Aldrich). Bacteria were grown on plates overnight at 37˚C (incubator).

6.3.1.9   *Bacteria culture for plasmid DNA preparation*

For "miniprep", 2 ml of SB medium with 100 µg/ml ampicillin was inoculated with one colony from the selection plate and incubated overnight at 37˚C (210 rpm; New Brunswick Excella E24 Shaker).

For "maxiprep", 10 ml of SB medium with 100 µg/ml ampicillin was inoculated with one colony from the selection plate and incubated for few hours at 37˚C (180 rpm; New Brunswick Excella E24 Shaker). Then the culture was transferred to 200 ml of medium and grown overnight at 37˚C (180 rpm).

6.3.1.10 *Plasmid DNA isolation*

Plasmid DNA was purified from bacteria cells with the use of Plasmid Mini Kit (QIAGEN, Hilden, Germany) or Plasmid Maxi Kit (QIAGEN), according to the manufacturer's instruction.

6.3.1.11 *Restriction enzyme digestion*

Purified plasmids were treated with specific restriction enzymes for 1 h at 37˚C (ThermoStat Plus, Eppendorf). The reaction mix contained 150-200 ng of plasmid DNA and 1 unit of restriction enzyme in appropriate buffer. After digestion, loading buffer was added to the reaction mix and DNA fragments were analyzed by electrophoresis.

Preparative restriction enzyme treatment was performed according to the manufacturer's recommendations (Fermentas), based on the assumption that 1 unit of enzyme digests 1 µg of DNA during 1 h. The reaction mix (100 µl) contained 5-10 µg of DNA, 10 units of restriction enzyme and the appropriate buffer. After digestion, DNA was precipitated, separated by preparative electrophoresis and purified from agarose gel.

6.3.1.12 *DNA dephosphorylation*

After restriction enzyme digestion, and in advance of ligation with the insert, 5' termini of linearized vector were dephosphorylated with the use of alkaline phosphatase (Promega) according to the manufacturer's instruction. After reaction, the enzyme was inactivated by 15 min incubation at 65˚C.

6.3.1.13 *Construction of recombinant baculovirus*

pAcGP67C vector encoding *A4GALT* fragment was utilized to the production of recombinant baculovirus by homologous recombination method (GenScript, Pistacaway Township, NJ, US).

6.3.1.14 High Five cell culture

High Five cells (BTI-TN-5B1-4), originated from the ovary of the cabbage looper (*Trichoplusia ni*), were cultured in ESF 921 medium (Expression Systems, Davis, CA, USA) supplemented with 10% fetal calf serum (Gibco, Carlsbad, CA, USA) at 27˚C, in non-humidified, 100% air atmosphere. After thawing, the cells were initially maintained in adherent culture (cooled incubator ST2; POL-EKO-APARATURA, Wodzisław Śląski, Poland) and were transferred to suspension (110 rpm, Ecotron incubator shaker; Infors HT, Bottmingen, Switzerland) after one or two passages.

6.3.1.15 High Five cells transduction with recombinant baculovirus

Before transduction, High Five cells were counted, centrifuged (5 min, 200 x g, room temperature; centrifuge 5702, Eppendorf) and suspended in ESF 921 medium at 3-4 x 10^6 cells/ml density. Recombinant baculovirus suspension was added to multiplicity of infection (MOI) = 5.

6.3.1.16 Purification of recombinant catalytic domain of human α-1,4-galactosyltransferase from the transduced High Five cell medium

48 h after transduction, High Five cell culture was centrifuged (15 min, 7500 x g, 4˚C; centrifuge J2-MC, Beckman Coulter). Supernatant was collected and concentrated 10 times by ultrafiltration with the use of Amicon Ultra-15 Centrifugal Filter Units with 10 kDa cut-off (Merck, Darmstadt, Germany). Then the concentrated supernatant was dialyzed into NPB buffer for 7 days at 4˚C, changing buffer every 12-24 h.

After dialysis, the preparation was centrifuged (30 min, 23700 x g, 4˚C; centrifuge J2-MC, Beckman Coulter) to remove insoluble proteins. Supernatant was loaded on column with Ni-NTA (nickel-nitrilotriacetic acid) agarose resin (Ni-NTA Agarose, QIAGEN), equilibrated with NPB buffer. Then the resin was washed with buffer containing 10 mM, 20 mM, 30 mM imidazole. Elution was performed with buffer containing 50 mM, 100 mM and 200 mM imidazole. Elution fractions were analyzed by dot blotting with anti-c-Myc antibody (9E10). Fractions positive for c-Myc antigen were pooled (separately eluted with 50 mM imidazole, eluted with 100 mM and 200 mM imidazole together) and concentrated 10 times by ultrafiltration with the use of Amicon Ultra-15 Centrifugal Filter Units with 10 kDa cut-off. Concentrated samples were dialyzed into TBS and analyzed by SDS-PAGE and CBB staining and by western blotting with anti-c-Myc antibody (9E10). After addition of glycerol to 50%, the samples containing recombinant α-1,4-galactosyltransferase were stored at -20˚C.

6.3.1.17 Protein quantification

Protein concentration was measured with the use of NanoDrop Lite Spectrophotometer (Thermo Fisher Scientific).

6.3.1.18 Dot blotting

2 µl of affinity chromatography elution fractions were applied to the nitrocellulose membrane. After soaking in TBS, the membrane was incubated for 1 h in 5% skim milk in TBS, washed 5 times (all washes done with TBS) and placed in anti-c-Myc antibody (9E10) solution (1:5, TBS) for 1 h. Then the membrane was washed and incubated with secondary antibody (anti-mouse IgG conjugated with alkaline phosphatase, 1:1000, TBS). After 5 washes, the membrane was soaked in 5-bromo-4-chloro-3-indolyl phosphate (BCIP, 0.2 mg/ml) / nitro blue tetrazolium (NBT, 0.4 mg/ml) solution.

6.3.1.19 Sodium dodecyl sulfate–polyacrylamide gel electrophoresis (SDS-PAGE)

Protein electrophoresis in polyacrylamide gel (4% v/v stacking, 10% separating Tris-Glycine gel) was performed in denaturing conditions. The samples were mixed with 5x concentrated loading buffer containing β-mercaptoethanol, incubated for 5 min at 95°C and applied to the gel. Electrophoresis was carried out at 200 V, 3 A, with the use of Mini-PROTEAN Tetra Cell system (Bio-Rad).

6.3.1.20 Coomassie Brilliant Blue (CBB) staining

The polyacrylamide gel after protein electrophoresis was incubated for 45 min in Coomassie Brilliant Blue (CBB) R-250 solution (0.6%, 45% methanol, 10% acetic acid). Then the gel was transferred into 35% methanol, 7% acetic acid solution and incubated until destaining of the background.

6.3.1.21 Electrophoretic transfer

After SDS-PAGE, proteins from the polyacrylamide gel were electrophoretically transferred to the nitrocellulose membrane at 100 V, 25 mA, with the use of Mini Trans-Blot module (Bio-Rad).

6.3.1.22 Western blotting

The nitrocellulose membrane after electrophoretic transfer was incubated for 1 h in 5% skim milk solution in TBS. Then it was washed and incubated with anti-c-Myc (9E10), followed by anti-mouse IgG antibody conjugated with alkaline phosphatase, as described in 6.3.1.18 section.

6.3.2 Glycosyltransferase assay with the use of Gal$_2$GlcNAc$_2$Man$_3$GlcNAc$_2$ nonasaccharide azide as an acceptor substrate

Gal$_2$GlcNAc$_2$Man$_3$GlcNAc$_2$ nonasaccharide azide was synthesized from sialoglycopeptide as described (Ullmann *et al.*, 2012) and kindly provided by Prof. Carlo Unverzagt (Bioorganische Chemie, Universität Bayreuth, Bayreuth, Germany).

Galactosylation of nonasaccharide acceptor by recombinant soluble α-1,4-galactosyltransferase (Fig. 9), as well as MS and NMR analysis of the reaction product was carried out at Bioorganische Chemie, Universität Bayreuth. 180 µl of the reaction mixture contained:

- ✓ 3 mg (1.8 µmol, 1 eq) of Gal$_2$GlcNAc$_2$Man$_3$GlcNAc$_2$ nonasaccharide azide;
- ✓ 233 µg of recombinant α-1,4-galactosyltransferase;
- ✓ 5.4 µmol (3 eq) of UDP-Gal (Promega, Madison, WI, USA);
- ✓ 50 mM sodium cacodylate buffer, pH 6.3;
- ✓ 1.2 mg/ml bovine serum albumin (Roth, Karlsruhe, Germany);
- ✓ 12 mU/µl alkaline phosphatase (EC 3.1.3.1, calf intestine);
- ✓ 1.2 mM MnCl$_2$ (Roth).
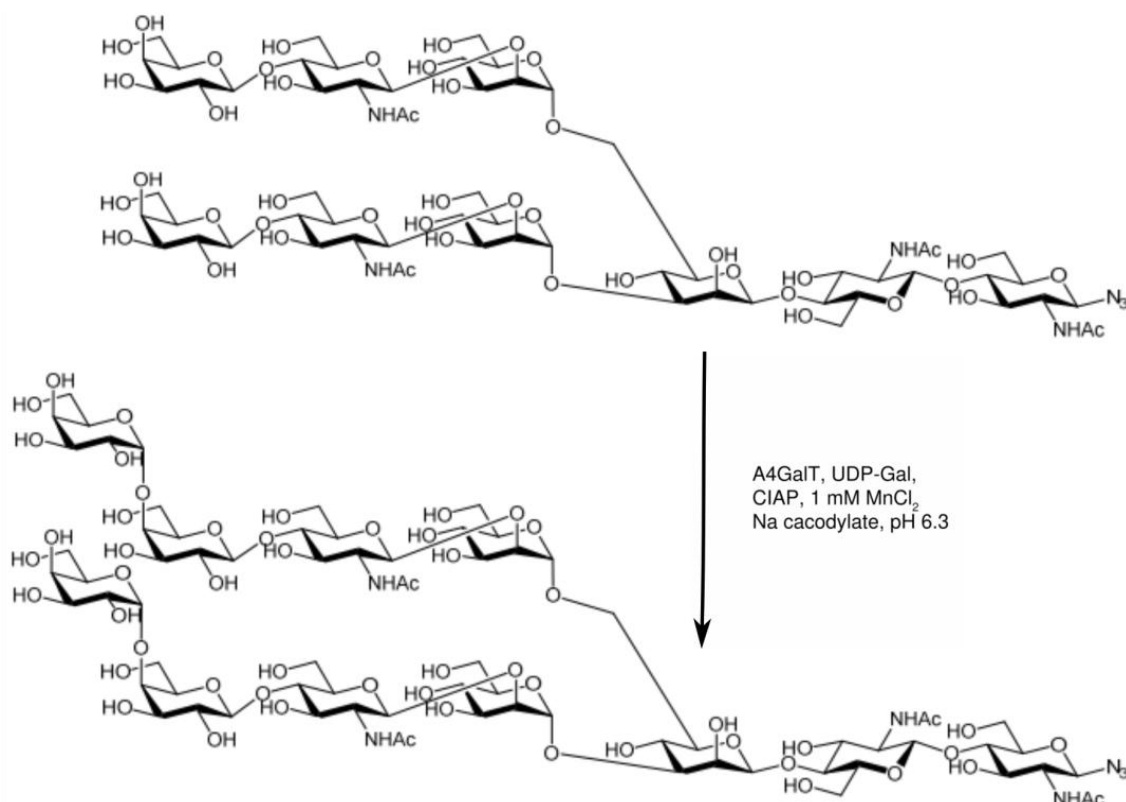
Fig. 9. Scheme of Gal$_2$GlcNAc$_2$Man$_3$GlcNAc$_2$ nonasaccharide azide galactosylation by recombinant human α-1,4-galactosyltransferase.

Reaction conditions were adapted from the protocol developed earlier in Laboratory of Glycobiology (Hirszfeld Institute of Immunology and Experimental Therapy) for enzymatic assays with the use of synthetic glycoconjugates carrying GSL-type glycans as acceptors. The reaction was performed at 30°C in Mastercycler Gradient PCR Thermal Cycler (Eppendorf). After 7 days the mixture was purified by size exclusion chromatography (HiLoad® 16/600 Superdex® 30 pg, 0.1 M NH_4HCO_3, flow: 0.6 ml/min) followed by an additional RP-HPLC (YMC Hydrosphere C18, 150 x 10 mm, 5 µm, gradient from 0-3% MeCN in H_2O, 0.1% formic acid) purification step.

6.3.2.1 ESI-TOF mass spectrometry analysis

ESI-TOF mass spectra were recorded with a Micromass LCT instrument coupled to a Waters H-Class UHPLC System. High resolution ESI mass spectra were recorded with a Thermo Q Exactive Orbitrap coupled to an Ultimate 3000 UHPLC System.

6.3.2.2 NMR analysis

NMR spectra were recorded with a Bruker Advance III HD 500 instrument. Product of α-1,4-galactosyltransferase reaction was characterized by ^{1}H and ^{13}C resonances from a couple of 1D and 2D NMR experiments (JMOD, HH-COSY, HH-TOCSY, HSQC, HSQC-TOCSY, NOESY). The spectra were calibrated using [D_4]-Methanol ($δ(^1H)$ = 3.31 ppm, $δ(^{13}C)$ = 49.00 ppm). Coupling constants are reported in Hz and the resonances are assigned according to Fig. 10.
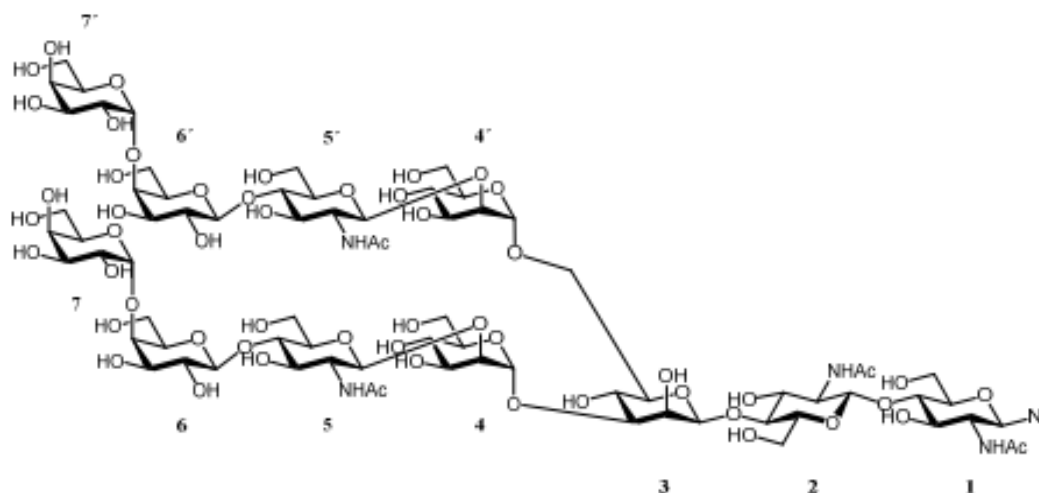
Fig. 10. Assignment of NMR resonances.

6.3.3 Glycosyltransferase assay with human recombinant saposin D glycoform as an acceptor substrate

The recombinant glycoprotein saposin D was synthesized as described (Graf *et al.*, 2017), as a nonasaccharide glycoform (SapD9) containing one N-linked glycan chain $Gal_2GlcNAc_2Man_3GlcNAc_2$. SapD9 was kindly provided by Prof. Carlo Unverzagt and its galactosylation by human recombinant soluble α-1,4-galactosyltransferase and MS analysis of the reaction product was carried out at Bioorganische Chemie, Universität Bayreuth, Bayreuth, Germany). 9.2 µl of the reaction mixture contained:

- ✓ 100 µg (9.3 nmol, 1 eq) of SapD9;
- ✓ 31 µg of recombinant α-1,4-galactosyltransferase;
- ✓ 37.7 nmol (4 eq) of UDP-Gal (Promega);
- ✓ 50 mM sodium cacodylate, pH 6.3;
- ✓ 10 mU/µl alkaline phosphatase (E.C. 3.1.3.1, calf intestine);
- ✓ 1 mM $MnCl_2$ (Roth).

The mixture was incubated at 30°C in Mastercycler Gradient PCR Thermal Cycler (Eppendorf). The reaction was monitored by HR-MS (ESI-MS in H_2O, 0.1% formic acid, flow 0.1 ml/min). After 7 days the reaction mix was purified by RP-HPLC (Supelco Discovery BIO Wide Pore C5, 50 x 2.1 mm, 5 µm, gradient: 20–80% MeCN in H_2O, 0.1% formic acid, flow: 0.5 ml/min) and fractions containing the product were pooled and lyophilized.

6.3.3.1 *Western blotting analysis of SapD*

SapD glycoforms were analyzed by western blotting with anti-P1 antibodies (P3NIL100 and 650). P1 glycotope containing ovalbumin purified previously by Dr Maria Duk (Laboratory of Glycobiology, Hirszfeld Institute of Immunology and Experimental Therapy) served as a positive control. Samples were subjected to non-reducing SDS-PAGE in 4-20% Tris-Glycine gel. After electrophoretic transfer, nitrocellulose membrane was blocked for 1 h in 5% cold fish gelatin in TBS, washed 5 times with TBS and incubated overnight in primary antibody (anti-P1, P3NIL100 or 650) solution (1:100, TBS/1% BSA). Then the membrane was washed and incubated for 1 h in biotin-conjugated secondary antibody solution (anti-human or anti-mouse polyvalent Ig, accordingly; 1:1000, TBS/1% BSA). After 5 washes the membrane was placed for 1 h in ExtrAvidin conjugated with alkaline phosphatase (1:5000, TBS/1% BSA). Bands were visualised using BCIP/NBT solution.

6.4 Testing of human α-1,4-galactosyltransferase activity toward glycoprotein acceptors *in vivo*

6.4.1 Cloning of human *A4GALT* ORF into pRRL-CMV-IRES-PURO vector

A4GALT and *A4GALT C631G* ORFs cloned into pRRL-CMV-IRES-PURO vector (kindly provided by Prof Didier Trono, École Polytechnique Fédérale de Lausanne, Switzerland) were used to recombinant lentiviruses production and obtaining high, stable expression in CHO-Lec2 cells. Map of the pRRL-CMV-IRES-PURO vector is presented on Fig. A3.

6.4.1.1 Polymerase chain reaction

Amplification of the *A4GALT* and *A4GALT C631G* ORFs was performed by PCR as described at 6.3.1.1 section, with PrimeSTAR GXL DNA polymerase (Takara Bio, Kusatsu, Japan) and the following primers: forward (5'→3') GGAATTCGATACCATGTCCAAGCCCCCCG and reverse (5'→3') GAACGCGTTCACAAGTACATTTTCATGGCCT. pCAG vector encoding the full-length human α-1,4-galactosyltransferase, either consensus or p.Q211E mutein, obtained from Dr Anna Suchanowska served as a template. Sequences recognized by EcoRI and MluI restriction enzymes were introduced in the forward and reverse primer, respectively.

Table 10. PCR conditions used for amplification of *A4GALT* ORF.

Reaction step	Reaction parameters		
	Temperature [°C]	Time [s]	Number of cycles
Initial denaturation	98	10	1
Denaturation	98	10	
Annealing	62	15	29
Extension	68	60	
Final extension	68	10	1

6.4.1.2 Ligation into pRRL-CMV-IRES-PURO vector

PCR products containing *A4GALT* and *A4GALT C631G* ORFs were subjected to EcoRI and MluI restriction enzyme digestion as described in 6.3.1.11 section. Purified DNA fragments were ligated into pRRL-CMV-IRES-PURO vector (vector map presented on Fig. A3) in 3:1 insert to vector molar ratio, as described in 6.3.1.5 section.

6.4.2 Lenti-X 293T cell culture

Lenti-X 293T cells (Clontech, Mountain View, CA, USA) were cultured in α-MEM (Laboratory of General Chemistry, Hirszfeld Institute of Immunology and Experimental Therapy) supplemented with 10% fetal bovine serum (FBS; Gibco) and 2 mM L-glutamine (Clontech). The culture was maintained at 37°C under humidified 5% CO_2 atmosphere. Cells

were subcultivated every 2-3 days with 0.25% trypsin/1 mM EDTA (Laboratory of General Chemistry, Hirszfeld Institute of Immunology and Experimental Therapy).

6.4.3 Transfection of Lenti-X 293T

Lenti-X 293T cells at 50-60% confluency in serum-free αMEM were co-transfected using 0.05 mg/ml polyethyleneimine (Sigma-Aldrich) with the following vectors (a generous gift from Prof Didier Trono, École Polytechnique Fédérale de Lausanne, Switzerland) as described (Owczarek *et al.*, 2013):

- ✓ 20 µg/ml of pRRL-CMV-A4GALT-IRES-PURO or pRRL-CMV-A4GALT.Q211E-IRES-PURO;
- ✓ 10 µg/ml of pMDL-g/p-RRE;
- ✓ 5 µg/ml of pRSV-REV;
- ✓ 5 µg/ml pMk-VSVG.

Cells were maintained at 37˚C and the medium was changed 24 h after transfection.

6.4.4 Purification of lentiviruses

Medium was harvested 72 h after transfection of Lenti-X 293T cells and centrifuged (400 x g, 5 min, 24˚C, centrifuge 5702, Eppendorf). Supernatants containing lentiviruses were concentrated 100 times on Amicon Ultra-15K:100 000 (Milipore).

6.4.5 CHO-Lec2 cell culture

CHO-Lec2 cells (American Type Culture Collection, Rockville, MD, USA) were cultured in DMEM/F12 (Gibco) supplemented with 10% FBS at 37˚C under humidified 5% CO_2 atmosphere. Cells were passaged every 3-4 days with 0.25% trypsin/1 mM EDTA.

For some experiments, CHO-Lec2 cells were cultured for 2 weeks in complete medium containing 3 µM N-[(1R,2R)-1-(2,3-dihydro-1,4-benzodioxin-6-yl)-1-hydroxy-3-pyrrolidin-1-ylpropan-2-yl]nonanamide (Genz-123346) (Merck), a glucosylceramide synthase inhibitor.

6.4.6 Lentiviral transduction of CHO-Lec2 cells

CHO-Lec2 cells were transduced with lentiviruses as described (Owczarek *et al.*, 2013). 2×10^4 cells were suspended in serum-free DMEM/F12, mixed with concentrated lentivirus (to the final volume of 1 ml) and centrifuged (2460 x g, 150 min, 24˚C, centrifuge 5702, Eppendorf). Then the cells were seeded on 6-well plates and after 24 h subjected to puromycin selection (CHO-Lec2 A4GALT 40 µg/ml and CHO-Lec2 A4GALT Q211E 15 µg/ml, respectively) to obtain stable clones.

6.4.7 *A4GALT* transcript quantification in CHO-Lec2 cells

mRNA isolation from CHO-Lec2 cells was performed using GeneMATRIX Universal RNA Purification Kit (EURx, Gdansk, Poland). Reverse transcription was accomplished as described in 6.2.5 section. 75 ng of cDNA served as a template in quantitative PCR performed as described in 6.2.6 section. *A4GALT* transcript level was determined with custom TaqMan assay targeting human *A4GALT* used in (Kaczmarek, Mikolajewicz, *et al.*, 2016). Results were normalized in reference to Chinese hamster *GAPDH* level, with the use of custom assay with following primers: forward (5'→3') TGGAAAGCTTGTCATCAAC and reverse (5'→3') GAAGACGCCAGTAGATTCC, and probe (5'→3') AGGCCATCACCATCTTCCAG.

6.4.8 Quantitative flow cytometry analysis of CHO-Lec2 cells

CHO-Lec2 cells were scraped, washed 5 times (all washes were done with PBS) and incubated 30 min on ice with human anti-P1 (P3NIL100, 1:400; all dilutions were done with 1% BSA in PBS) and mouse anti-P1 (1:200) antibodies. After 5 washes the cells were incubated with secondary FITC-conjugated antibodies: anti-human IgM (1:100) or anti-mouse IgM (1:100), accordingly. To assess the level of Gb3 alone, cells were incubated for 30 min with FITC-conjugated anti-CD77 (1:100). After incubation with FITC-conjugates cells were washed, resuspended in 500 µl of cold PBS and subjected to flow cytometry analysis on FACSCalibur (BD Biosciences, Franklin Lakes, NJ, USA). 1×10^5 of events from the gated population were analyzed by Flowing Software (Perttu Terho, University of Turku, Turku, Finland). As described in 6.2.8 section, Quantum calibration microspheres (Bio-Rad) were used for quantitative measurements.

6.4.9 CHO-Lec2 cell lysis

CHO-Lec2 cells were harvested and lysed in CelLytic M (Sigma-Aldrich) supplemented with protease inhibitor cocktail by shaking for 15 min at room temperature. Then the lysate was separated from cell debris by centrifugation (15 min, 21130 x g, centrifuge 5424 R, Eppendorf).

6.4.10 CHO-Lec2 cell lysate digestion with PNGase F

PNGase F treatment of CHO-Lec2 protein lysates was performed as described (Maszczak-Seneczko *et al.*, 2011), with the use of recombinant PNGase F kindly provided by Prof. Mariusz Olczak (Department of Biochemistry, Faculty of Biotechnology, University of Wroclaw, Wroclaw, Poland). Briefly, 1 µl of 10% SDS and 0.7 µl 1M DTT was added to 60 µg of cell lysate and the samples were incubated in 60°C for 5 minutes. Then they were de-N-glycosylated with recombinant PNGase F in 50 mM sodium phosphate buffer, pH 7.5 for 2 h in 37°C.

6.4.11 Western blotting analysis of CHO-Lec2 cell lysates

60 μg of cell lysate per lane was subjected to SDS-PAGE on 10% Tris-Glycine gel and transferred to nitrocellulose membrane, similarly as described in sections 6.3.1.19 and 6.3.1.21; however, without addition of β-mercaptoethanol to the loading buffer and at lower temperature of denaturation (60˚C instead of 95˚C).

Before analysis with the use of anti-A4GALT (5C7) antibody (obtained by Prof. Arkadiusz Miążek, Laboratory of Tumor Immunology, Hirszfeld Institute of Immunology and Experimental Therapy, Wroclaw, Poland; Mikolajczyk *et al.*, 2021) the membrane was blocked in 5% skim milk in TBS, and before incubation with anti-P1 antibodies and lectins the membrane was blocked in 5% cold fish gelatin in TBS. Then the membrane was treated as described in 6.3.3.1 section, with the use of biotinylated secondary antibodies or lectins followed by ExtrAvidin-alkaline phosphatase.

6.4.12 Isolation of neutral glycosphingolipids from CHO-Lec2 cells

Isolation of CHO-Lec2 neutral GSLs was performed as described (Suchanowska *et al.*, 2012). Briefly, GSLs were extracted with chloroform/methanol, desalted on Sephadex G-25 (Sigma-Aldrich), purified from phospholipids by their saponification and separated from gangliosides on DEAE-Sephadex (Sigma-Aldrich).

6.4.13 HPTLC analysis of neutral glycosphingolipids

High-performance thin layer chromatography (HPTLC) analysis of neutral GSLs was carried out as described (Suchanowska *et al.*, 2012). GSLs solubilized in chloroform/methanol (2:1, v/v) were applied to HPTLC plates (Kieselgel 60, Merck, Darmstadt, Germany) and developed with chloroform/methanol/water (55:45:9, v/v/v).

6.4.14 HPTLC orcinol staining

Dried HPTLC plates were sprayed with 0.2% orcinol solution in 3 M H_2SO_4 and incubated at 120˚C for 7 min in drying and heating chamber ED115 with natural convection (BINDER, Tuttlingen, Germany).

6.4.15 HPTLC antibody assay

For antibody assays, dried HPTLC plates were incubated in 0.05% polyisobutylmethacrylate (Sigma-Aldrich) in hexane for 1 min, dried and immersed in TBS. Then the plates were blocked in 5% BSA in TBS for 1 h. After that, the plates were treated analogously as membranes in western blotting analysis described in 6.3.3.1 section, with the use of biotinylated secondary antibodies and ExtrAvidin-alkaline phosphatase conjugate.

6.4.16 Matrix-assisted laser desorption/ionization-time of flight (MALDI-TOF) analysis of neutral glycosphingolipids

MALDI-TOF mass spectrometry analysis of neutral GSLs isolated from CHO-Lec2 cells was carried out on an Autoflex III TOF/TOF™ instrument (BrukerDaltonics, Bremen, Germany). Peptide Calibration Standard (BrukerDaltonics) was used as external calibration and Norharmane (9H-Pyrido[3,4-b]indole; Sigma) as a matrix (10 mg/ml, chloroform:methanol, 2:1, v/v). 1 µl of GSLs dissolved in chloroform/methanol (2:1, v/v) was applied to the plate. Spectra were scanned in the range of *m/z* 700–2000 in the reflectron-positive mode.

6.5 Analysis of Shiga toxin interactions with P1 and Gb4 glycosphingolipids

Recombinant B subunits of Stx1a and Stx2b used in HPTLC and ELISA were a kind gift from Dr Enoch Y. Park (Laboratory of Biotechnology, Shizuoka University, Shizuoka, Japan). Stx1B and Stx2B production and characteristic is described (Kato *et al.*, 2015). Recombinant B subunit of Stx1a used in SPR analysis was obtained by Bartosz Bednarz M.Sc. (Laboratory of Molecular Biology of Microorganisms, Hirszfeld Institute of Immunology and Experimental Therapy), as described (Szymczak-Kulus *et al.*, 2021).

6.5.1 HPTLC Stx assay

HPTLC analysis of neutral GSLs isolated from human RBCs and CHO-Lec2 cells was performed as described in 6.4.15 section. HPTLC plates were incubated with 1 µg/ml recombinant B subunit of Stx1 or Stx2 (Stx1B or Stx2B) containing His-tag, then with anti-6x-His Tag antibody (HIS.H8, 1:1000), biotinylated anti-mouse polyvalent Ig (1:1000) and ExtrAvidin conjugated with alkaline phosphatase (1:5000).

6.5.2 Analysis of synthetic glycoconjugates by enzyme-linked immunosorbent assay (ELISA)

Nunc MaxiSorp 96 well plates (Thermo Fischer) were coated overnight with 20 µg/ml solutions of Lac-PAA, P1-PAA, Gb4-PAA and NOR-PAA synthetic glycoconjugates (Synthaur LLC, Moscow, Russia; structures shown in Table 11) in 50 mM phosphate buffer, pH 7.4 with 5 mM MgCl$_2$. Then the wells were washed five times (all washes done with PBS, pH 7.4, containing 0.05% Tween 20) and blocked overnight with 5% BSA in PBS. After five washes followed 1 h incubation with Stx1B or Stx2B at the concentration of 1 µg/ml in 1% BSA/0.05% Tween 20/PBS. Then the wells were washed and incubated for 1 h with anti-6x-His Tag antibody (HIS.H8, 1:1000), followed by incubations with biotinylated anti-mouse polyvalent Ig (1:1000) and ExtrAvidin conjugated with alkaline phosphatase (1:5000). After

washing twice with water, 1 mg/ml of *p*-nitrophenol phosphate (Sigma-Aldrich) in 0.1 M Tris-HCl, pH 9.6, 1 mM MgCl$_2$, was added to the wells. Absorbance was measured at 405 nm on EnSpire 2300 Multilabel Reader (Perkin Elmer, Waltham, MA, USA).

Table 11. Structures of synthetic PAA glycoconjugates used in this study.

Glycoconjugate	Structure
Lac-PAA	Galβ1→4Glc-PAA
P1-PAA	Galα1→4Galβ1→4GlcNAcβ1→3Galβ1→4Glc-PAA
Gb4-PAA	GalNAcβ1→3Galα1→4Galβ1→4Glc-PAA
NOR-PAA	Galα1→4GalNAcβ1→3Galα1→4Galβ1→4Glc-PAA

6.5.3   Biotinylation of P1-PAA and Gb4-PAA glycoconjugates

To immobilize P1-PAA and Gb4-PAA on SPR sensor chip, the glycoconjugates were subjected to biotinylation. 500 µg of biotin N-hydroxysuccinimide ester (Sigma-Aldrich) were dissolved in 50 µl methanol and diluted with 1.95 ml of PBS to 0.025% solution. 50 µl of 1 mg/ml glycoconjugate solution was added to 50 µl of PBS and then mixed with 160 µl of 0.025% biotin ester. After 30 min incubation at room temperature, the samples were dialyzed for 2 h against water (Slide-A-Lyzer Dialysis Cassettes, 10K MWCO, Thermo Scientific) and overnight against HBS-N buffer (GE Healthcare).

6.5.4   Analysis of synthetic glycoconjugates by surface plasmon resonance (SPR)

Interactions of Stx1B and Stx2B (analytes) with biotinylated glycoconjugates P1-PAA and Gb4-PAA (ligands) were evaluated by SPR on Biacore T-200 (GE Healthcare), using HBS-N supplemented with 0.005% surfactant P20 (GE Healthcare) as the running buffer for immobilization and measurements. Immobilization of ligands on Sensor Chip SA (GE Healthcare), covered with high affinity streptavidin, was performed with 100 µg/ml solutions of biotinylated P1-PAA and Gb4-PAA. The final immobilization levels of P1-PAA and Gb4-PAA were approximately 20 and 60 response units (RU), respectively. Unmodified flow cells served as reference surface. For binding analysis, 1.06 µM Stx1B was injected over the sensor surface for 1 min. For affinity analysis, Stx1B, at the following concentrations: 0.025, 0.074, 0.222, 0.667 (repeated twice), 2 µM, was injected for 1 min at the flow rate 30 µl/min and the dissociation was monitored for 5 min. For binding analysis, 6.67 µM Stx2B was injected over the sensor surface for 1 min. For affinity analysis, Stx2B, at the following concentrations: 0.12, 0.37, 1.11 (repeated twice), 3.33, 10 µM, was injected for 1 min at the flow rate 30 µl/min and the dissociation was controlled for 5 min. For regeneration of the sensor surface 50 mM NaOH was injected for 1 min at the flow rate 30 µl/min. All measurements were performed at 25˚C

and analyzed using BIAevaluation Software 4.0 (GE Healthcare). K_D was determined by fitting to the Steady State Affinity model.

6.5.5 Cloning of human *B3GNT5* and *B3GALNT1* ORFs into pCAG vector

Amplification of the *B3GNT5* and *B3GALNT1* ORFs was performed by PCR as described at 6.3.1.1 section, with PrimeSTAR GXL DNA polymerase (Takara Bio, Kusatsu, Japan). The following primers were used for *B3GNT5* amplification: forward (5'→3') AAAAAAGGTACCATGAGAATGTTGGTTAGTGG and reverse (5'→3') AAAAAAGCGGCCGCTTAGATAAACGCAGCCCTAC, and for *B3GALNT1*: forward (5'→3') AAAAAAGGTACCATGGCCTCGGCTCTCTG and reverse (5'→3') AAAAAAGCGGCCGCTTAATAATGGCATGTGGTGTTCC. pcDNA3 vectors encoding the full-length human β-1,3-*N*-acetylglucosaminyltransferase and β-1,3-*N*-acetylgalactosaminyltransferase, obtained from Dr Radosław Kaczmarek served as templates. Sequences recognized by KpnI and NotI restriction enzymes were introduced in the forward and reverse primers, respectively. PCR reactions were performed in conditions described in Table 10. PCR products containing *B3GNT5* and *B3GALNT1* were subjected to the restriction enzyme digestion as described in 6.3.1.11 section. Purified DNA fragments were ligated into pCAG vector (kindly provided by Prof. Peter Andrews, University of Sheffield) in 1:2 insert to vector molar ratio, as described in 6.3.1.5 section. Vector map is presented on Fig. A4.

6.5.6 Namalwa cell culture

Namalwa cells (Cell Bank of Hirszfeld Institute of Immunology and Experimental Therapy, Wroclaw, Poland) were cultured in DMEM/F12 (Gibco) supplemented with 10% FBS at 37˚C under humidified 5% CO_2 atmosphere. Cells were grown in suspension and subcultured by dilution with a fresh medium.

6.5.7 Transfection of Namalwa cells

pCAG-B3GNT5 and pCAG-B3GALNT1 vectors were introduced into Namalwa cells transfected before by Dr Radosław Kaczmarek with vector encoding the consensus α-1,4-galactosyltransferase and cultured in the presence of 0.25 μg/ml puromycin. Electroporation of Namalwa cells was performed with the use of Neon Transfection System (Invitrogen). 5.6×10^4 of Namalwa A4GALT cells was transferred to the tube containing 3 μg of plasmid DNA and gently mixed. The cell-DNA mixture was aspirated into 10 μl Neon Tip and the Neon Pipette was inserted into Neon Tube with 3 ml of electrolytic buffer placed in the Neon Pipette Station. After delivering the electric pulse (1.4 kV, 20 ms, 2 pulses), the cell-DNA mixture was immediately transferred into prewarmed culture medium. The next day a selection antibiotic, 500 μg/ml of G418 (InvivoGen, Toulouse, France), was added to the medium. For the next two

weeks the medium was exchanged every day and then the cells were examined by flow cytometry.

6.5.8   Flow cytometry analysis of Namalwa cells

Namalwa cells were washed with PBS, incubated with anti-CD77, anti-P1 (650), anti-P1 (P3NIL100), anti-Gb4 (a generous gift from Dr Tetsuya Okuda, Bioproduction Research Institute, National Institute of Advanced Industrial Science and Technology, Tsukuba, Japan), Stx1B, Stx2B and prepared for flow cytometry analysis as described in 6.4.8 section.

6.5.9   Incorporation of synthetic glycoconjugates into CHO-Lec2 cells

P^k (Gb3) trisaccharide (Galα1$\rightarrow$4Galβ1$\rightarrow$4Glc), as well as Galili trisaccharide (Galα1$\rightarrow$3Galβ1$\rightarrow$4GlcNAc) as control, was incorporated into CHO-Lec2 cells as part of the synthetic FSL construct, consisting of the functional component (F), spacer (S) and diacyl lipid (L). Sonicated P^k-FSL and Galili-FSL constructs (10 µM in PBS; Kode Biotech Ltd., Auckland, New Zealand) were incubated with 1 x 10^5 untransduced CHO-Lec2 cells for 1 h at 37°C, under gentle agitation (100 rpm) on a shaker (Celltron, Infors HT). Efficiency of the incorporation was tested in flow cytometry analysis of the cells performed as described in 6.4.8 section. For the cytotoxicity assays the incorporation of P^k-FSL and Galili-FSL to CHO-Lec2 cells was performed for 1.5 h in serum-free DMEM/F12. Obtained CHO-Lec2 P^k and CHO-Lec2 Galili cells, along with CHO-Lec2 NAT and CHO-Lec2 A4GALT, were subjected to the cytotoxicity assays with the use of Stx1 and Stx2, as described in 6.6.4 section.

6.6   Analysis of Shiga toxin interactions with glycoprotein products of human α-1,4-galactosyltransferase

Stx1B and Stx2B used in western blotting and flow cytometry analysis were a kind gift from Dr Enoch Y. Park (Laboratory of Biotechnology, Shizuoka University, Shizuoka, Japan). Stx1B used in SPR analysis was kindly provided by Bartosz Bednarz M.Sc. (Laboratory of Molecular Biology of Microorganisms, Hirszfeld Institute of Immunology and Experimental Therapy).

6.6.1   Western blotting

Western blotting analysis of SapD samples was carried out as described in 6.3.3.1 section, and analysis of CHO-Lec2 lysates as described in 6.4.11 section with membrane blocking in 5% cold fish gelatin in TBS. The membranes were incubated with 1 µg/ml Stx1B or Stx2B, then with anti-6x-His Tag antibody (HIS.H8, 1:1000), biotinylated anti-mouse polyvalent Ig (1:1000) and ExtrAvidin conjugated with alkaline phosphatase (1:5000).

6.6.2 Analysis of SapD glycoforms by SPR

Interactions of Stx1B (analyte) with SapD9 and SapD11 (ligands) were analyzed on Biacore T-200 (GE Healthcare), using HBS-N (GE Healthcare) as the running buffer. All measurements were performed at 25°C. Ligands were immobilized on Series S Sensor Chip CM5 with the use of the Amine Coupling Kit (GE Healthcare). Ligands were diluted to the concentration of 10 µg/ml in 10 mM sodium acetate buffer, pH 4.5. The final immobilization levels of SapD9 and SapD11 were approximately 70 and 60 response units (RU), respectively. Reference surface constituted unmodified flow cells served. For binding analysis, 93.97 µM Stx1B was injected over the sensor surface for 1 min. For affinity analysis, Stx1B, at the following concentrations: 4.16, 8.31, 16.62 (repeated twice), 33.25, 66.5 µM, was injected for 1 min at the flow rate 50 µl/min and the dissociation was monitored for 5 min. The flow of running buffer was sufficient to regenerate the surface. Data were analyzed using BIAevaluation Software 4.0 (GE Healthcare) and K_D was determined by fitting to the Steady State Affinity model. Measurements with Stx2B as the analyte were impossible to accomplish due to vain attempts of sensor surface regeneration.

6.6.3 Quantitative flow cytometry

Quantitative flow cytometry analysis of human RBCs was performed as described in 6.2.8 section, but excepting of prior papain treatment of the cells. Analysis of CHO-Lec2 cells was carried out as described in 6.4.8 section. The cells were firstly incubated with 1 µg/ml Stx1B or Stx2B, then with anti-6x-His Tag antibody (HIS.H8, 1:1000) and anti-mouse IgG conjugates with FITC (1:100). For statistical analysis of Stx1B binding capacity per RBC quantified with the use of Quantum microspheres for different *A4GALT* genotypes, a Mann-Whitney U-test was performed.

6.6.4 Cytotoxicity assays

2×10^4 CHO-Lec2 cells were seeded in 96-well plates (Wuxi NEST Biotechnology Co., Ltd, China) in complete DMEM/F12. After 24 h medium was replaced by 100 µl/well of serum-free DMEM/F12 containing 0.01, 0.05, 0.1, 0.5, 1 ng/ml of Stx1 or Stx2 holotoxins from *E. coli* O157 (Sigma-Aldrich). After 20 h of toxin incubation, 20 µl/well of MTS tetrazolium compound (CellTiter 96 AQueous One Solution Assay, Promega) was added to the wells. After 2.5 h incubation in humidified, 5% CO_2 atmosphere, absorbance at 490 nm was recorded on EnSpire 2300 Multilabel Reader (Perkin Elmer). Background absorbance registered at zero cells/well was subtracted from the data and the absorbance of wells incubated in medium without addition of Stx was taken as 100% of cell viability. All concentrations were run in triplicates and

each experiment was performed at least three times. Results were analyzed using the t-test for independent groups with Holm-Bonferroni correction.

7. Results

7.1 SNPs at *A4GALT* locus and the genetic background of P_1/P_2 polymorphism

It is generally accepted that P_1/P_2 phenotype diversity is related to the *A4GALT* transcript level (production of P1 antigen arise from the elevated transcript level). In turn, several SNPs at *A4GALT* locus were proposed to influence the gene transcription rate (Thuresson, Westman and Olsson, 2011; Lai *et al.*, 2014). However, SNPs reported by different authors were not confronted in an independent experiment and were never studied in the $P^{1NOR}P^1$ and $P^{1NOR}P^2$ individuals. In this study, 109 individuals were tested for five SNPs (rs8138197, rs2143918, rs2143919, rs5751348 correlating with P_1/P_2 polymorphism, and rs397514502 responsible for p.Q211E substitution), *A4GALT* transcript level and quantity of P^k (Gb3) and P1 antigens on RBCs. Agglutination of RBCs revealed that 84 individuals were P1-positive (P_1, including 10 NOR-positive), 24 were P1-negative (P_2) and one person displayed the null phenotype (p) (Table A3). For 91.7% of donors (100 individuals), the results of *A4GALT* genotyping were consistent for all tested SNPs. The rs2143919 presented the weakest association with the phenotype, as reported before (Lai *et al.*, 2014). In two cases, rs8138197 predicted P^1P^1 homozygosity, while other three SNPs suggested P^1P^2. One P^2P^2 (according to all four SNPs) individual was typed P_1 in the agglutination test.

HPTLC analysis of neutral GSLs isolated from RBCs of different genotypes (Fig. 11) showed that anti-P1 (650) binds to both P1 and P^k (Gb3) antigens, while anti-P1 (P3NIL100) binds to the P1 antigen only. Anti-NOR antibody recognized only the NOR antigen represented by NOR1 and NOR2 GSLs.
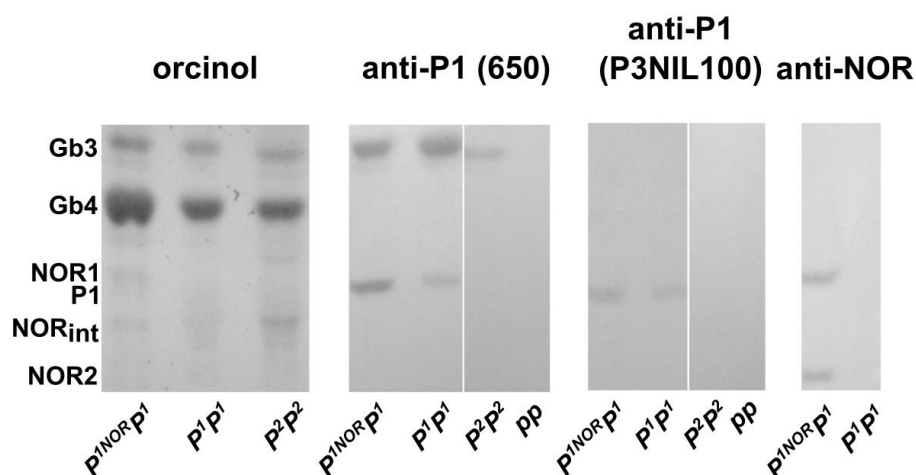
Fig. 11. HPTLC analysis of neutral GSLs isolated from RBCs of different genotypes.

Flow cytometry analysis of RBCs of different *A4GALT* genotypes showed the highest binding of anti-P1 antibodies (650 and P3NIL100) to P^1P^1, and the lowest binding to P^2P^2 (Fig. 12). There was no binding to RBCs of *pp* genotype. Only $P^{1NOR}P^1$ and $P^{1NOR}P^2$ RBCs were bound by anti-NOR antibody.
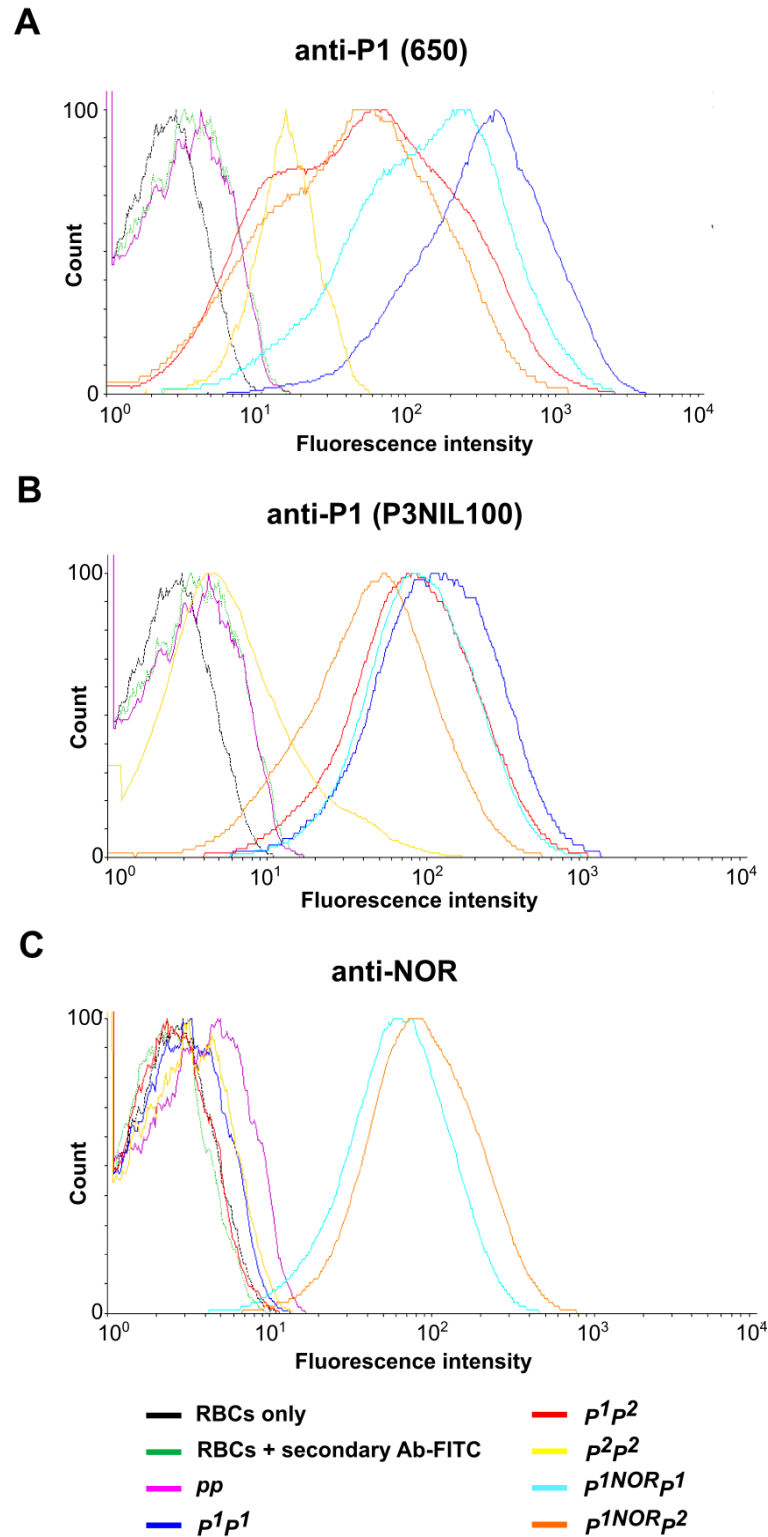
Fig. 12. Flow cytometry analysis of human RBCs of different *A4GALT* genotypes with the use of anti-P1 (650) (A), anti-P1 (P3NIL100) (B) and anti-NOR (C) antibodies.

Quantitative flow cytometry analysis of RBCs with the use of anti-P1 (650), anti-P1 (P3NIL100) and anti-NOR antibodies revealed wide intragroup distributions in all genotypes except the P^2P^2 (Fig. 13). The scatter plots of antibody binding capacities (ABCs) showed substantial intercohort overlaps. Interestingly, RBCs of all the cohorts except P^1P^1 showed higher anti-P1 (P3NIL100) than anti-P1 (650) binding capacity (Fig. 13A, B), which stands in the opposition to their specificity assessed in HPTLC assays. The higher binding capacities of anti-P1 (P3NIL100), which is specific for P1 antigen, in comparison to anti-P1 (650), which recognizes both P^k (Gb3) and P1 antigens, are presumably related with the accessibility of antigens expressed on the cell surface. Despite its abundance, P^k (Gb3) was shown to be hardly detectable for binding proteins when anchored in the cell membrane, in contrast to the longer and more protruding P1 (Mahfoud *et al.*, 2010). Henceforth, anti-P1 (650) antibody is assumed to favor the P1 antigen in flow cytometry and its binding capacity may not accurately reflect the combined amount of P^k (Gb3) and P1 antigens.
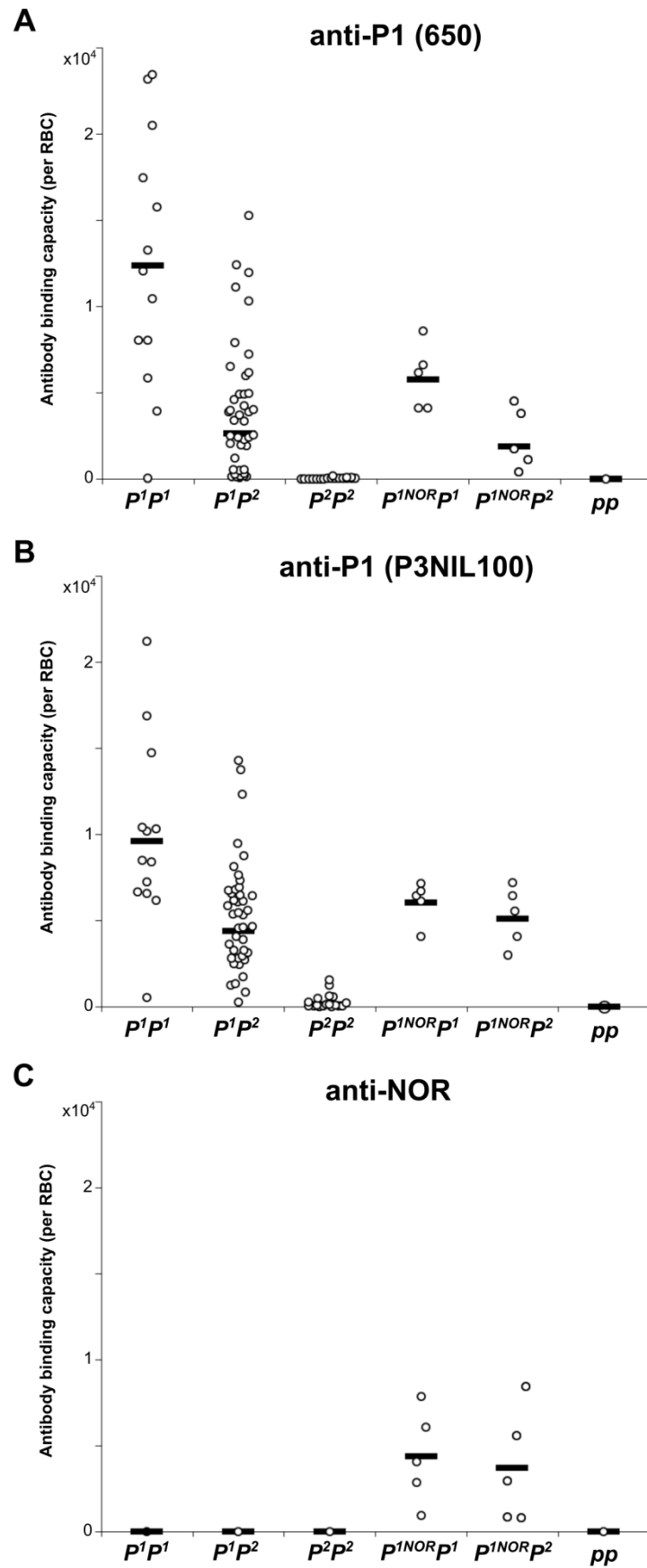
Fig. 13. Quantitative flow cytometry analysis of anti-P1 (650) (A), anti-P1 (P3NIL100) (B) and anti-NOR (C) binding capacity per RBC in individuals of different genotypes (the lines are medians).

In turn, the results of quantitative analysis of *A4GALT* transcript level were less widely distributed (Fig. 14). The average ratio of transcript levels for P^1P^1, P^1P^2 and P^2P^2 genotypes was assessed as 10:3:1.
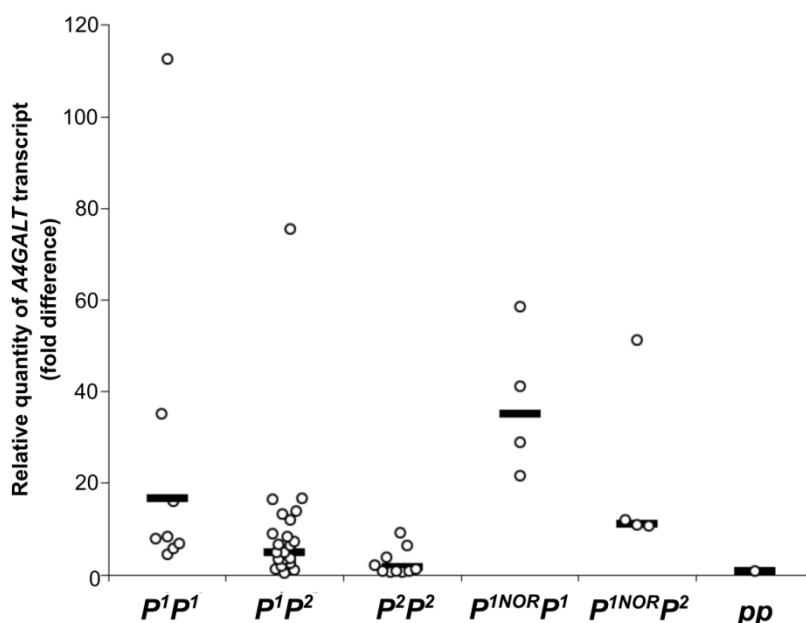
Fig. 14. Quantitative analysis of *A4GALT* transcripts in individuals of different genotypes (the lines are medians).

To evaluate whether the effect of the P_1/P_2-differentiating SNPs is significant across the three genotypes (P^1P^1 versus P^1P^2 and P^1P^2 versus P^2P^2), the ABC means were compared between groups. NOR-positive individuals were left out of this analysis to eliminate the potential confounding effect of the altered enzyme activity. The two anti-P1 antibodies (P3NIL100 and 650) performed consistently insofar that in the case of both reagents the mean differences were statistically significant between P^1P^1 and P^1P^2, and P^1P^2 and P^2P^2, with large effect sizes (Table 12). The rs5751348 showed the strongest association with anti-P1 antibody binding capacity, although ABCs of RBCs with different genotypes overlapped extensively.

Table 12. Statistics of the effect of rs5753148 SNP on the anti-P1 (P3NIL100 and 650) binding level and *A4GALT* transcript level.

Statistic	Compared cohorts					
	anti-P1 (P3NIL100) ABC		anti-P1 (650) ABC		*A4GALT* transcript level	
	P^1P^1 versus P^1P^2	P^1P^2 versus P^2P^2	P^1P^1 versus P^1P^2	P^1P^2 versus P^2P^2	P^1P^1 versus P^1P^2	P^1P^2 versus P^2P^2
Mean difference	5219	4250	9753	2586	11.9	3.2
P	0.0003	4.6×10^{-15}	4.5×10^{-6}	9.6×10^{-18}	0.0175	0.0116
95% CI for the mean difference	2520 to 7918	3441 to 5059	5932 to 13574	2178 to 2993	2.3 to 21.5	0.7 to 5.7
Effect size (g)	1.3	3.0	1.7	-	1.2	1.0
Post-hoc power	85%	99.99997%	85%	99.99997%	54%	70.3%

The anti-P1 (650) antibody binding capacity of $P^{1NOR}P^1$ RBCs was reduced by 54% in comparison with NOR-negative P^1P^1 individuals and the anti-P1 (P3NIL100) binding capacity of $P^{1NOR}P^1$ RBCs was decreased by 37% in comparison to P^1P^1 (Fig. 13). However, comparison of NOR-positive ($P^{1NOR}P^2$) and NOR-negative P^1P^2 individuals (P^1P^2) generated conflicting results with anti-P1 (650) antibody showing 29% lower ABC of $P^{1NOR}P^2$ RBCs, yet anti-P1 (P3NIL100) showing 16% higher ABC of these RBCs (Fig. 13). While the differences between $P^{1NOR}P^1$ and P^1P^1 groups were statistically significant, the differences between $P^{1NOR}P^2$ and P^1P^2 were not (Table 13).

Table 13. Statistics of the effect of c.631C>G (NOR) mutation on the anti-P1 (P3NIL100 and 650) level.

Statistic	Compared groups				
	anti-P1 (P3NIL100) ABC		anti-P1 (650) ABC		anti-NOR ABC
	$P^{1NOR}P^2$ versus P^1P^2	$P^{1NOR}P^1$ versus P^1P^1	$P^{1NOR}P^2$ versus P^1P^2	$P^{1NOR}P^1$ versus P^1P^1	$P^{1NOR}P^1$ versus $P^{1NOR}P^2$
Mean difference	704	-3581	-747	-6615	647
P	0.4632	0.0094	0.5811	0.0029	0.74
95% CI for the mean difference	-1375 to 2783	-6144 to -1017	-3452 to 1959	-10602 to -2627	-3749 to 5043
Effect size (g)	-	-	0.3	-	0.2
Post-hoc power	6.4%	42%	8.4%	42%	5.9%

7.2 Testing of human α-1,4-galactosyltransferase activity toward glycoprotein acceptors *in vitro*

For years, the human α-1,4-galactosyltransferase was considered as an enzyme strictly specific for glycosphingolipids. However, our early flow cytometry analysis of Shiga toxin 1 B subunit (Stx1B) binding to human RBCs suggested that Galα1→4Gal structures may be present also on glycoproteins. Typically, the flow cytometry analysis of RBCs glycosphingolipid epitopes is preceded by papain treatment to allow their efficient interaction with antibodies. Therefore, binding of anti-P1 antibodies (650 and P3NIL100) to human RBCs is elevated after papain treatment, because accessibility of GSLs for the antibodies was better after removing extracellular proteins (Fig.15A, B). Strikingly, this is not the case with Stx1B binding, which is decreased after digestion or RBCs with papain (Fig. 15C). These results suggested loss of some epitopes (presumably Galα1→4Gal structures) recognized by Stx1B due to protease treatment.
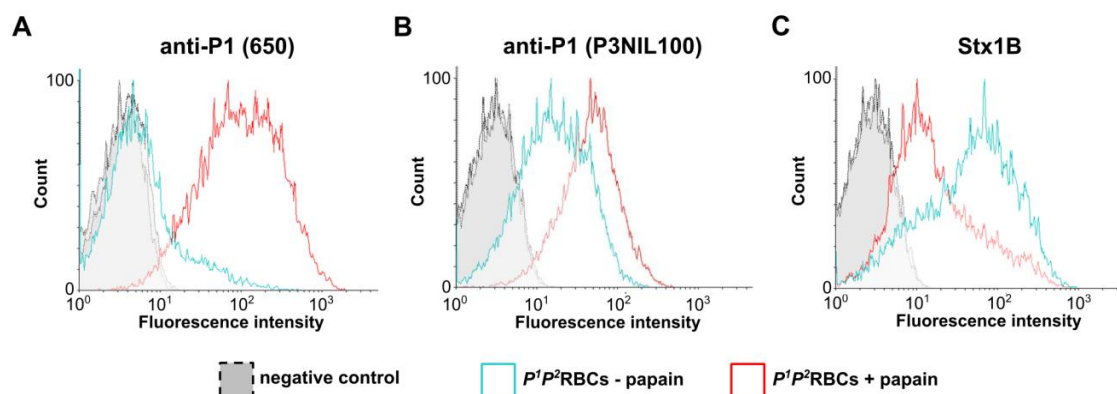
Fig. 15. Flow cytometry analysis of P^1P^2 RBCs, untreated or treated with papain, with the use of anti-P1 (650) (A), anti-P1 (P3NIL100) (B) and Stx1B (C).

To answer the question whether α-1,4-galactosyltransferase may be responsible for formation of Galα1→4Gal structures on glycoproteins, the recombinant enzyme was used in reaction with synthetic N-glycan acceptor. Expression and purification of recombinant soluble catalytic domain of human α-1,4-galactosyltransferase was already optimized for our earlier studies of its activity toward glycosphingolipid acceptors (Kaczmarek, Duk, *et al.*, 2016). The catalytic domain of consensus α-1,4-galactosyltransferase (A4GalT) and p.Q211E mutein (A4GalT p.Q211E) were produced in High Five insect cells upon transduction with recombinant baculoviruses and secreted into the medium. The recombinant proteins containing an N-terminal 6x-His Tag were purified in a single-step affinity chromatography on Ni-NTA agarose resin. Fractions eluted with 100 mM and 200 mM imidazole showed high purity (Fig. 16) and

after concentration to 7.75 mg/ml (A4GalT) and 2.75 mg/ml (A4GalT p.Q211E) were used for *in vitro* enzymatic assays.
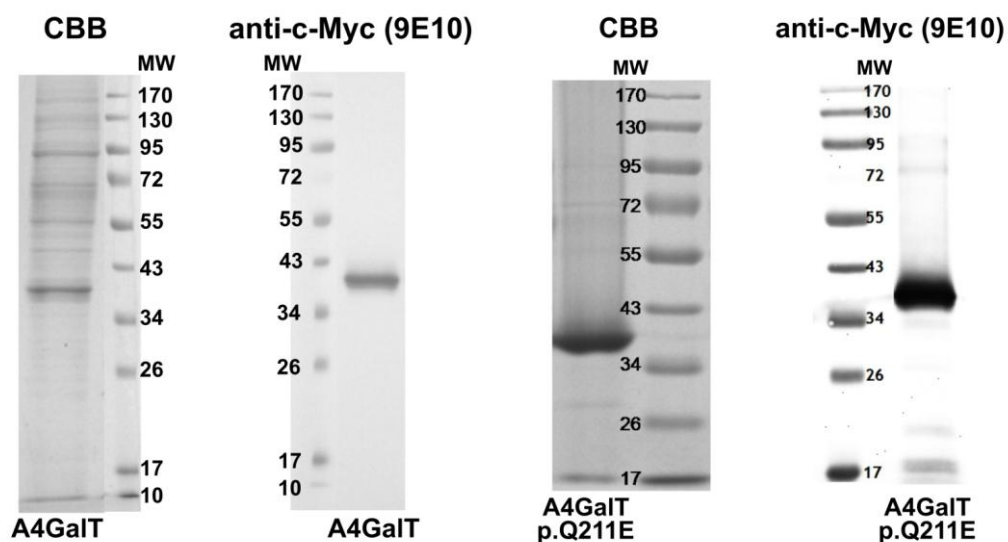
Fig. 16. CBB and western blotting analysis of purified A4GalT (A) and A4GalT p.Q211E (B).

The activity of A4GalT and A4GalT p.Q211E was evaluated using the $Gal_2GlcNAc_2Man_3GlcNAc_2$ nonasaccharide azide with two terminal lactosamine units as an acceptor substrate (Fig. 17). This study was done in cooperation with Prof. Carlo Unverzagt (Bioorganische Chemie, Universität Bayreuth, Bayreuth, Germany). Synthesis of the acceptor was performed at the laboratory of Prof. Carlo Unverzagt (Ullmann *et al.*, 2012), as well as A4GalT and A4GalT p.Q211E reactions and analysis of the product.
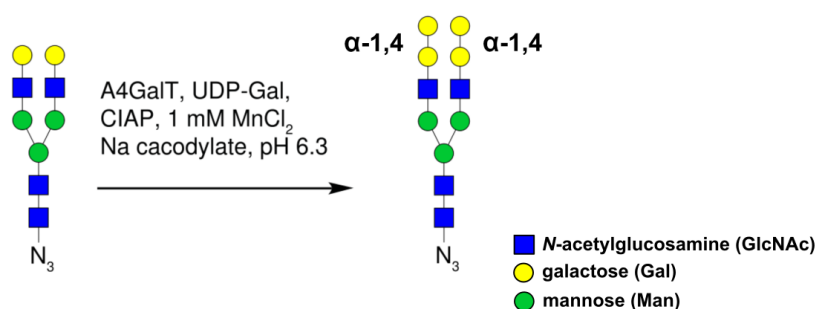
Fig. 17. Reaction scheme of α-galactosylation of synthetic N-glycan carried out by A4GalT.

After 24 h, both reaction mixtures were analyzed by LC-MS, which revealed 77% of unreacted acceptor substrate for A4GalT. In contrast, in the case of the A4GalT p.Q211E the percentage of unreacted substrate was 38%. The decasaccharide intermediate contribution was determined as 21% (A4GalT) and 48% (A4GalT p.Q211E), and the undecasaccharide product as 2% (A4GalT) and 14% (A4GalT p.Q211E) (Fig. 18, 19).
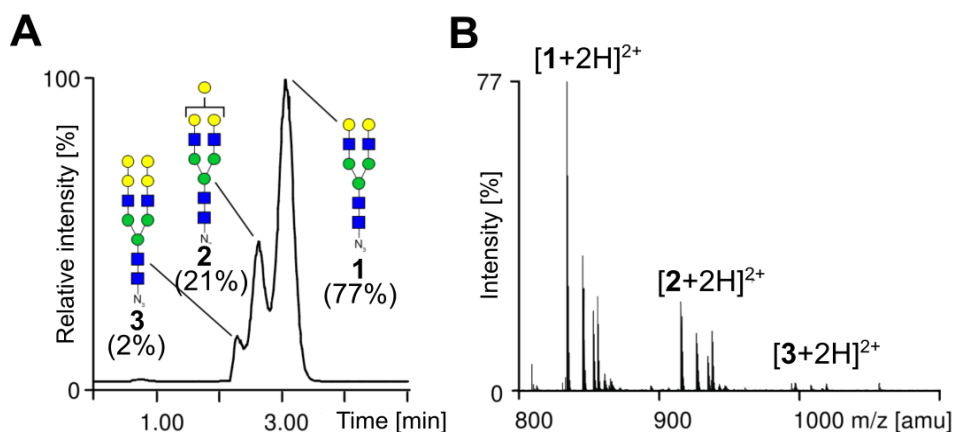
Fig. 18. A) Total ion count (TIC) from HR-LC-MS of nonasaccharide azide incubated for 24 h with A4GalT; B) summed up mass spectrum from TIC. 1 – nonasaccharide substrate; 2 – decasaccharide intermediate; 3 – undecasaccharide product.
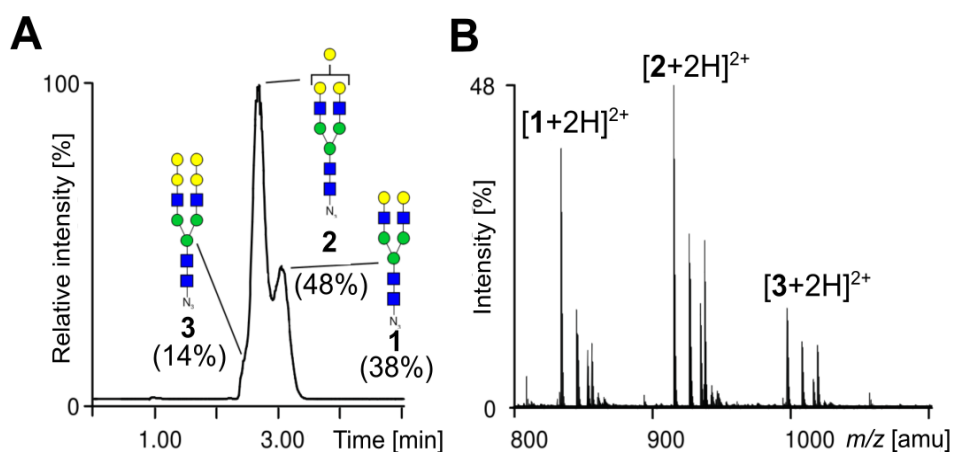
Fig. 19. A) Total ion count (TIC) from HR-LC-MS of nonasaccharide azide incubated for 24 h with A4GalT p.Q211E; B) summed up mass spectrum from TIC. 1 – nonasaccharide substrate; 2 – decasaccharide intermediate; 3 – undecasaccharide product.

Both A4GalT and A4GalT p.Q211E were able to use nonasaccharide azide as an acceptor substrate, but A4GalT p.Q211E used it more efficiently, and this enzyme was selected for subsequent experiments. To examine the linkage of the galactose units transferred by A4GalT p.Q211E to nonasaccharide acceptor, a preparative reaction was carried out. After 7 days of incubation, undecasaccharide product was purified by gel filtration and UHPLC (Fig. 20). The product was obtained in 84% yield and was subjected to LC-MS and NMR analyses.
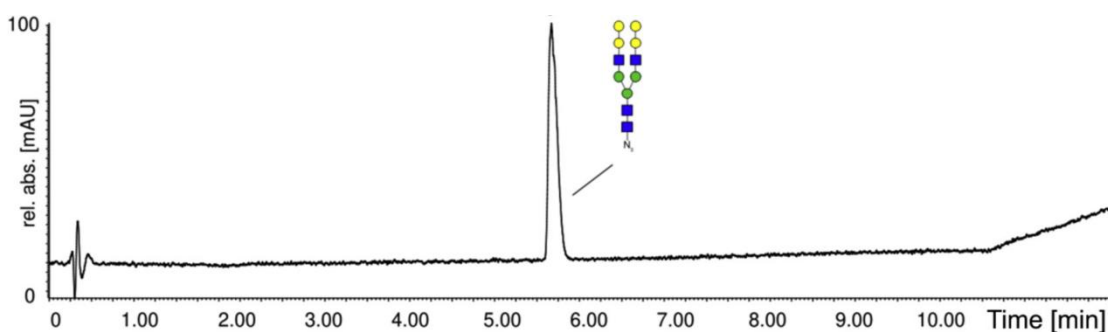
Fig. 20. UHPLC trace of purified undecasaccharide azide product of A4GalT p.Q211E reaction.

500 MHz NMR analysis revealed that spectrum the anomeric signals (H-1) of the two galactoses transferred by A4GalT p.Q211E, H-1^7 and H-1$^{7'}$, overlap with H-1^4 but show a small coupling constant indicating their α-configuration (Fig. 21). This is further confirmed by the large $^1J_{CH}$ coupling constants for H-1^7, C-1^7 and H-1$^{7'}$, C-1$^{7'}$ of 170.6 Hz. Both newly transferred α-galactoses 7 and 7' are attached to O-4 of the β-galactoses 6 and 6' leading to the typical downfield shift of the ring carbon after glycosylation (C-4^6 and C-4$^{6'}$ at 78.2 ppm).
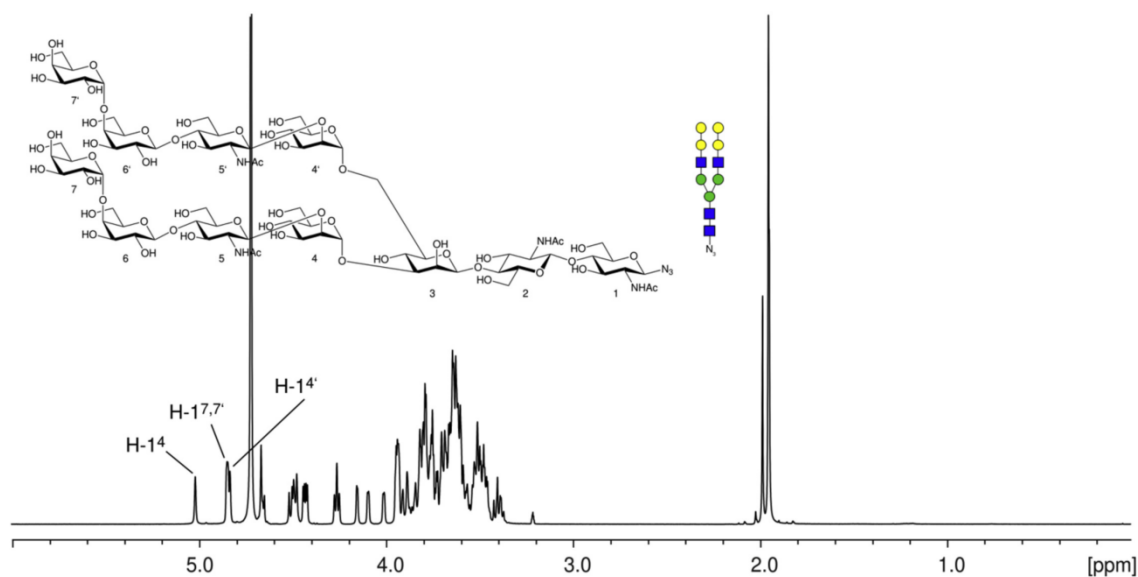
Fig. 21. ^{1}H-NMR spectrum of the undecasaccharide azide product of A4GalT p.Q211E reaction. ^{1}H-NMR (500 MHz, D$_2$O, [D$_4$]-methanol as internal standard): δ = 5.12 (d, 1H, $J_{1,2}$ < 1 Hz, H-1^{4}α), 4.96 to 4.92 (m, 3H, H-1^{7}α, H-1$^{7'}$α, H-1$^{4'}$α), 4.77 to 4.74 (m, 2H, H-1^{3}β, H-1^{1}β), 4.63 to 4.56 (m, 3H, H-1^{2}β, H-1^{5}β, H-1$^{5'}$β), 4.55 to 4.50 (m, 2H, H-1^{6}β, H-1$^{6'}$β), 4.40 to 4.32 (m, 2H, H-5^7, H-5$^{7'}$), 4.25 (dd, 1H, $J_{1,2}$, $J_{2,3}$ < 1 Hz, H-2^3), 4.19 (dd, 1H, $J_{1,2}$, $J_{2,3}$ < 1 Hz, H-2^4), 4.11 (dd, 1H, $J_{1,2}$, $J_{2,3}$ < 1 Hz, H-2$^{4'}$), 4.06 to 3.53 (m, 59H, H-4^6, H-4$^{6'}$, H-4^7, H-4$^{7'}$, H-6a^3, H-6a^2, H-6a^6, H-6a$^{6'}$, H-3^6, H-3$^{6'}$, H-6a^4, H-6a$^{4'}$, H-3^7, H-3$^{7'}$, H-3^4, H-3$^{4'}$, H-6a^1, H-6b^2, H-2^7, H-2$^{7'}$, H-6b^6, H-6b$^{6'}$, H-2^2, H-5^6, H-5$^{6'}$, H-3^2, H-6b^3, H-3^3, H-4^2, H-4^1, H-4^3, H-5^1, H-6b^1, H-2^1, H-2^5, H-5^4, H-5$^{4'}$, H-2$^{5'}$, H-6a,b^7, H-6a,b$^{7'}$, H-6a,b^5, H-6a,b$^{5'}$, H-3^5, H-3$^{5'}$, H-4^5, H-4$^{5'}$, H-6b^4, H-6b$^{4'}$, H-5^2, H-3^1, H-5^3, H-5^5, H-5$^{5'}$, H-2^6, H-2$^{6'}$), 3.53 to 3.45 (m, 2H, H-4^4, H-4$^{4'}$), 2.10 to 2.02 (m, 12H, NAc).

The activity of A4GalT p.Q211E was then examined in an assay involving recombinant glycoprotein, human saposin D (SapD) (Fig. 22). This small lysosomal sphingolipid activator protein contains single N-glycosylation site (Tatti *et al.*, 1999). SapD glycoform with a $Gal_2GlcNAc_2Man_3GlcNAc_2$ nonasaccharide glycan chain (SapD9) was synthesized as described (Graf *et al.*, 2017), at the laboratory of Prof. Carlo Unverzagt (Bioorganische Chemie, Universität Bayreuth, Bayreuth, Germany). The reaction catalyzed by A4GalT p.Q211E and MS analysis of the product was also performed there.
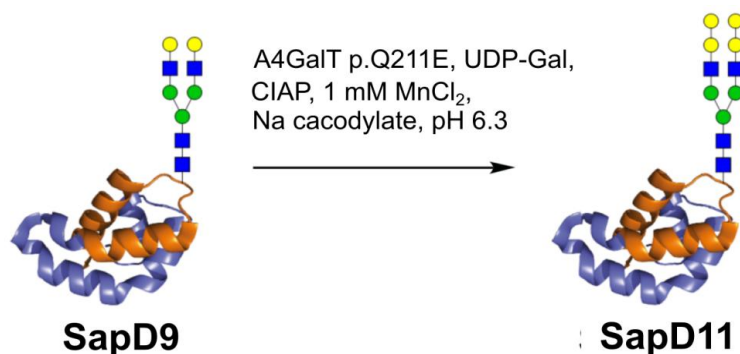
Fig. 22. Reaction scheme of SapD9 α-galactosylation carried out by A4GalT p.Q211E.

Treatment of SapD9 with A4GalT p.Q211E in the presence of UDP-Gal resulted in production of the new SapD glycoform bearing $Gal_2Gal_2GlcNAc_2Man_3GlcNAc_2$ undecasaccharide N-glycan (SapD11). SapD11 was obtained with the yield of 78% (Fig. 23).
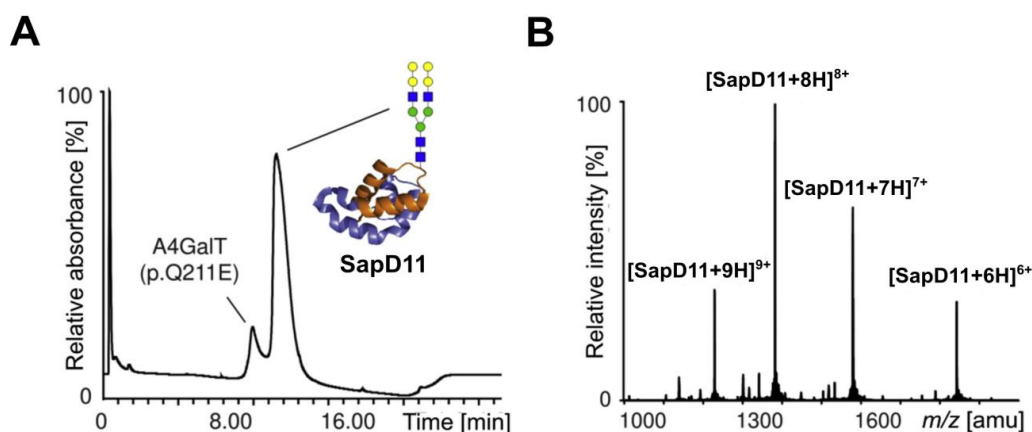
Fig. 23. A) UHPLC trace of the synthesis of SapD11. B) HR-MS spectrum of purified SapD11.

HR-MS analysis of SapD11 purified by UHPLC showed the addition of two hexose units and virtual identity of the deconvoluted and the simulated spectrum (Fig. 24). Western blotting analysis of SapD9 and SapD11 with the use of anti-P1 antibodies (P3NIL100 and 650) confirmed the presence of terminal Galα1→4Galβ1→4GlcNAc structures on the N-glycan of SapD11 (Fig. 25).
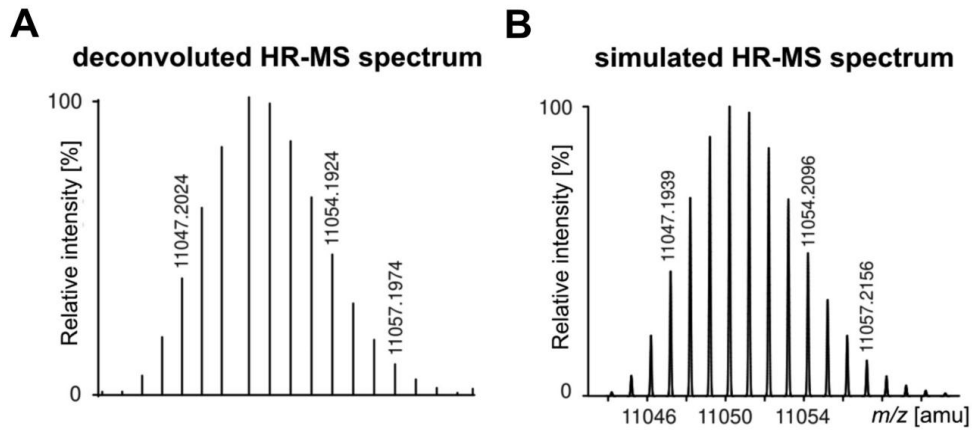
Fig.24. Deconvoluted (A) and simulated (B) HR-MS spectrum of the $[M+9H]^{9+}$ peak of SapD11.
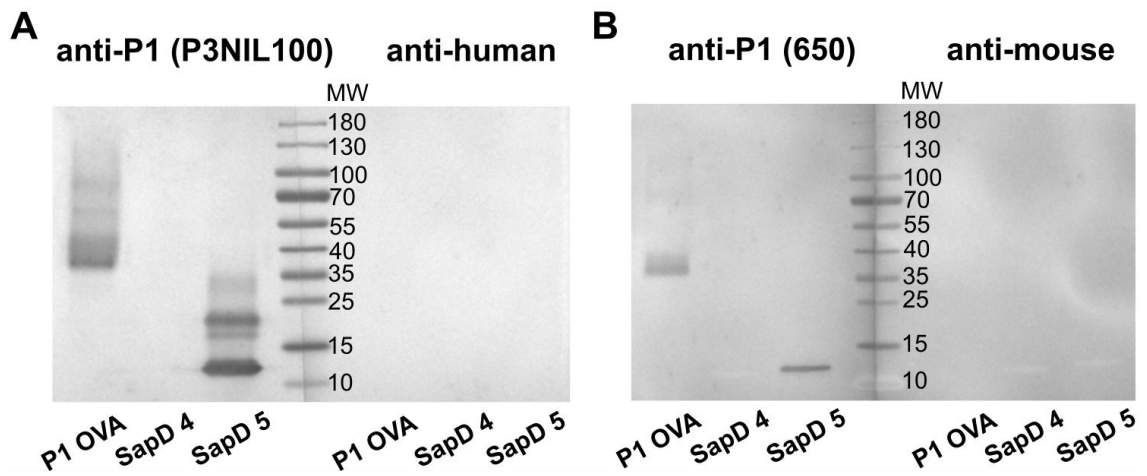
Fig.25. Western blotting analysis of SapD9 and SapD11 using anti-P1 antibodies: P3NIL100 (A), 650 (B). The bands of higher molecular weight than 11 kDa are presumably artifacts caused by boiling the sample. P1 OVA – pigeon egg ovalbumin containing P1 glycotope used as the positive control.

7.3   Testing of human α-1,4-galactosyltransferase activity toward glycoprotein acceptors *in vivo*

To examine whether human α-1,4-galactosyltransferase can synthesize Galα1→4Gal structures on glycoproteins *in vivo*, the full-length consensus enzyme and p.Q211E mutein were expressed in CHO-Lec2 cells. CHO-Lec2 cells were selected because they do not express an endogenous α-1,4-galactosyltransferase. Moreover, they are deficient in CMP-sialic acid transporter, which makes CHO-Lec2 incapable of sialylation, and this is an important issue, because adding sialyl acid residues may compete with α-galactosylation during biosynthesis of N-glycans (Stanley, 1983; Takahashi *et al.*, 2001; Patnaik and Stanley, 2006). CHO-Lec2 cells were transduced with lentiviral vectors encoding consensus α-1,4-galactosyltransferase (CHO-Lec2 A4GALT) and p.Q211E mutein (CHO-Lec2 A4GALT Q211E) and grown in a selection medium containing puromycin. The selection was monitored by flow cytometry analysis of the cells with the use of antibodies detecting products of the enzymes (Fig. 26).
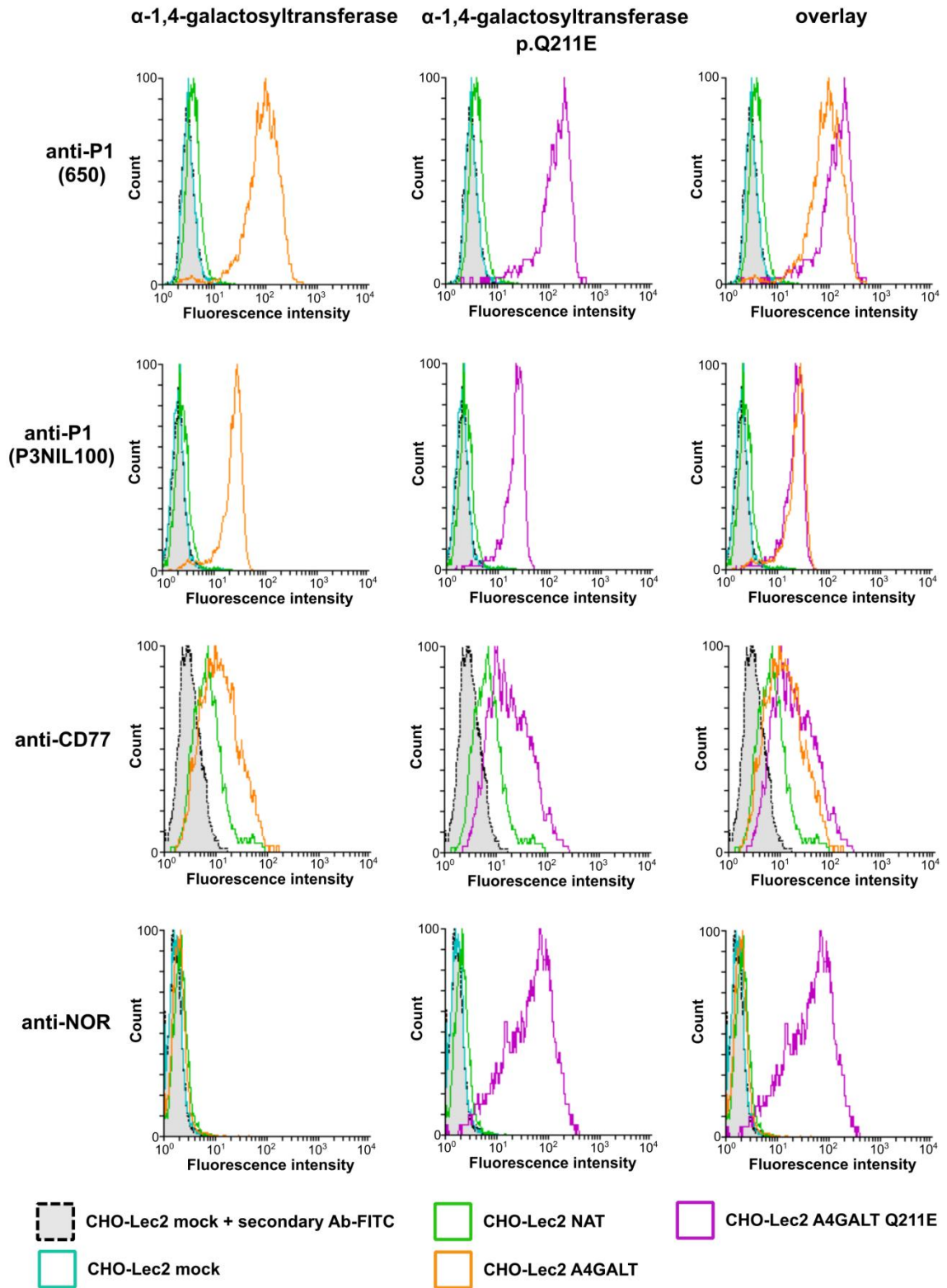
Fig. 26. Flow cytometry analysis of CHO-Lec2 cells expressing consensus α-1,4-galactosyltransferase or p.Q211E mutein. Mock – cells transduced with empty lentivirus; NAT – untransduced cells; A4GALT – cells transduced with vector encoding consensus α-1,4-galactosyltransferase; A4GALT Q211E – cells transduced with vector encoding p.Q211E mutein.

Neutral glycosphingolipids isolated from CHO-Lec2 A4GALT and CHO-Lec2 A4GALT Q211E were analyzed by HPTLC orcinol staining and antibody assays. The P^k antigen (Gb3) was identified in both CHO-Lec2 A4GALT and CHO-Lec2 A4GALT Q211E, whereas P1 antigen was not detected (Fig. 27). Presumably, P1 is not produced in CHO-Lec2 due to the lack of its precursor, nLc4. CHO-Lec2 A4GALT Q211E showed elevated production of P^k antigen (Gb3) and presence of NOR1, NOR$_{int}$ and NOR2.
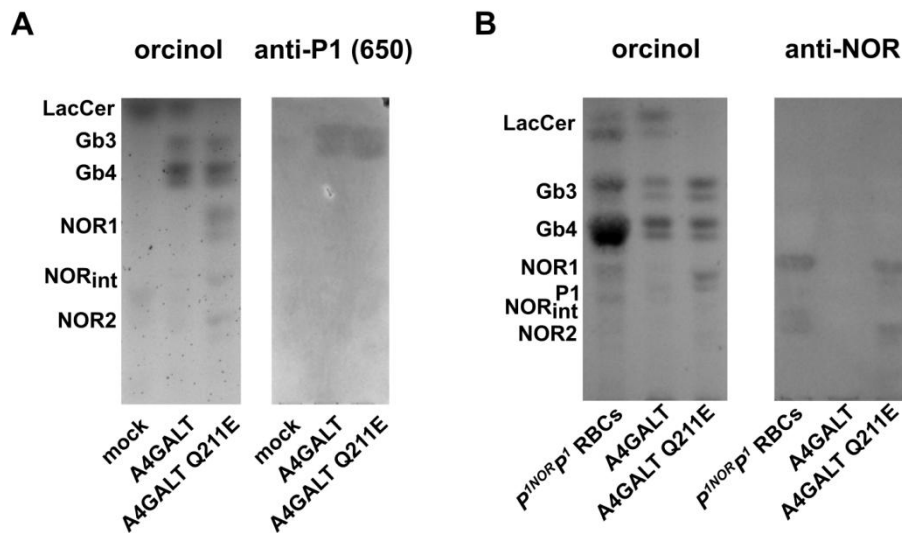
Fig. 27. HPTLC analysis of neutral GSLs purified from CHO-Lec2 cells stained with orcinol and anti-P1 (650) (A) or orcinol and anti-NOR (B). A4GALT − CHO-Lec2 A4GALT; A4GALT Q211E, - CHO-Lec2 A4GALT Q211E; mock − CHO-Lec2 transduced with empty lentivirus; $P^{1NOR}P^1$ RBCs − neutral GSLs from human $P^{1NOR}P^1$ RBCs used as the positive control.

Western blotting analysis revealed binding of anti-P1 antibodies (P3NIL100 and 650) to CHO-Lec2 A4GALT and CHO-Lec2 A4GALT Q211E cell lysates, indicating the presence of P1 glycotopes (Galα1→4Galβ1→4GlcNAc) on glycoproteins (Fig. 28A). Binding to CHO-Lec2 A4GALT Q211E lysate was stronger in comparison to CHO-Lec2 A4GALT. After treatment of CHO-Lec2 A4GALT Q211E lysate with PNGase F, kindly provided by Prof. Mariusz Olczak (Department of Biochemistry, Faculty of Biotechnology, University of Wroclaw, Wroclaw, Poland), no anti-P1 (P3NIL100) binding was detected, suggesting that P1 glycotopes were present only on N-linked, but not O-linked glycan chains (Fig. 28B).
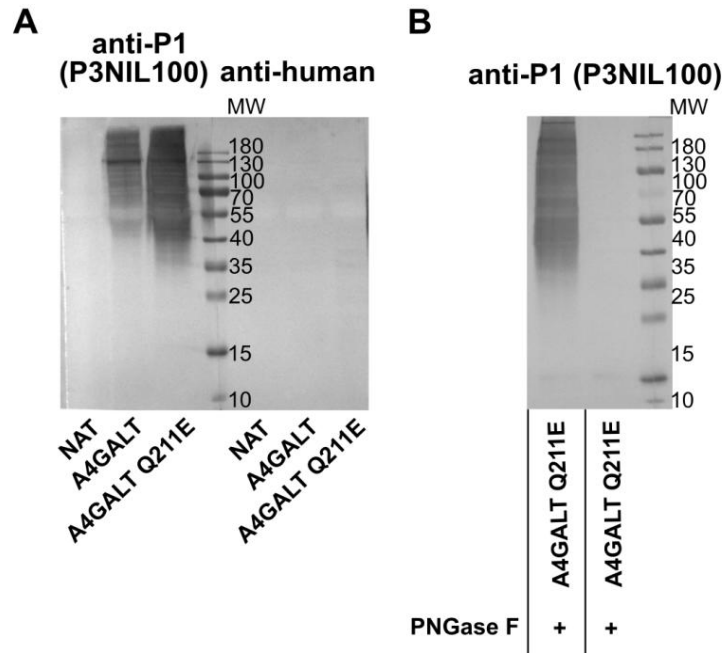
Fig. 28. A) Western blotting analysis of CHO-Lec2 cell lysates stained with anti-P1 (P3NIL100) antibody. B) Analysis of PNGase F-treated and untreated lysates of CHO-Lec2 A4GALT Q211E cells.

Additionally, to exclude cross-reactivity with Galα1→3Gal structures, GSL I B4 lectin blotting analysis of the lysates was performed. The lectin, which is specific toward Galα1→3Gal (Iskratsch *et al.*, 2009), did not bind to CHO-Lec2 A4GALT and CHO-Lec2 A4GALT Q211E cell lysates (Fig. 29A). Likewise, anti-NOR antibody did not detect any glycoproteins in CHO-Lec2 cell lysates, indicating a lack of Galα1→4GalNAc structures (Fig. 29B).
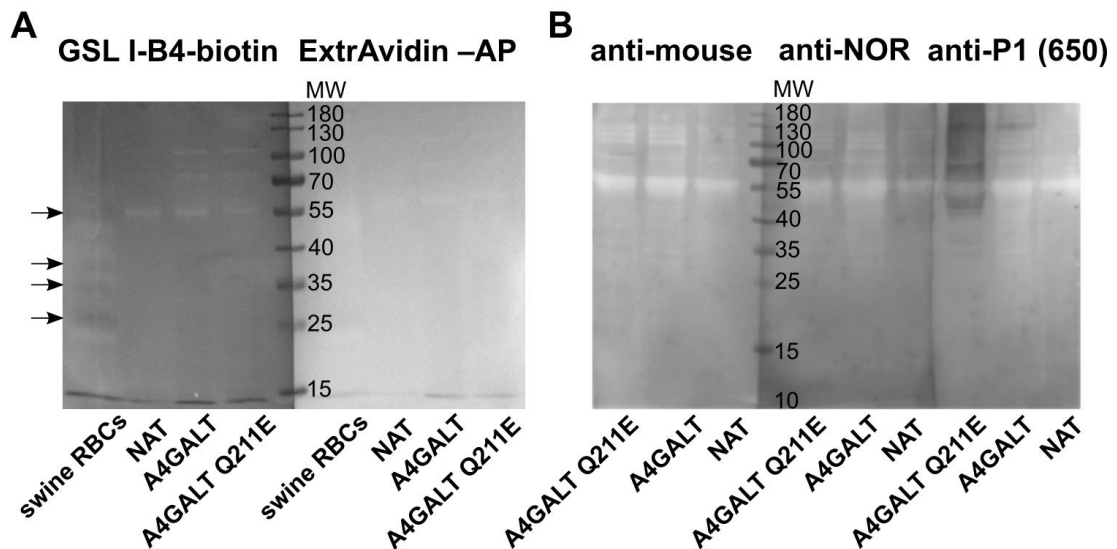
Fig. 29. A) Analysis of CHO-Lec2 cell lysates stained with biotinylated GSL I-B4 lectin. B) Analysis of CHO-Lec2 cell lysates stained with anti-P1 (650) and anti-NOR antibodies. Swine RBCs – lysates of swine RBC membranes used as the positive control.

To elucidate whether α-1,4-galactosyltransferase produces P1 glycotopes on GSLs only, or on GSLs and glycoproteins, CHO-Lec2 cells were cultured in the presence of glucosylceramide synthase inhibitor Genz-123346 (Liu, Hill and Li, 2013). MALDI-TOF analysis of GSLs isolated from CHO-Lec2 A4GALT Q211E treated for 2 weeks with Genz-123346 detected only hexosylceramide (presumably galactosylceramide) (Fig. 30). Notably, binding of anti-P1 antibody (P3NIL100) to the lysates of Genz-123346-treated cells in western blotting was increased in comparison to the binding to the untreated cell lysates (Fig. 31).
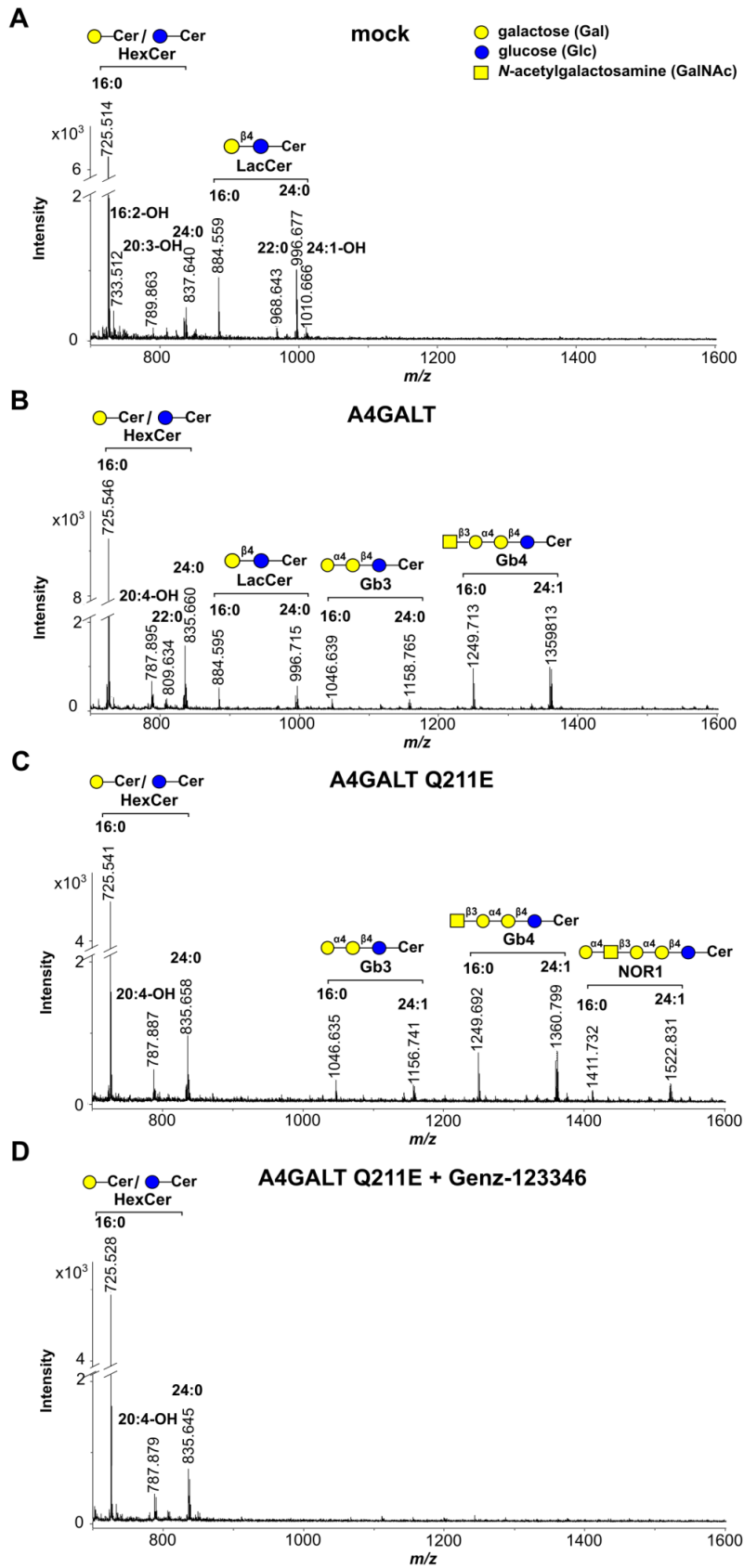
Fig. 30. MALDI-TOF analysis of neutral glycosphingolipids isolated from the mock-transfected CHO-Lec2 cells (A), CHO-Lec2 A4GALT (B), CHO-Lec2 A4GALT Q211E (C) and CHO-Lec2 A4GALT Q211E cells cultured in the presence of Genz-123346.

anti-P1 (P3NIL100)
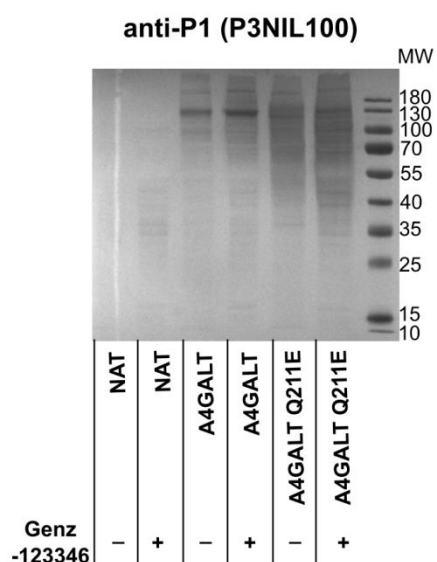
Fig.31. Western blotting analysis of Genz-123346-treated and untreated CHO-Lec2 cell lysates.

The CHO-Lec2 cells, untreated and cultured in medium containing Genz-123346, were also analyzed by quantitative flow cytometry with the use of anti-P1 (P3NIL100 and 650) and anti-CD77. It was found that both anti-P1 antibodies recognize Galα1→4Gal structures not only on GSLs but also on glycoproteins; on the other hand, anti-CD77 binds solely P^k antigen (Gb3). The binding levels of anti-P1 (P3NIL100) to CHO-Lec2 A4GALT and CHO-Lec2 A4GALT Q211E cultured in the presence of Genz-123346 and untreated cells were similar (Fig. 32). In comparison, binding of anti-P1 (650) to Genz-123346-treated cells was increased. Thus, it may be argued that the CHO-Lec2 A4GALT and CHO-Lec2 A4GALT Q211E cells treated with Genz-123346 synthesize at least similar amount of P1 glycotopes on glycoproteins as untreated cells. On the other hand, anti-CD77 antibody did not bind to CHO-Lec2 A4GALT and CHO-Lec2 A4GALT Q211E treated with Genz-123346, suggesting that these cells did not produce P^k antigen (Gb3) at all.

A

B
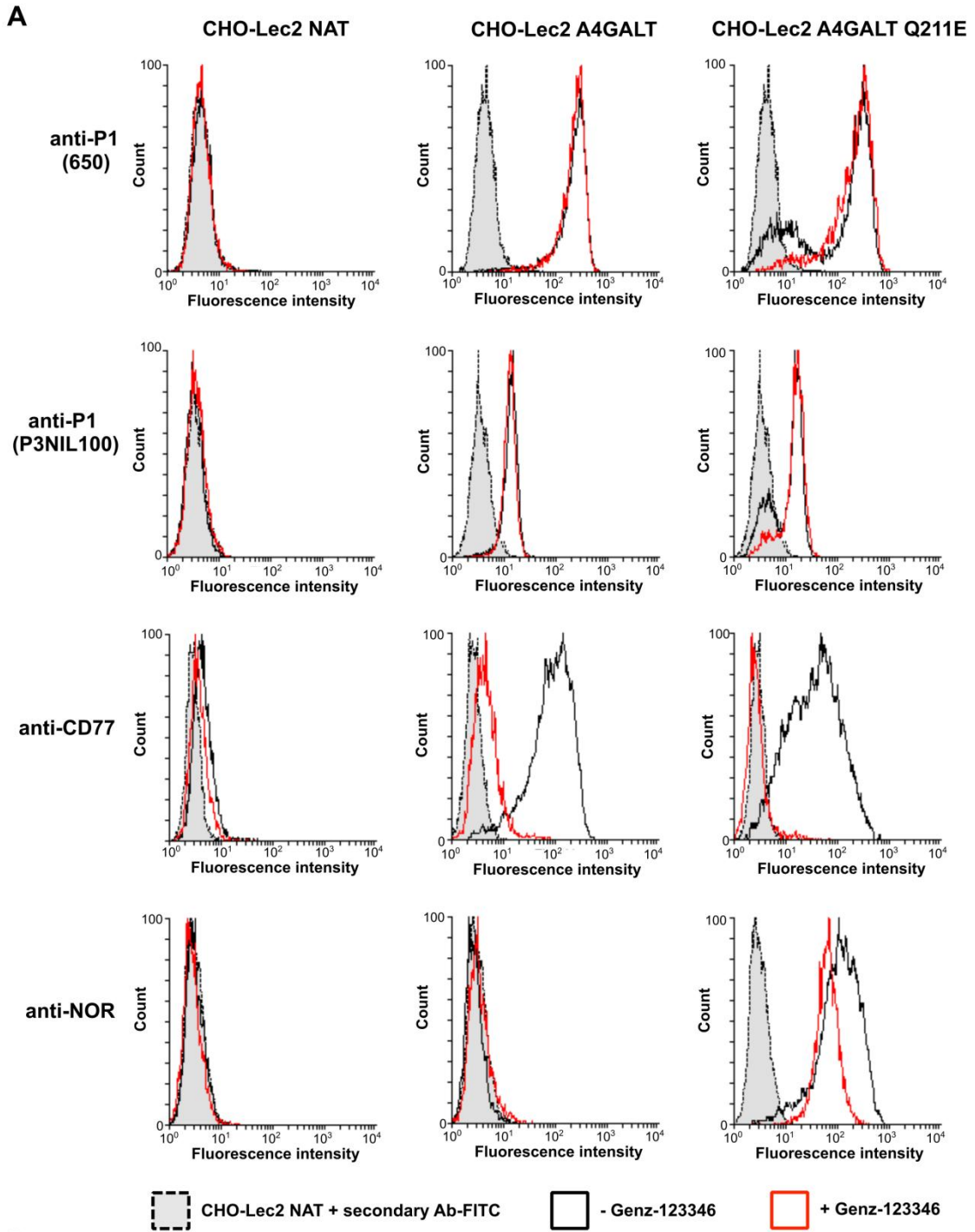
Fig. 32. A) Flow cytometry analysis of CHO-Lec2 cells with the use of anti-P1 (P3NIL100), anti-P1 (650), anti-CD77 and anti-NOR antibodies. B) Quantitative flow cytometry analysis of anti-P1 (P3NIL100), anti-P1 (650) and anti-CD77 binding capacity per CHO-Lec2 cell (displayed as median from at least three replicates; error bars represent interquartile ranges).

The HPTLC, western blotting and flow cytometry analyses suggested that there is higher level of P1 glycotopes in CHO-Lec2 A4GALT Q211E in comparison to the CHO-Lec2 A4GALT. To determine whether this phenomenon is a result of elevated amount of p.Q211E mutein or its higher activity, the levels of *A4GALT* transcript and α-1,4-galactosyltransferase protein were evaluated. Quantitative analysis of *A4GALT* mRNA revealed CHO-Lec2 A4GALT Q211E express approximately 10 times (in untreated cells) to 20 times (in Genz-123346-treated cells) less transcript than CHO-Lec2 A4GALT (Table 14). Accordingly, western blotting analysis of CHO-Lec2 cell lysates showed stronger anti-A4GALT (clone 5C7, produced by Prof. Arkadiusz Miążek, Laboratory of Tumor Immunology, Hirszfeld Institute of Immunology and Experimental Therapy, Wroclaw, Poland) staining in the case of CHO-Lec2 A4GALT (Fig. 33).

Table 14. Quantitative analysis of *A4GALT* transcripts in CHO-Lec2 cells. RQ, relative quantity.

	ΔCt	ΔΔCt	RQ
NAT	15.7123	0	1
A4GALT	-0.1155	-15.8278	**58163.7**
A4GALT Q211E	3.2034	-12.5089	**5828.3**
NAT + Genz-123346	16.4905	0	1
A4GALT + Genz-123346	-0.6479	-17.1384	**144269.5**
A4GALT Q211E + Genz-123346	3.5537	-12.9369	**7841.2**
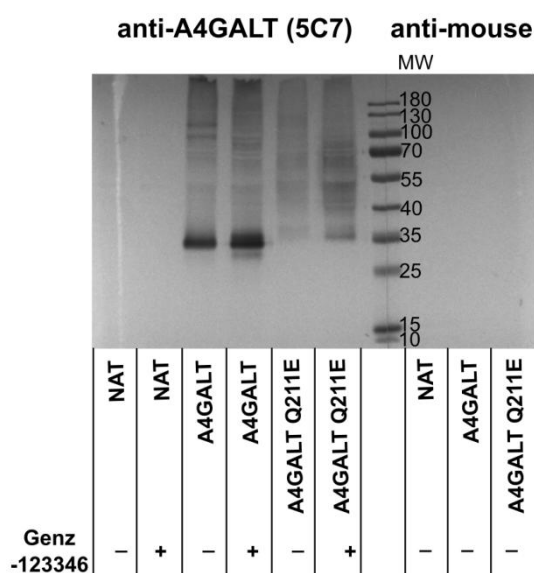
Fig. 33. Western blotting analysis of CHO-Lec2 cell (cultured in presence or absence of Genz-123346) lysates stained with anti-A4GALT (5C7) antibody.

To precisely determine the structure of N-glycans from CHO-Lec2 A4GALT and CHO-Lec2 A4GALT Q211E, the N-glycans were examined by porous graphitized carbon LC-MS by Prof. Manfred Wuhrer team (Center for Proteomics and Metabolomics, Leiden University Medical Center, Leiden, The Netherlands). The LC-MS analysis revealed that untransduced CHO-Lec2 cells produced mainly oligomannosidic N-glycans (Fig. 34). The major complex-type glycans were determined as a biantennary, fully galactosylated N-glycans with and without core fucose. The N-glycan profiles of CHO-Lec2 A4GALT and CHO-Lec2 A4GALT Q211E were predominantly similar to that of untransduced cells; however, they displayed an additional decasaccharide N-glycan at *m/z* 901.33 [M-2H]$^{2-}$ (Fig. 35A) with a relative abundance of 0.77% (standard deviation 0.10%) and 1.07% (standard deviation 0.03%), respectively (Fig. 35B). In particular, tandem mass spectrometry analysis of this decasaccharide N-glycan revealed a ^{1,3}A4 fragment ion at *m/z* 586.21 indicating the addition of a hexose to one of the antennae (Fig. 36). The D ion at *m/z* 688.13 and D-18 ion at *m/z* 670.13 indicated this modification to present on the three-linked antenna rather than on the six-linked antenna. When the tandem mass spectra were screened for the diagnostic ion of *m/z* 586.21, no other N-glycans with an additional antennary hexose were found. However, these additional hexose-modified N-glycans may be present, albeit below the detection limit of the LC-MS method. Together, results of the LC-MS analysis indicate the addition of a hexose to the three-linked antenna of a biantennary complex type N-glycan in CHO-Lec2 cells upon expression of α-1,4-galactosyltransferase, which points to the presence of an antennary Galα1→4Galβ1→4GlcNAc motif.
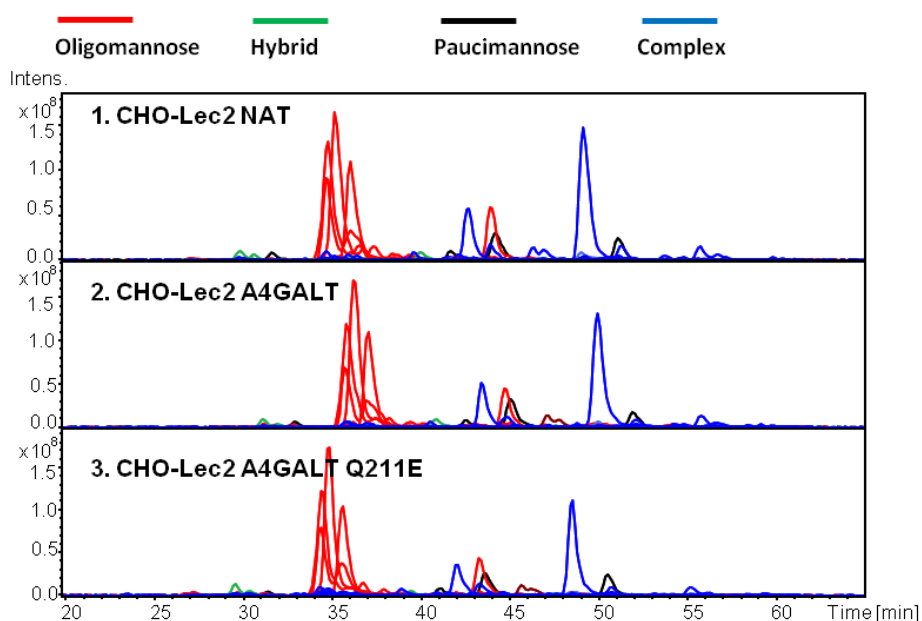
Fig. 34. Combined extracted ion chromatograph of high abundant N-glycans released from CHO-Lec2 NAT, CHO-Lec2 A4GALT and CHO-Lec2 A4GALT Q211E cells.
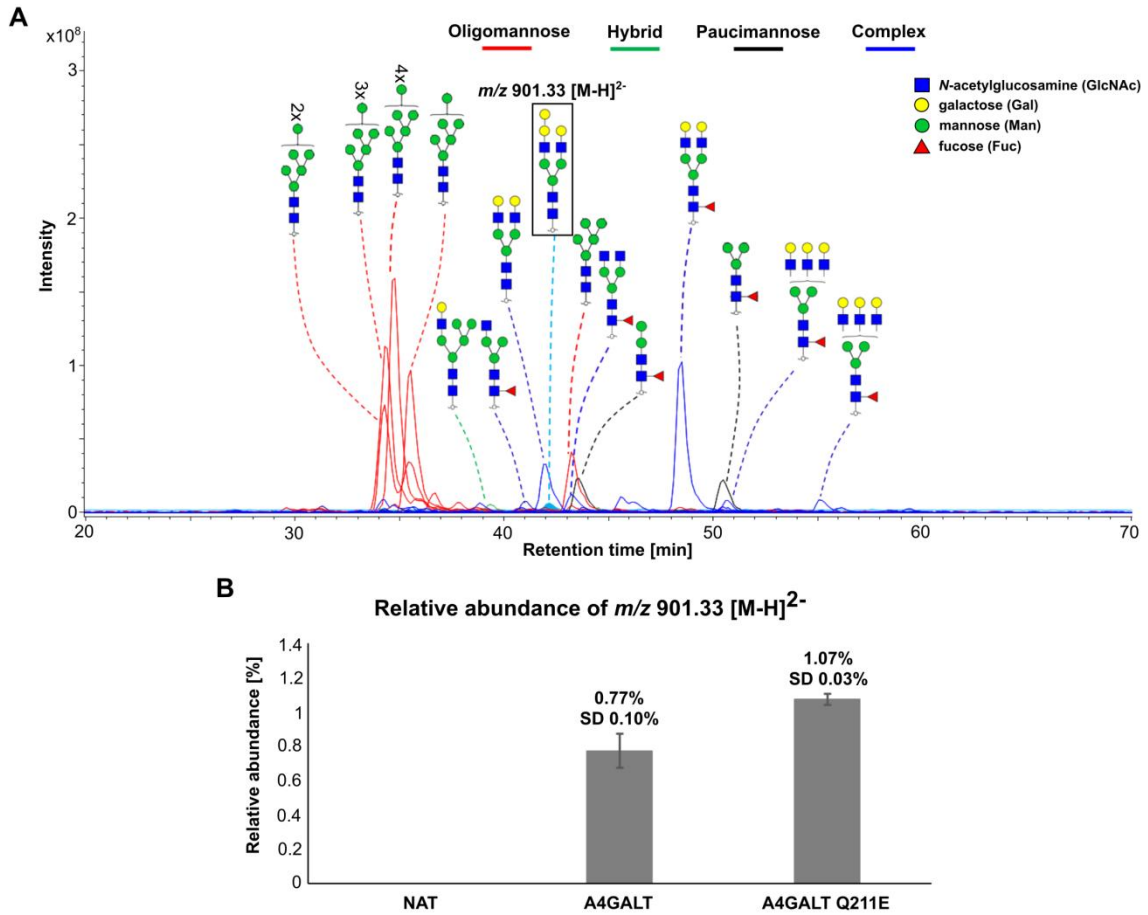
Fig. 35. Analysis of the top 15 most abundant N-glycans released from 0.5 x 10^6 CHO-Lec2 A4GALT Q211E cells on PGC nano-LC-ESI-MS/MS. A) Combined extracted ion chromatograms (EICs) of top 15 N-glycans. B) Relative abundance of the N-glycan at *m/z* 901.33 [M-H]$^{2-}$ displayed as mean relative abundance with standard deviation (SD); N=3.
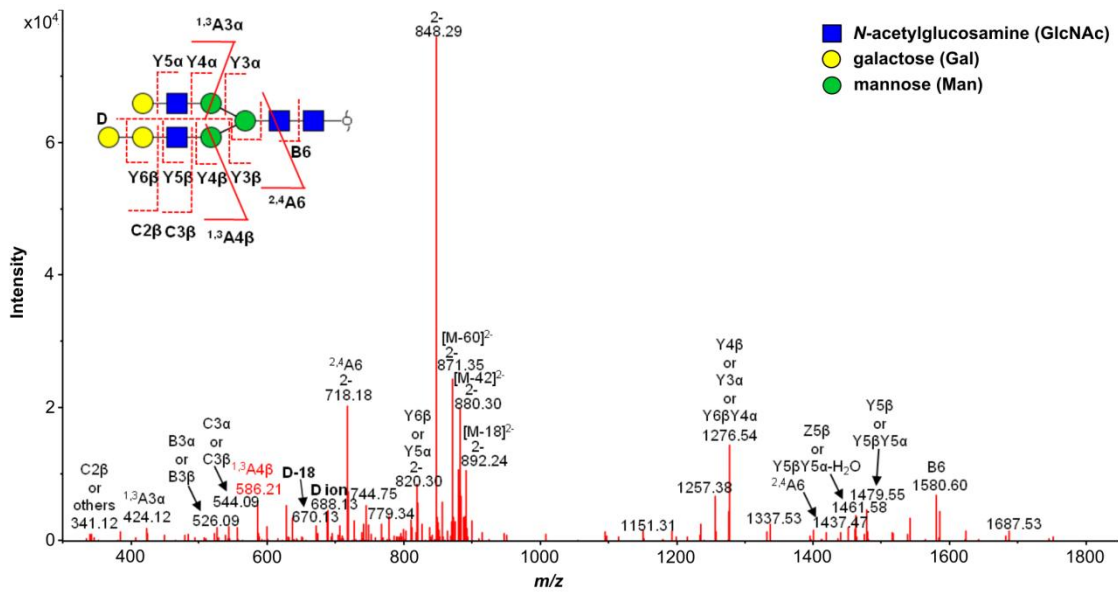
Fig. 36. Tandem MS spectrum of an N-glycan at *m/z* 901.34 $^{2-}$ of the CHO-Lec2 A4GALT Q211E analyzed by PGC nano-LC-ESI-MS/MS in negative ion mode.

7.4 Analysis of Shiga toxin interactions with P1 and Gb4 glycosphingolipids

While Shiga toxin interaction with the P^k antigen (Gb3) is a well-studied phenomenon, binding to the P1 antigen has never been under investigation. The role of Gb4, a related GSL formed by addition of GalNAcβ1→3 to the P^k antigen (Gb3), remains also controversial. Some reports indicate Stx can bind Gb4 and possibly use it as a receptor; however, other studies suggest rather artefactual character of this interaction (Yiu and Lingwood, 1992; Detzner, Pohlentz and Müthing, 2020; Lingwood, 2020).

HPTLC analysis of human $P^{1NOR}P^1$ RBCs showed Stx1B binding to P^k antigen (Gb3), Gb4 and P1 (Fig. 37). Stx2B bound P^k and Gb4. Stx1B and Stx2B were a generous gift from Dr Enoch Y. Park (Laboratory of Biotechnology, Shizuoka University, Shizuoka, Japan). The NOR antigens were not recognized by Stxs.
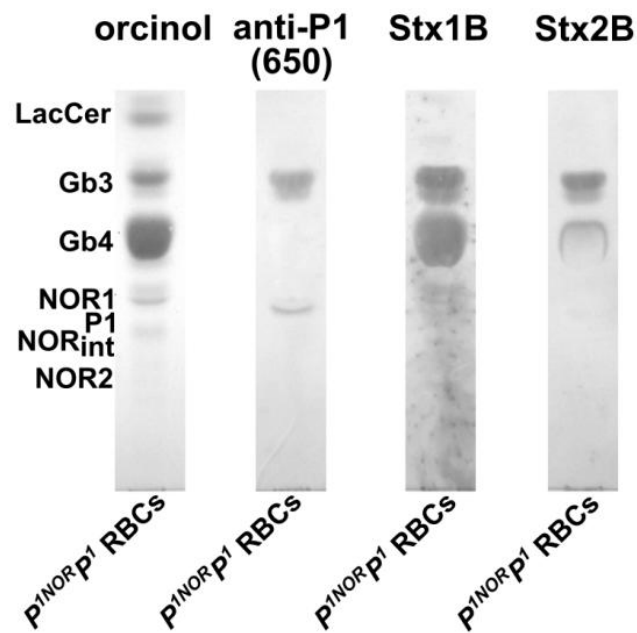
Fig. 37. HPTLC analysis of GSLs isolated from $P^{1NOR}P^1$ RBCs, stained with orcinol, anti-P1 (650), Stx1B and Stx2B.

Furthermore, the Stx1B and Stx2B were tested in ELISA assay on plates coated with synthetic glycoconjugates Lac-PAA, P1-PAA, Gb4-PAA, NOR-PAA (structures in Table 11), kindly provided by Prof. Nicolai Bovin (Laboratory of Carbohydrate Chemistry, Institute of Bioorganic Chemistry, Russian Academy of Sciences, Russian Federation). Only P1-PAA was found to be recognized by Stx1B (Fig. 38).
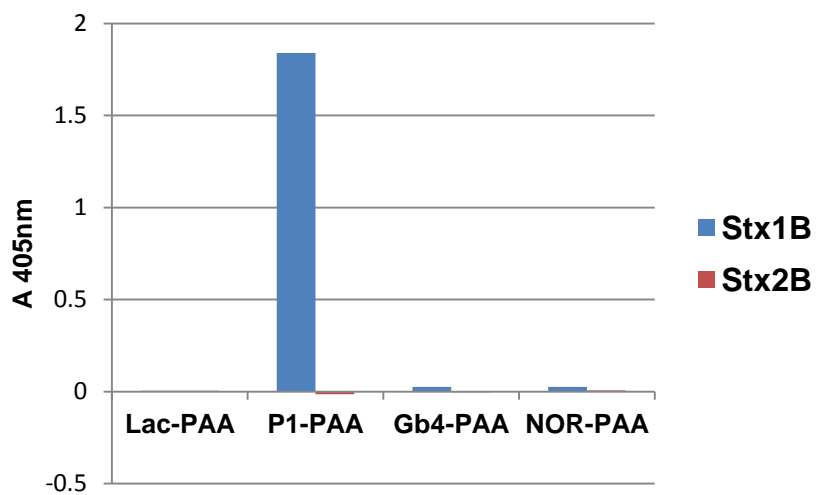
Fig. 38. Analysis of Stx1B and Stx2B interactions with synthetic glycoconjugates: Lac-PAA, P1-PAA, Gb4-PAA, NOR-PAA.

Interactions of the Stx1B and Stx2B with P1-PAA and Gb4-PAA immobilized on SA chip were examined by SPR (Fig. 39). Stx1B used in SPR analysis was kindly provided by Bartosz Bednarz M.Sc. (Laboratory of Molecular Biology of Microorganisms, Hirszfeld Institute of Immunology and Experimental Therapy), and Stx2B by Dr Enoch Y. Park (Laboratory of Biotechnology, Shizuoka University, Shizuoka, Japan). In the initial binding analysis, both P1-PAA and Gb4-PAA appeared to bind Stx1B; however, in the affinity analysis only interaction with P1-PAA has been confirmed. The analysis with Stx1B in different concentrations (0.025, 0.074, 0.222, 0.667, 2 μM) revealed the calculated dissociation constant $K_D = 5.06 \times 10^{-7}$ M. The affinity analysis was conducted only once because of the limited amount of Stx1B that was available at the time.
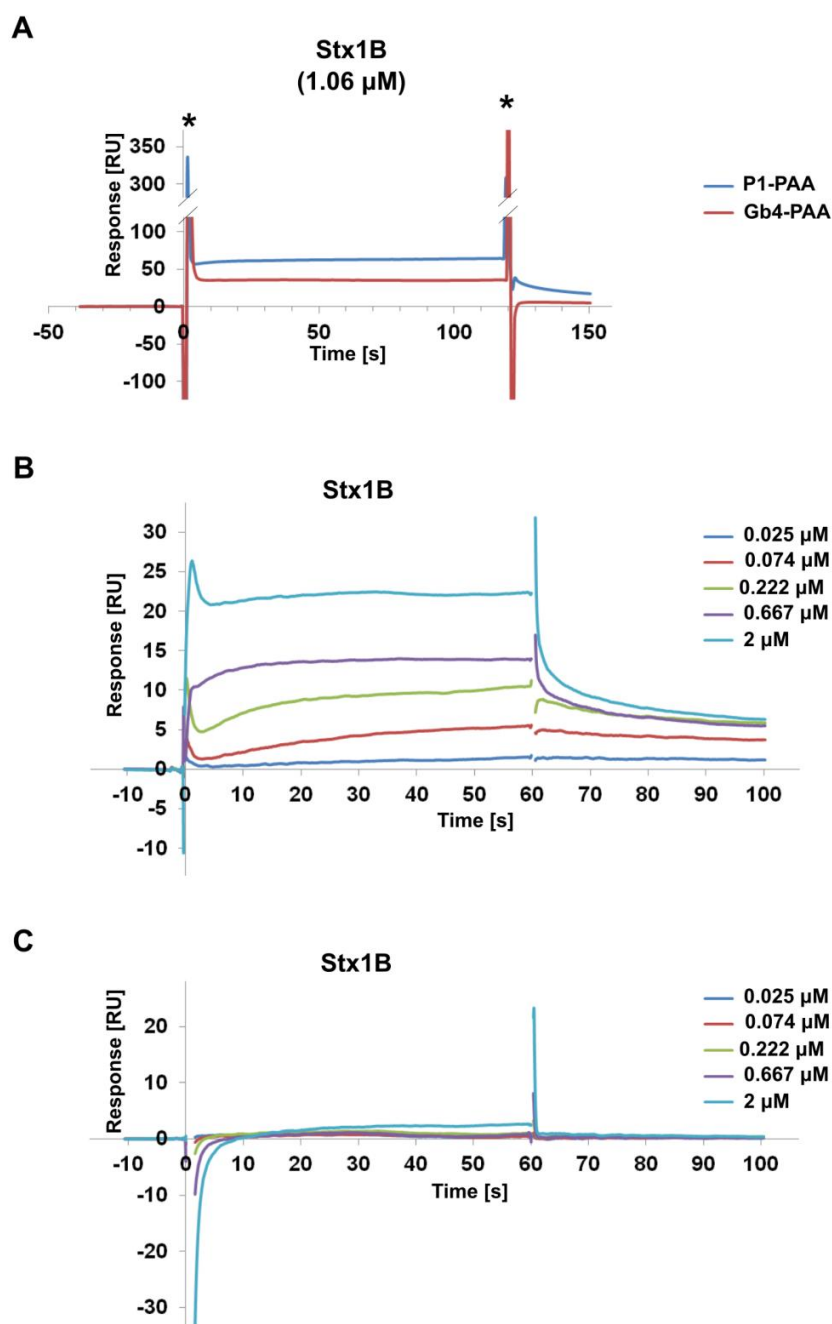
Fig. 39. A) SPR binding analysis of Stx1B to P1-PAA and Gb4-PAA. B) SPR affinity analysis of Stx1B interaction with P1-PAA. C) SPR affinity analysis of Stx1B interaction with Gb4-PAA. ∗ - spikes resulted from the difference between composition of the running buffer and sample buffer.

The binding analysis with the use of Stx2B showed interaction with Gb4-PAA, but not with P1-PAA (Fig. 40). However, the affinity analysis with Stx2B in different concentrations (0.12, 0.37, 1.11, 3.33, 10 µM) indicated that interaction with Gb4-PAA was merely a nonspecific artifact.
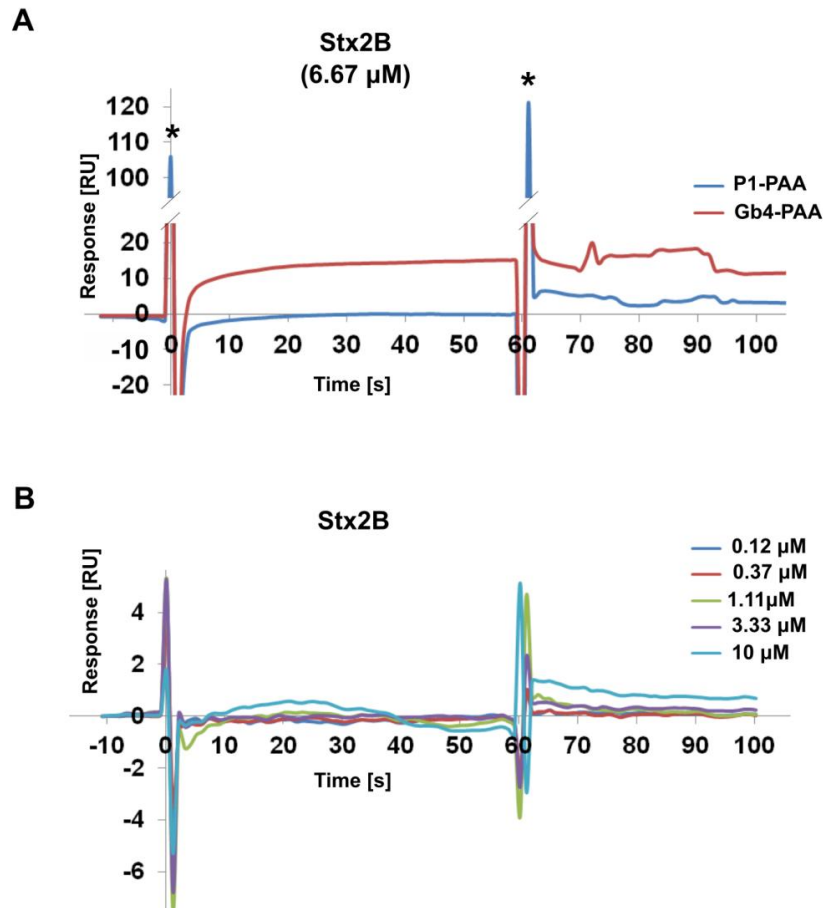
Fig. 40. A) SPR binding analysis of Stx2B to P1-PAA and Gb4-PAA. B) SPR affinity analysis of Stx2B interaction with Gb4-PAA. ∗ - spikes resulted from the difference between composition of the running buffer and sample buffer.

The ELISA and SPR analysis suggested that Stx1B can bind P1-PAA; thus, a question emerged whether P1 or Gb4 may be recognized by Stx *in vivo* and act as functional receptors. Developing of a suitable cellular model was challenging, since α-1,4-galactosyltransferase is responsible for the biosynthesis of both P1 and P^k antigen (Gb3), which is the main Stx receptor. P^k (Gb3) is also a precursor of Gb4, and all three GSLs originate from lactosylceramide, so it is not possible to obtain synthesis of P1 or Gb4 without the P^k (Gb3) formation. Therefore, the Namalwa cells overexpressing human α-1,4-galactosyltransferase (Namalwa A4GALT) obtained by Dr Radoslaw Kaczmarek were further modified to generate cells producing α-1,4-galactosyltransferase and human β-1,3-*N*-acetylglucosaminyltransferase (Namalwa A4GALT/B3GNT5) or α-1,4-galactosyltransferase and human β-1,3-*N*-acetylgalactosaminyltransferase (Namalwa A4GALT/B3GALNT1) to increase the level of P1 or Gb4, respectively (Fig. 41). The Namalwa cell line was chosen due to the very low expression level of endogenous α-1,4-galactosyltransferase resulting in production of only trace amounts of P^k (Gb3) and the lack of P1 antigen (despite relatively high expression of its precursor,

paragloboside). The objective was to compare the level of Stx B subunit binding capacity by quantitative flow cytometry and elucidate the influence of P1 and Gb4.
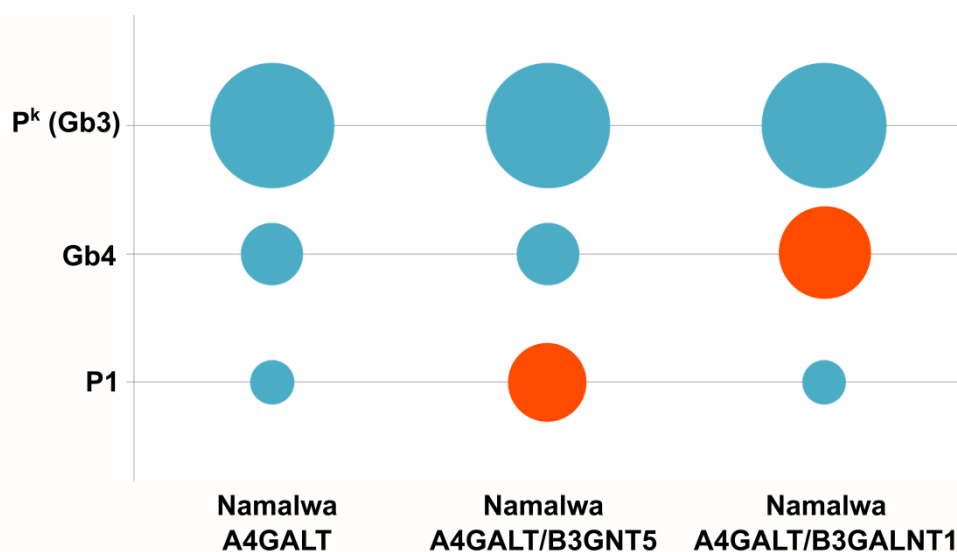
Fig. 41. Outline of the conception of Namalwa A4GALT cells transfection. The circles represent estimated amounts of P^k (Gb3), Gb4 and P1 antigen produced by the cells. The orange circles indicate the expected increased amount of P1 antigen or Gb4 in Namalwa A4GALT/B3GNT5 or Namalwa A4GALT/B3GALNT1, respectively, in comparison to Namalwa A4GALT cells.

Flow cytometry analysis of Namalwa cells revealed that there was a slight increase of P1 antigen (in Namalwa A4GALT/B3GNT5) or Gb4 (in Namalwa A4GALT/B3GALNT1) production in comparison to the Namalwa A4GALT cells (Fig. 42). Gb4 level was evaluated with the use of anti-Gb4 antibody kindly provided by Dr Tetsuya Okuda (Bioproduction Research Institute, National Institute of Advanced Industrial Science and Technology, Tsukuba, Japan). However, the elevated level of P1 antigen in Namalwa A4GALT/B3GNT5 cells was accompanied by an unexpected increase of P^k (Gb3) synthesis. A similar increase of P^k (Gb3) production was also observed in the Namalwa A4GALT/B3GALNT1 cells. Stx1B and Stx2B binding to Namalwa A4GALT/B3GNT5 and Namalwa A4GALT/B3GALNT1 was increased in comparison to the Namalwa A4GALT cells and correlated to P^k (Gb3) level. Since the unexpected increase of P^k (Gb3) production in Namalwa A4GALT/B3GNT5 and Namalwa A4GALT/B3GALNT1 masked the effect of elevated synthesis of P1 and Gb4, evaluation of their influence on Stx binding was not possible using this experimental model.
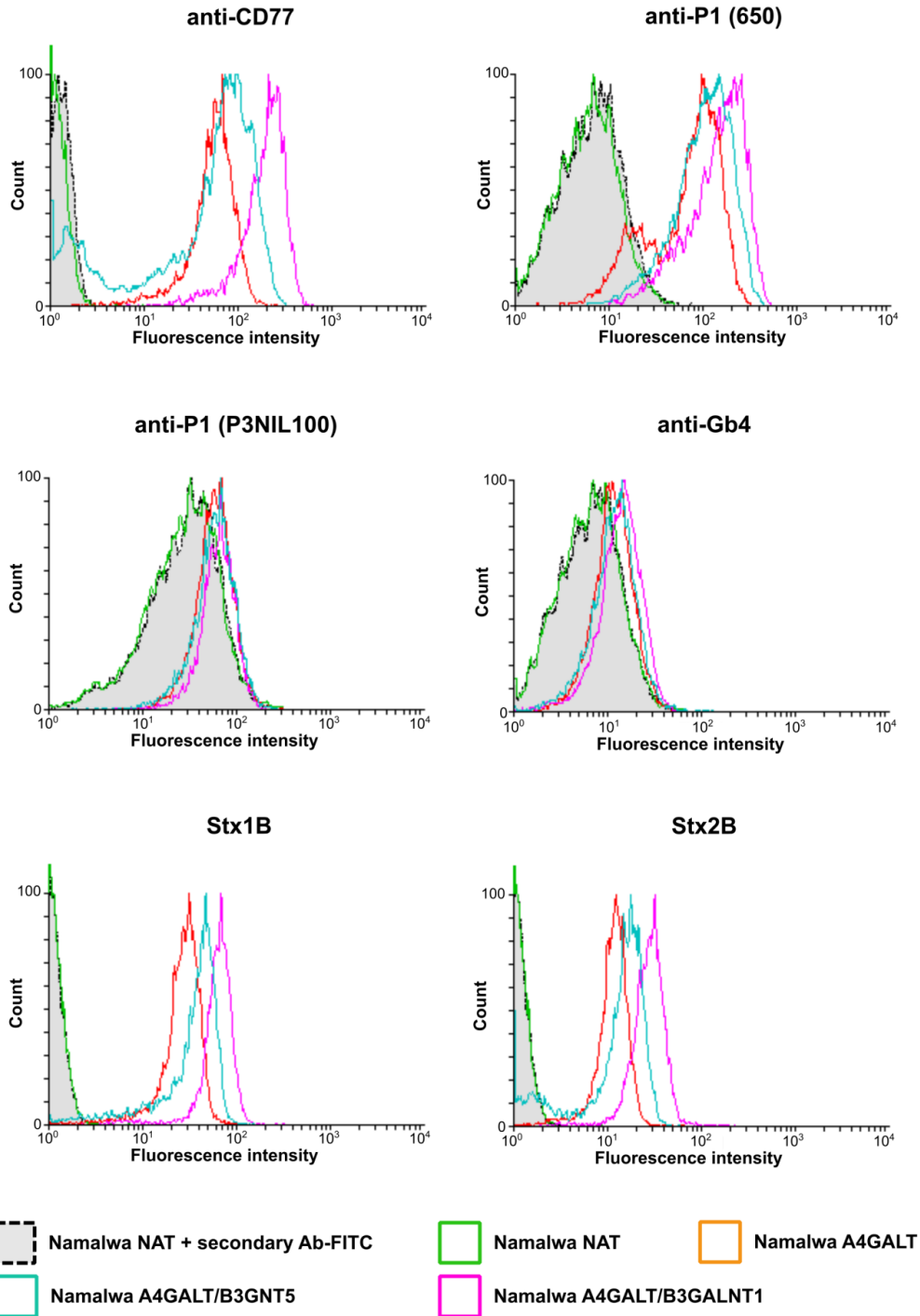
Fig. 42. Flow cytometry analysis of Namalwa cells with the use of anti-CD77, anti-P1 (650), anti-P1 (P3NIL100), anti-Gb4, Stx1B and Stx2B.

Another attempt to address the role of P1 and Gb4 in binding of Stx *in vivo* was incorporation of synthetic glycoconjugates obtained from Prof. Nicolai Bovin (Laboratory of Carbohydrate Chemistry, Institute of Bioorganic Chemistry, Russian Academy of Sciences, Russian Federation) into living cells and performing Stx binding and cytotoxicity assays. This concept was tested with P^k-FSL glycoconjugate as a positive control. After incorporation of the

P^k-FSL into CHO-Lec2 cells lacking endogenous α-1,4-galactosyltransferase and P^k (Gb3) expression, flow cytometry analysis showed the binding of anti-P1 (650) antibody, as well as binding of Stx1B and Stx2B (Fig. 43). However, the Stx1 and Stx2 cytotoxicity assays did not reveal any difference between CHO-Lec2 NAT P^k and CHO-Lec2 NAT Galili (cells with incorporated Galα1→3Galβ1→4GlcNAc glycoconjugate, Galili-FSL, as a negative control) sensitivity, suggesting that synthetic glycoconjugates are unable to confer the toxin internalization and exert cytotoxicity (Fig. 44).
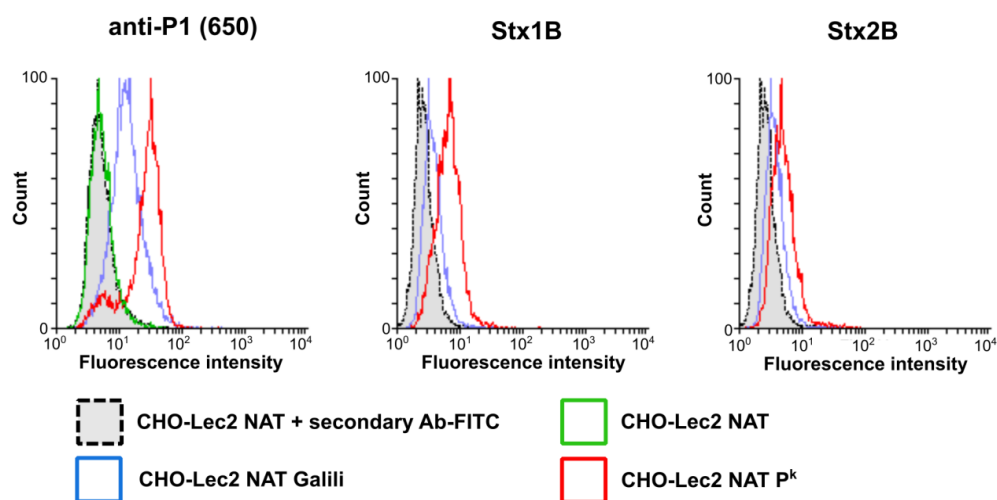
Fig. 43. Flow cytometry analysis of CHO-Lec2 NAT P^k and CHO-Lec2 NAT Galili cells with the use of anti-P1 (650), Stx1B and Stx2B.

A

B
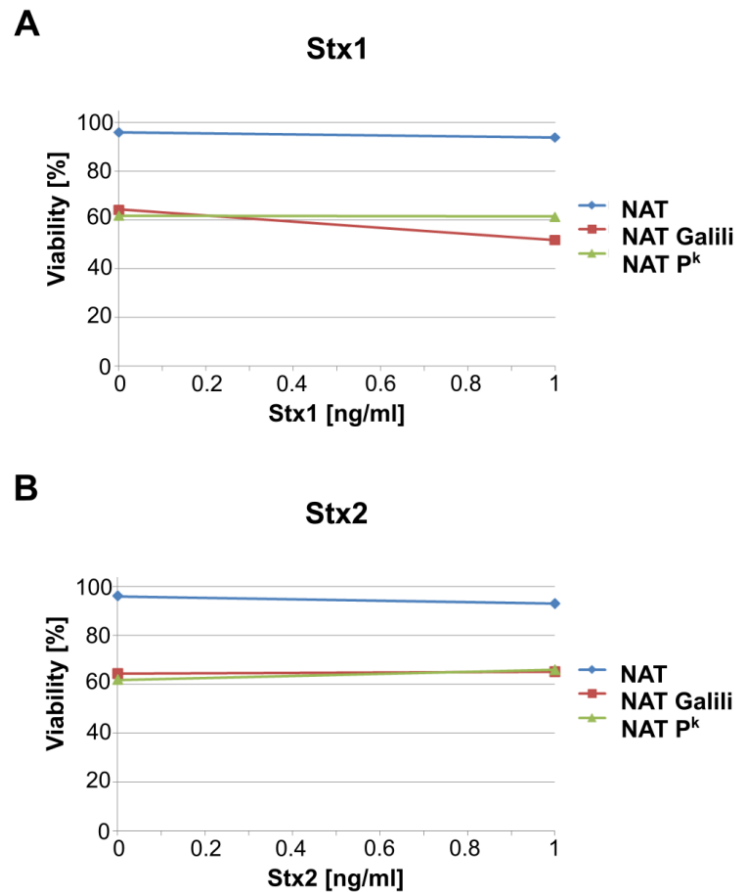
Fig. 44. Viability of CHO-Lec2 NAT cells after the incorporation of synthetic glycoconjugates and treatment with Stx1 (A) and Stx2 (B) holotoxins.

7.5 Analysis of Shiga toxin interactions with glycoprotein products of human α-1,4-galactosyltransferase

To characterize the interactions of Stxs with N-glycoproteins carrying P1 glycotopes (Galα1→4Galβ1→4GlcNAc), the binding of recombinant Stx1 and Stx2 B subunits (Stx1B and Stx2B) to SapD11 and CHO-Lec2 cells was examined. The SapD11 produced by α-1,4-galactosyltransferase in addition to its precursor glycoform SapD9 and the pigeon egg ovalbumin containing P1 glycotope (P1 OVA) were analyzed by western blotting with the use of Stx1B and Stx2B. Stx1B showed binding to P1 OVA and SapD11, but not SapD9, whereas Stx2B did not bind any glycoproteins (Fig. 45).
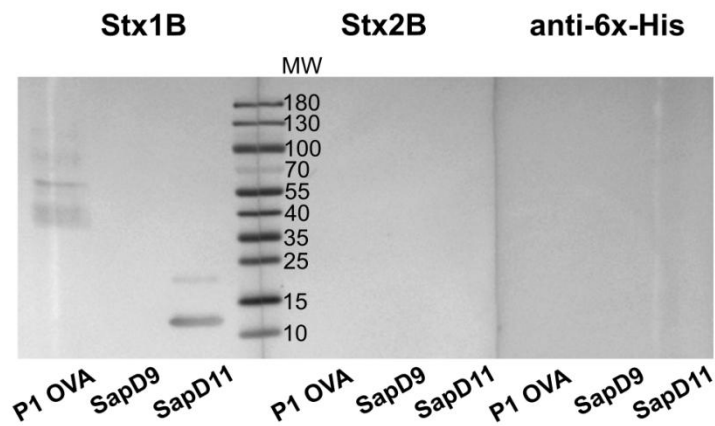
Fig. 45. Western blotting analysis of SapD9 and SapD11 with Stx1B and Stx2B. The band of molecular weight at approximately 22 kDa is presumed to be a SapD11 artefact. P1 OVA, pigeon egg ovalbumin containing P1 glycotope, was used as the positive control.

Interactions of Stx1B with SapD9 and SapD11 immobilized on CM5 chip were analyzed by SPR. The binding analysis displayed binding of Stx1B to SapD11, but not SapD9 (Fig. 46A). The interaction was confirmed in the affinity analysis with Stx1B in different concentrations (4.16, 8.31, 16.62, 33.25, 66.5 µM), which reported calculated dissociation constant K_D = 3.31 x 10^{-5} M (Fig. 46B). The affinity analysis was conducted only once due to the limited amount of Stx1B. Analysis with the use of Stx2B was not possible because of its nonspecific interactions with CM5 chip surface.
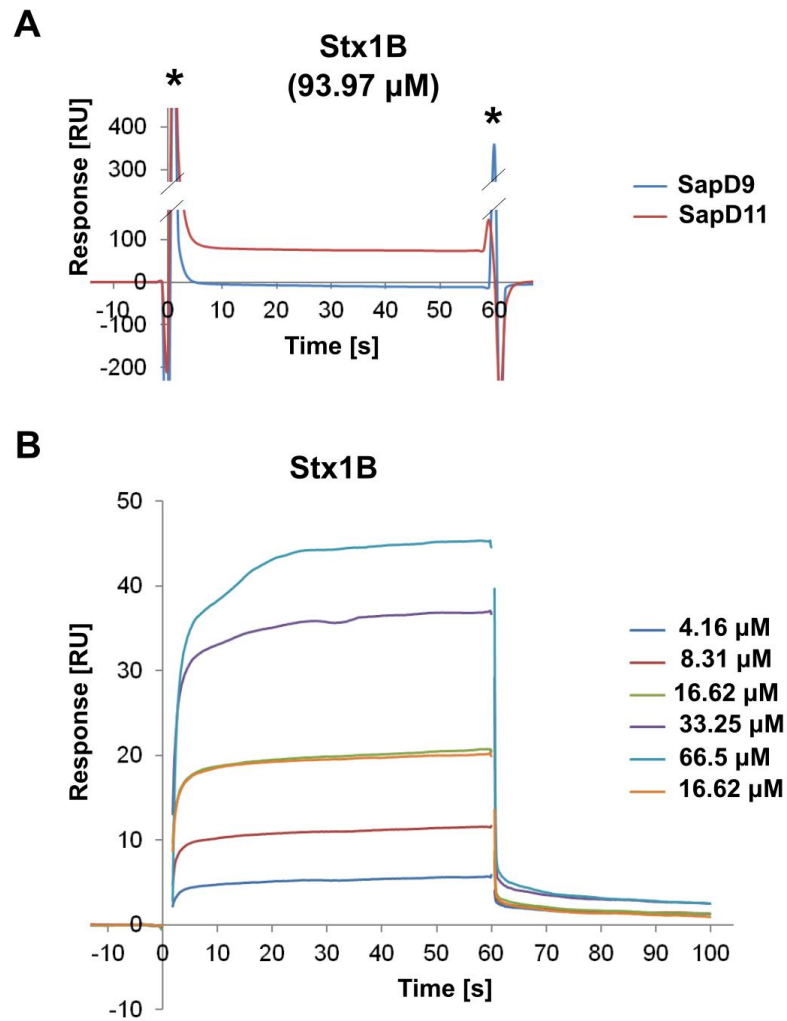
Fig. 46. A) SPR binding analysis of Stx1B to SapD9 and SapD11. B) SPR affinity analysis of Stx1B interaction with SapD11. ∗ - spikes resulted from the difference between composition of the running buffer and sample buffer.

The CHO-Lec2 cells were analyzed in flow cytometry with the use of Stx1B and Stx2B. Both toxins showed similar binding to the CHO-Lec2 A4GALT and CHO-Lec2 A4GALT Q211E cells (Fig. 47). There was no binding to the untransduced cells. The results suggest that products of consensus α-1,4-galactosyltransferase and p.Q211E mutein are recognized by Stx1B and Stx2B.
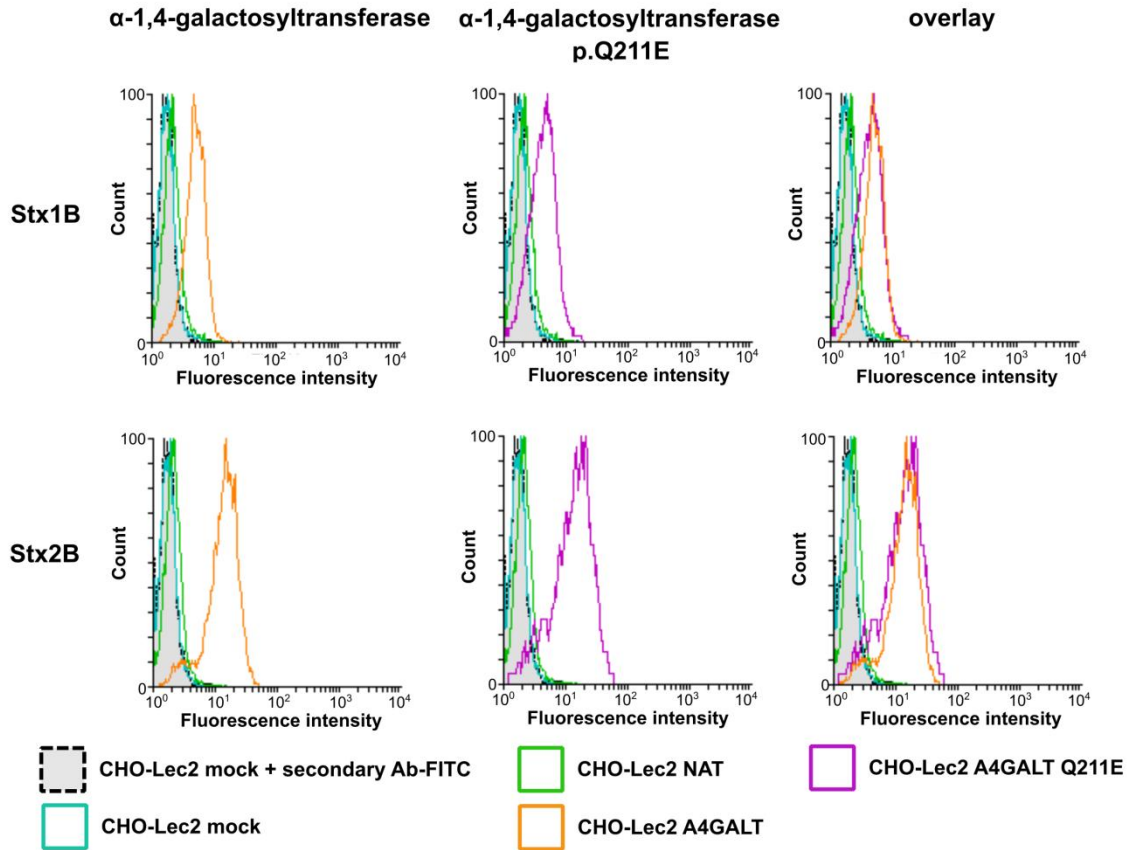
Fig. 47. Flow cytometry analysis of CHO-Lec2 cells with the use of Stx1B and Stx2B.

Furthermore, CHO-Lec2 cell lysates were tested in western blotting with the use of Stx1B and Stx2B. Stx1B detected several glycoproteins in CHO-Lec2 A4GALT and CHO-Lec2 A4GALT cell lysates, while Stx2B did not bind to any proteins (Fig. 48).
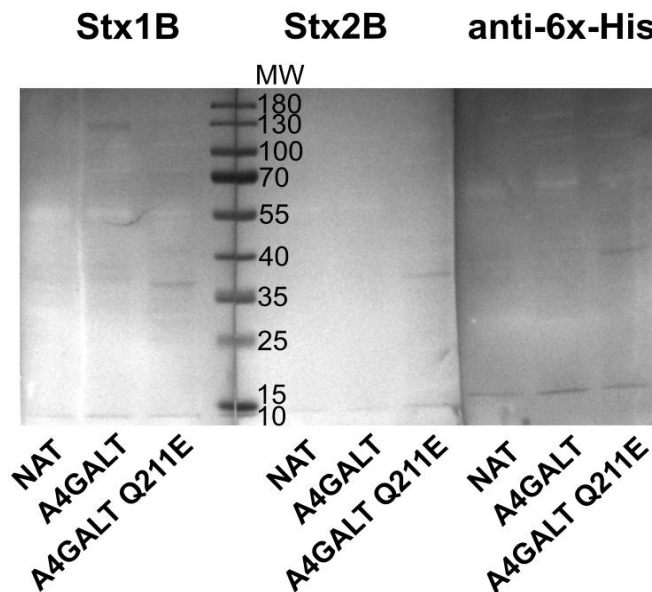
Fig. 48. Western blotting analysis of CHO-Lec2 cell lysates stained with Stx1B and Stx2B.

To elucidate the contribution of glycoproteins in Stx1B and Stx2B binding, quantitative flow cytometry analysis of untreated and treated with Genz-123346 CHO-Lec2 cells was performed. Strikingly, the binding of Stx1B to Genz-123346-treated CHO-Lec2 A4GALT and CHO-Lec2 A4GALT Q211E cells was elevated in comparison to the untreated cells (Fig. 49). On the other hand, Stx2B binding to CHO-Lec2 A4GALT and CHO-Lec2 A4GALT Q211E cells was completely abolished after Genz-123346 treatment.

Moreover, Stx1B binding capacity of untreated and Genz-123346-treated cells was elevated in the case of CHO-Lec2 A4GALT Q211E, compared to the CHO-Lec2 A4GALT. The untreated CHO-Lec2 A4GALT Q211E cells showed also increased Stx2B binding capacity (Fig. 49B).
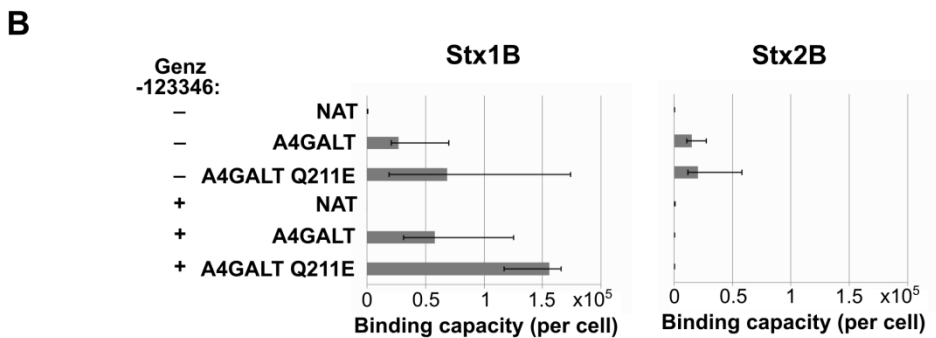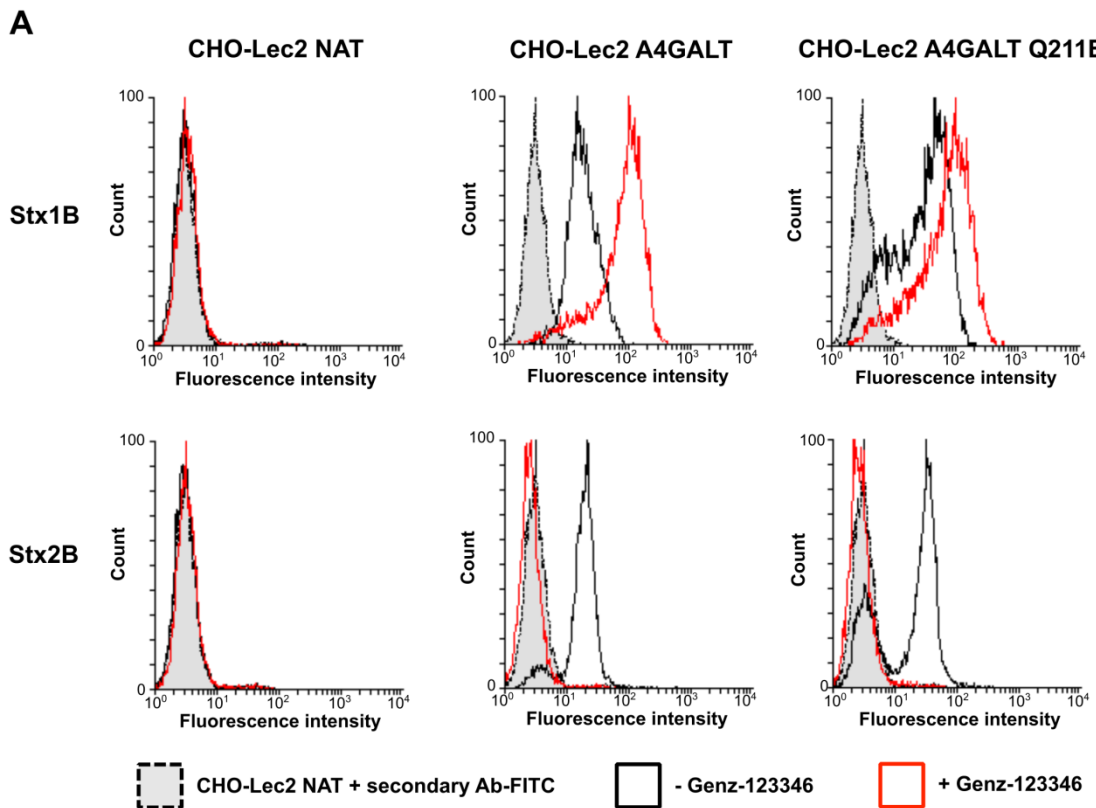
Fig. 49. A) Flow cytometry analysis of CHO-Lec2 cells with the use of Stx1B and Stx2B. B) Quantitative flow cytometry analysis of Stx1B and Stx2B binding capacity per CHO-Lec2 cell (displayed as median from at least three replicates; error bars represent interquartile ranges).

Neutral GSLs isolated from the untreated CHO-Lec2 cells and the cells grown in the presence of Genz-123346 were analyzed by HPTLC with the use of Stx1B. The toxin subunit recognized P^k antigen (Gb3) and Gb4 in the untreated CHO-Lec2 A4GALT and CHO-Lec2 A4GALT Q211E, but did not bind any GSLs from Genz-123346-treated cells (Fig. 50). These results suggest that Stx1B binds Genz-123346-treated CHO-Lec2 A4GALT and CHO-Lec2 A4GALT Q211E cells (Fig. 49) due to the interactions with glycoproteins, but not with the GSL products of α-1,4-galactosyltransferase or p.Q211E mutein.
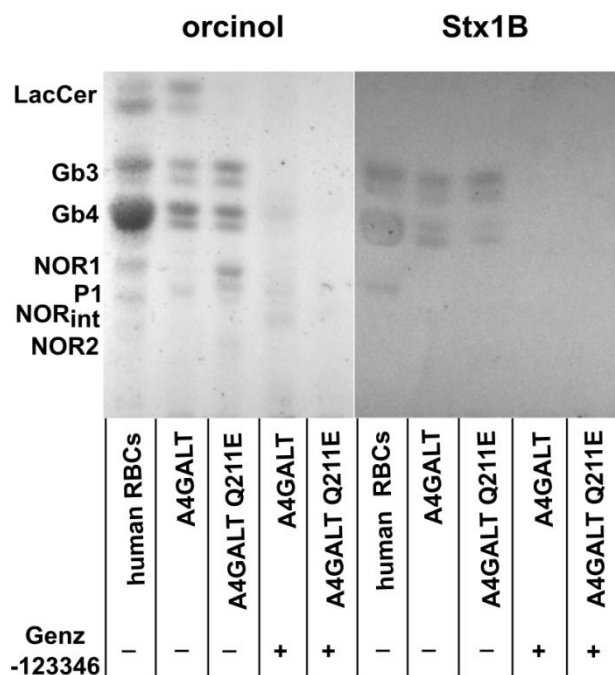
Fig.50. HPTLC analysis of neutral GSLs purified from CHO-Lec2 cells, untreated or cultured in the presence of Genz-123346, stained with orcinol and Stx1B.

The results of flow cytometry, HPTLC and western blotting analyses of CHO-Lec2 cells suggested that p.Q211E mutein has bigger activity that the consensus α-1,4-galactosyltransferase. In contrast, the flow cytometry analysis of human RBCs suggested that p.Q211E mutein exhibits lower activity than consensus α-1,4-galactosyltransferase. To determine the influence of p.Q211E on Stx binding to human RBCs, the RBCs of different *A4GALT* genotypes were analyzed using quantitative flow cytometry. $P^{1NOR}P^1$ and $P^{1NOR}P^2$ genotypes showed increased Stx1B binding compared with P^1P^1 and P^1P^2, respectively (Fig. 51).
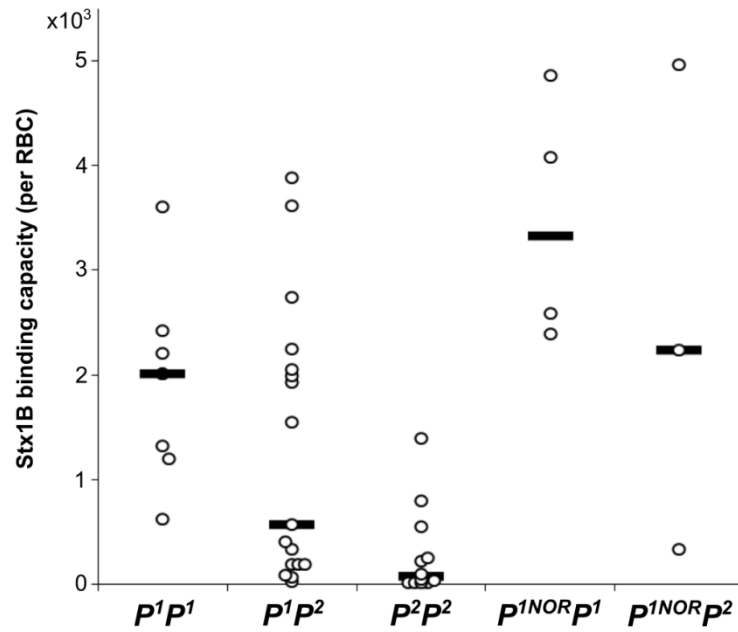
Fig. 51. Quantitative flow cytometry analysis of Stx1B binding capacity per RBC in individuals of different genotypes (the lines are medians).

Since glycoproteins produced by the consensus α-1,4-galactosyltransferase and p.Q211E mutein are recognized by Stx1B, the question arises whether such glycoproteins may act as functional toxin receptors. The preliminary flow cytometry analysis of untreated and Genz-123346-treated CHO-Lec2 A4GALT Q211E cells, incubated with Stx1B and Stx2B in conditions allowing Stx B subunit internalization, showed that both Stx1B and Stx2B were detected at the lower level after internalization on the untreated cells (Fig. 52). A similar shift was observed in Stx1B binding to the cells treated with Genz-123346, suggesting glycoproteins may confer Stx1B internalization.
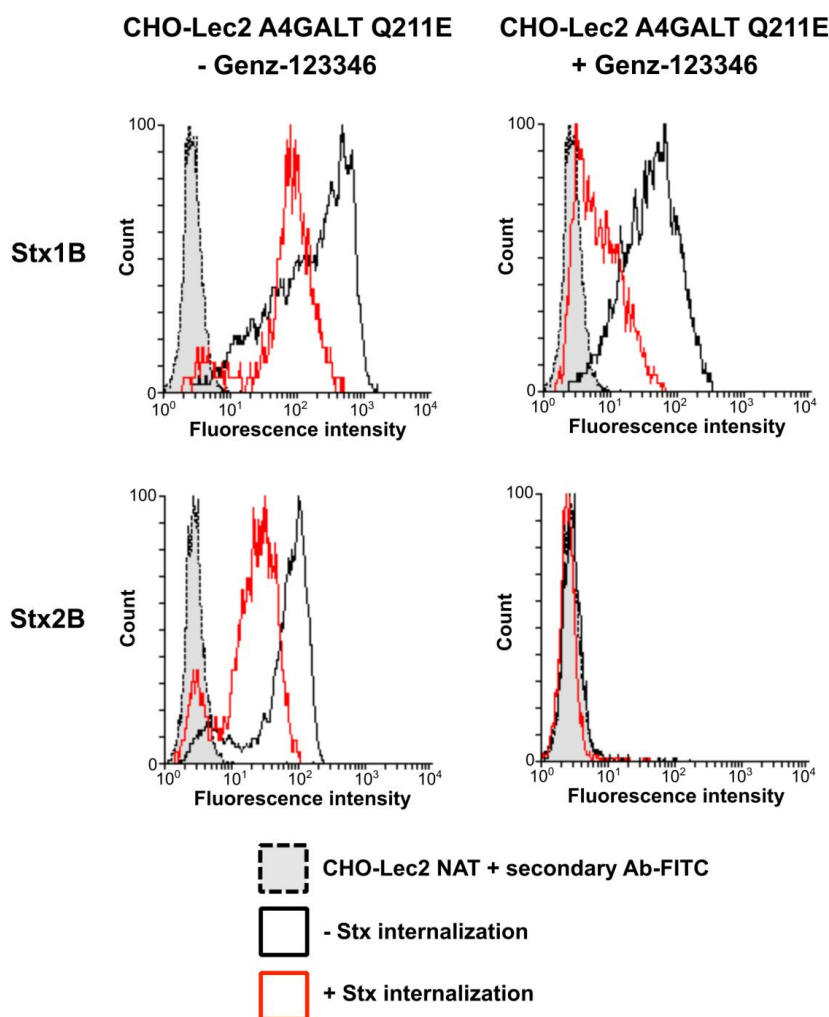
Fig. 52. Flow cytometry analysis of Stx1B and Stx2B binding to CHO-Lec2 A4GALT Q211E cells, untreated and cultured in the presence of Genz-123346, before and after Stx internalization.

To determine the role of glycoproteins in Stx binding and internalization, cytotoxicity assays with the use of five different concentrations (0.01, 0.05, 0.1, 0.5, 1 ng/ml) of Stx1 and Stx2 holotoxins were performed. The untransduced CHO-Lec2 cells were not sensitive to Stx1 and Stx2 (Fig. 53). In contrast, viability of CHO-Lec2 A4GALT and CHO-Lec2 A4GALT Q211E cells was decreased after incubation with Stx1 and Stx2 in concentrations 0.05-1 ng/ml. After Genz-123346 treatment, both CHO-Lec2 A4GALT and CHO-Lec2 A4GALT Q211E cells became insensitive to Stx2 (Fig. 54). However, a decrease of CHO-Lec2 A4GALT Q211E cell viability was detected in the concentration range 0.1-1 ng/ml of Stx1, whereas CHO-Lec2 A4GALT appeared to be completely insensitive.

A

B
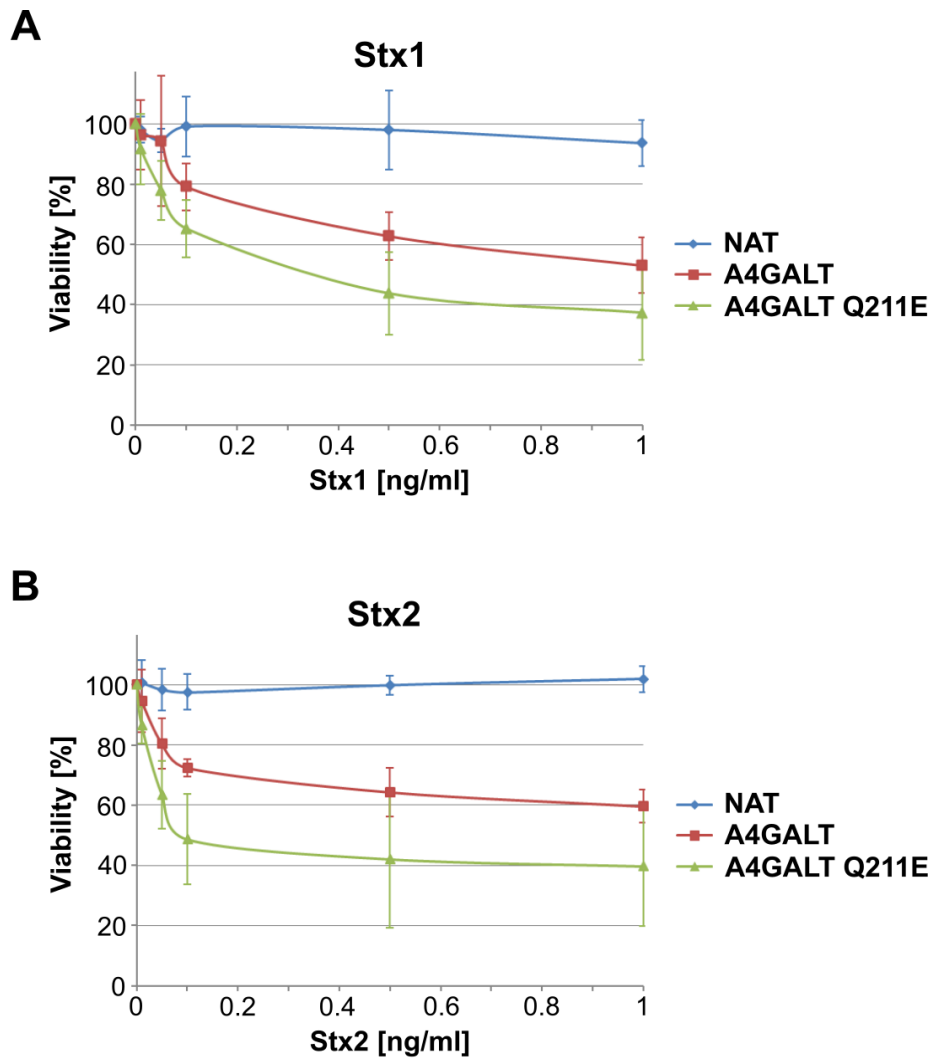
Fig. 53. Viability of CHO-Lec2 cells after exposure to Stx1 (A) or Stx2 (B) (at least three independent experiments were conducted, each with three technical replicates; error bars are standard deviations).

A

B
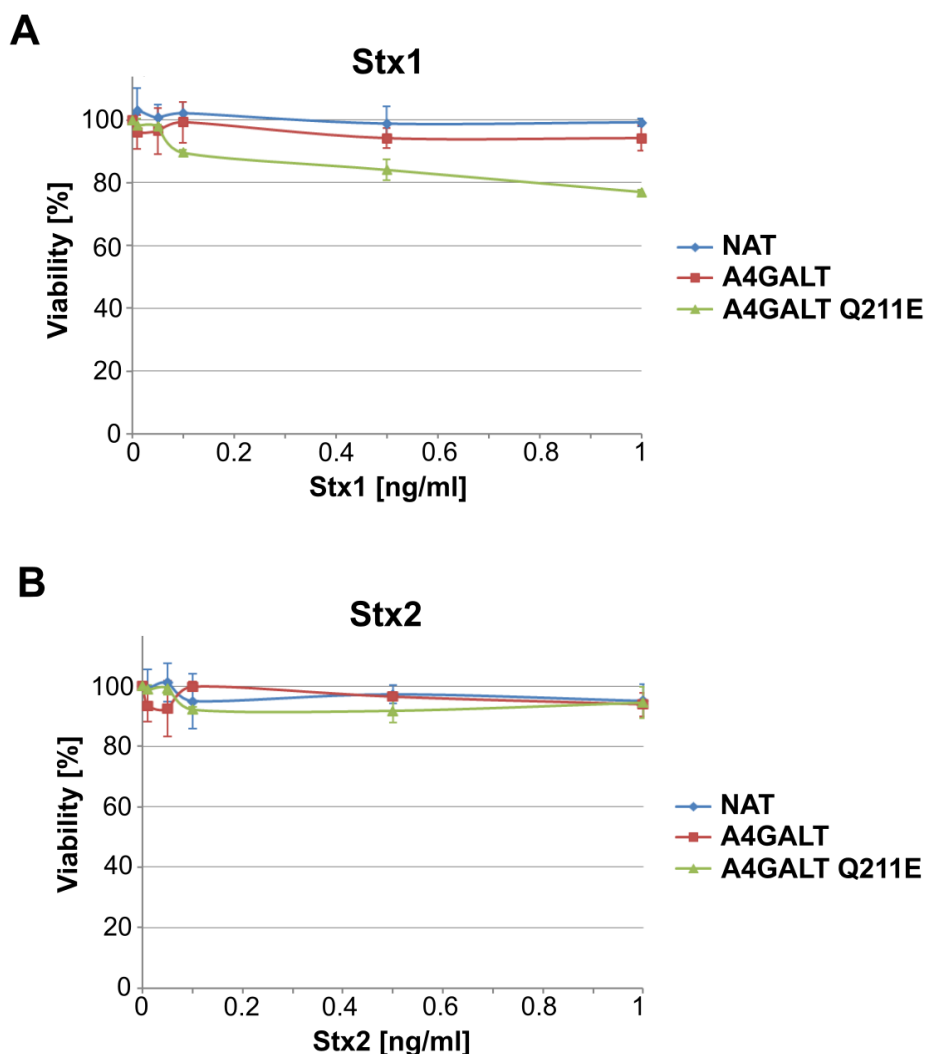
Fig. 54. Viability of CHO-Lec2 cells cultured in the presence of Genz-123346 treated with Stx1 (A) or Stx2 (B) (at least three independent experiments were conducted, each with three technical replicates; error bars are standard deviations).

When CHO-Lec2 A4GALT and CHO-Lec2 A4GALT Q211E cells were incubated with Stx1 at concentration 1 ng/ml, the viability of the cells was decreased to 53% and 37%, respectively, and after incubation with 1 ng/ml Stx2, to 60% and 40% (Fig. 55). The lack of susceptibility of Genz-123346-treated CHO-Lec2 A4GALT and CHO-Lec2 A4GALT Q211E cells to Stx2 suggests that glycoproteins cannot be utilized as receptors by this toxin. However, the Stx1 cytotoxicity analysis of the cells treated with Genz-123346 revealed that CHO-Lec2 A4GALT cells are completely insensitive to toxin, in contrast to the CHO-Lec2 A4GALT Q211E cells, which viability was reduced to 77%. These results suggest that glycoproteins produced in CHO-Lec2 A4GALT Q211E cells may act as functional receptors for Stx1. Presumably, the lack of susceptibility of Genz-123346-treated CHO-Lec2 A4GALT cells is related with the insufficient level of glycoproteins carrying P1 glycotopes, which expression is strongly reduced in comparison to the CHO-Lec2 A4GALT Q211E cells.

A

Stx1 (1 ng/ml)

	NAT (+ Genz-123346)	A4GALT	A4GALT (+ Genz-123346)	A4GALT Q211E	A4GALT Q211E (+ Genz-123346)
NAT	0.0944	< 0.0001	0.7624	< 0.0001	< 0.0001
NAT (+ Genz-123346)		< 0.0001	0.1659	< 0.0001	< 0.0001
A4GALT			< 0.0001	0.0038	< 0.0001
A4GALT (+ Genz-123346)				< 0.0001	< 0.0001
A4GALT Q211E					< 0.0001

B

Stx2 (1 ng/ml)

	NAT (+ Genz-123346)	A4GALT	A4GALT (+ Genz-123346)	A4GALT Q211E	A4GALT Q211E (+ Genz-123346)
NAT	0.0031	< 0.0001	0.0018	< 0.0001	0.0014
NAT (+ Genz-123346)		< 0.0001	0.7046	< 0.0001	0.8385
A4GALT			< 0.0001	0.0023	< 0.0001
A4GALT (+ Genz-123346)				< 0.0001	0.8411
A4GALT Q211E					< 0.0001

Fig. 55. CHO-Lec2 cells viability cultured in the presence or absence of Genz-123346 after 20 h of 1 ng/ml Stx1 (A) or Stx2 (B) treatment (mean; error bars are standard deviations). Tables contain p values of the t test with Holm–Bonferroni correction ($p < 0.05$; $p < 0.01$; $p < 0.001$).

8. Discussion

8.1 *A4GALT* genotype and P_1/P_2 polymorphism, finally united

Although α-1,4-galactosyltransferase is the only enzyme involved in the biosynthesis of P1PK antigens, elucidation of genetic background of this histo-blood group system was extremely challenging. P1 antigen has been unequivocally shown to be a product of α-1,4-galactosyltransferase many years after the first report suggesting this fact (Iwamura *et al.*, 2003; Kaczmarek, Duk, *et al.*, 2016). At the time of performing and publishing results of the first part of this thesis, it was only assumed that P1 antigen production is related with the elevated level of *A4GALT* transcript, and several SNPs in *A4GALT* gene were proposed to underlie this phenomenon (Thuresson, Westman and Olsson, 2011; Lai *et al.*, 2014).

Results of this study indicated that the level of P^k (Gb3) and P1 antigens on RBCs surface, as well as *A4GALT* transcript levels were associated with *A4GALT* genotype established on the basis of four SNPs (rs8138197 proposed by Thuresson, Westman and Olsson, 2011; rs2143918, rs2143919 and rs5751348 proposed by Lai *et al.*, 2014). The rs5751348 was shown to be the most credible among tested SNPs in determining the P_1/P_2 phenotypic polymorphism. These results are not confounded by the influence of later uncovered glycoprotein products of α-1,4-galactosyltransferase, since RBCs were pretreated with protease (papain).

Results of this study were the first independent report collating the significance of *A4GALT* SNPs found before by different groups (Thuresson, Westman and Olsson, 2011; Lai *et al.*, 2014). Later, a study based on whole genome sequencing with nucleotide frequency correlation and serologic correlation determined rs8138197, rs2143918 and rs5751348 correlating with P_1/P_2 polymorphism (Lane *et al.*, 2019). Recently, the same three SNPs were tested among Thai population and all of them consistently correlated with P_1/P_2 phenotype diversity (Thinley *et al.*, 2021). Moreover, a multiplex PCR for P_1/P_2 genotyping has been developed based on rs2143918 and rs5751348 (Thinley *et al.*, 2021).

In line with the results of this study, in the rs5751348G region (*P^1* allele) putative binding motifs for several transcription factors involved in hematopoietic system were identified, such as EGR1 (transcription factor early growth response 1), RUNX1 (Runt-related transcription factor 1), KLF1 (Krüppel-like factor 1) (Westman *et al.*, 2018; Yeh *et al.*, 2018). RUNX1 was found to bind *P^1*-, but not *P^2*-specific probes and silencing of *RUNX1* expression resulted in downregulation of *A4GALT* transcript level (Westman *et al.*, 2018). Moreover, EGR1 was shown to bind specifically to the rs5751348G genomic region and to induce the transcription

of the P^1 allele (Yeh *et al.*, 2018). On the other hand, KLF1 did not demonstrated binding to the rs5751348G region (Westman *et al.*, 2018). However, it seems that KLF1 may be involved in inducing *A4GALT* transcription indirectly, possibly by interaction with RUNX1 and/or EGR1. The results of this study showing wide and largely overlapping distributions of *A4GALT* transcript level, as well as P^k and P1 antigen expression on RBCs allow to speculate that regulation of *A4GALT* transcription is based on the interplay of different transcription factors.

8.2 Human α-1,4-galactosyltransferase activity expands on glycoproteins

After discovery that p.Q211E substitution is responsible for broadening enzyme acceptor specificity, one would not expect to uncover more products of α-1,4-galactosyltransferase. However, the presence of P1 glycotope (Galα1→4Galβ1→4GlcNAc) on human glycoproteins was suggested by (Marcus, 1971) and tested by (Haselberger and Schenkel-Brunner, 1982), who showed that P1-antiserum recognized band 4.5 (GLUT1) and, to a lesser extent, other RBC membrane proteins. However, those results were contradicted by a report demonstrating a complete depletion of P1 determinants from RBC membrane glycoproteins upon treatment with *n*-butanol, which removes GSLs (Yang, Bergström and Karlsson, 1994). Since then, there was a general agreement that the sole carrier of P1 glycotope is GSL P1 antigen. Recently, (Stenfelt *et al.*, 2019) suggested that some human P1 RBCs may exhibit P1 not just on GSLs, but also on glycoproteins, presumably GLUT1 and Band 3. However, the evidence was limited to western blotting results.

Results of this thesis demonstrate that the soluble catalytic domain of human α-1,4-galactosyltransferase and the p.Q211E mutein can readily transfer galactose residues to both antennae of synthetic N-glycan acceptor. The p.Q211E mutein provided a faster reaction, hence it was selected to another *in vitro* experiment with the use of synthetic glycoform of human saposin D (SapD9) carrying a complex nonasaccharide N-glycan with both antennae terminating in Galβ1→4GlcNAc. The enzyme was found to attach galactose residues to both antennae of the N-glycan of SapD9, resulting in production of P1 glycotopes.

In the *in vivo* approach, CHO-Lec2 cells transduced with vector encoding either consensus α-1,4-galactosyltransferase or p.Q211E mutein were shown to produce glycoproteins which contain P1 glycotopes, with the mutein being the more efficient enzyme. Removal of N-glycans rendered the glycoproteins undetectable by the anti-P1 (P3NIL100) antibody, indicating that P1 glycotopes were present only on N-, but not O-linked glycan chains. To ensure the absence of GSLs as potential confounders in CHO-Lec2 protein lysates, the cell culture was maintained

in the presence of Genz-123346, which is an inhibitor of glucosylceramide synthase. As expected, the cells exposed to Genz-123346 did not produce any GSL substrates or products of α-1,4-galactosyltransferase. At the same time, more P1 glycotopes was expressed on glycoproteins in comparison to the cells not treated with Genz-123346. Mass spectrometric analysis of the released N-glycans confirmed the presence of P1 glycotope on a biantennary N-glycan upon expression of consensus α-1,4-galactosyltransferase or p.Q211E mutein.

Recently, these results were corroborated by a report indicating production of P1 glycotopes on glycoproteins after overexpression of human α-1,4-galactosyltransferase in HeLa cells with silenced genes encoding glucosylceramide and galactosylceramide synthases (Morimoto *et al.*, 2020).

Although astonishing in the case of human α-1,4-galactosyltransferase, the ability to synthesize glycan chains of both glycoproteins and GSLs by one enzyme is not uncommon. One example is ABO histo-blood group system transferases, both of which synthesize A and B blood group antigens on different N-, O-, and Cer-linked glycans depending on the cell type (Cooling, 2015). It is estimated that 80% of ABH determinants on RBCs are present on glycoproteins and 20% on GSLs (Watkins *et al.*, 1988). Moreover, human β-1,3-galactosyltransferases 1, 2, and 5, and β-1,4-galactosyltransferase 1 and 5 can act on glycoproteins as well as on GSLs (Amado *et al.*, 1998; Van Die *et al.*, 1999; Zhou, Berger and Hennet, 1999; Zhou *et al.*, 2000). Likewise, human β-1,3-*N*-acetylglucosaminyltransferase 5 uses GSLs and glycoproteins as acceptors (Henion *et al.*, 2001).

8.3 Consensus α-1,4-galactosyltransferase vs. p.Q211E mutein – which is more efficient?

Besides broadening α-1,4-galactosyltransferase acceptor specificity, the p.Q211E substitution may influence the enzyme efficiency. The results of this study suggested seemingly contradictory conclusions. The quantitative flow cytometry analysis showed decreased binding of anti-P1 antibody (P3NIL100) to $P^{1NOR}P^1$ in comparison to P^1P^1 RBCs, which may raise speculation that the p.Q211E enzyme's superpromiscuity comes at the cost of P1 antigen synthesis. Presumably, it may be estimated that the p.Q211E mutein produces one NOR molecule for one P1 molecule, so the number of P1 molecules decreases. On the other hand, RBCs of $P^{1NOR}P^1$ and $P^{1NOR}P^2$ genotypes showed the increased binding of Stx1B in comparison with P^1P^1 and P^1P^2 genotypes, respectively. This discrepancy is probably caused by methodological and molecular differences between the anti-P1 and Stx1B binding assays. Prior to anti-P1 antibody analysis, RBCs are treated with papain to allow efficient detection of GSL

epitopes, which otherwise may be cloaked by membrane proteins. Papain is a nonselective protease, so it may remove P1 glycoproteins along with the other proteins. In contrast, papain treatment decreases Stx1B binding and it was not used in the Stx1B flow cytometry analysis. Moreover, Stx1B and antibodies have different affinities for P^k (Gb3) and P1 GSLs and greatly differ in size, so these receptors may be less accessible to antibodies (Johannes and Römer, 2010; Volynsky *et al.*, 2017).

In turn, the p.Q211E mutein expressed in CHO-Lec2 cells was found to produce more P^k antigen (Gb3) and P1 glycotopes on glycoproteins in comparison with the consensus α-1,4-galactosyltransferase, despite its lower expression at the mRNA and protein level. The P1 antigen was not synthesized by the consensus enzyme nor p.Q211E mutein presumably due to the lack of GSL precursor.

Taken together, it may be assumed that the p.Q211E mutein produces the P1 antigen less efficiently (hence the decreased anti-P1 binding to protease-treated RBCs), but it synthesizes the P^k antigen (Gb3) and P1 glycotopes on glycoproteins at higher level in comparison with the consensus α-1,4-galactosyltransferase.

8.4 Glycoprotein products of human α-1,4-galactosyltransferase – the back door entry for Shiga toxin 1

While the general opinion maintains that P^k antigen (Gb3) is the main receptor for Stx, the role of Gb4 still requires clarification. In addition, the role of P1 antigen has never been under investigation. The results of this study did not confirm postulated Stx1B or Stx2B binding to the Gb4-PAA but instead showed interaction of Stx1B with P1-PAA. Since this analysis was performed with the use of synthetic glycoconjugates, the results must be treated with caution. Unfortunately, an attempt to clarify this issue using the *in vivo* approach employing the Namalwa cell line exerimental model did not produce any conclusive results.

For many years, it was taken for granted that human α-1,4-galactosyltransferase could act exclusively on GSLs, so glycoproteins were never considered as potential Stx receptors. The only report suggested the existence of putative mammalian proteins recognized by Stx1 and Stx2 in P^k antigen (Gb3) deficient Vero cells (Devenish, Gyles and LaMarre, 1998). However, the P1 glycotope-containing glycoproteins have been found in birds and amphibians (Suzuki, Laskowski and Lee, 2006). Pigeon egg white ovomucoid displaying P1 on N-glycans is recognized by Stx1 and can be used in affinity chromatography for purification of the toxin (Miyake, Utsuno and Noda, 2000; Takahashi *et al.*, 2001). In glycan array analysis, Stx1 recognized a synthetic biantennary glycan $Gal_4GlcNAc_2Man_3$ with both antennae carrying P1

glycotopes (Gallegos *et al.*, 2012). P1 glycotopes were expressed on O-glycans of recombinant mucin-type fusion protein PSGL-1/mIgG$_{2b}$ produced in CHO-K1 cells, cotransfected with vectors encoding the pigeon homolog of human α-1,4-galactosyltransferase and human core 2 β1,6-*N*-acetylglucosaminyltransferase (Maria Cherian *et al.*, 2014). That glycoprotein, along with human serum albumin conjugated with the P^k (Gb3) glycan, was shown to be recognized by Stx1, but not Stx2.

In this study, Stx1B (but not Stx2B) was shown to recognize a synthetic model glycoprotein carrying P1 glycotope (SapD11), as well as unidentified glycoproteins on CHO-Lec2 cells overexpressing human consensus α-1,4-galactosyltransferase or p.Q211E mutein. Furthermore, the cytotoxicity assays revealed that CHO-Lec2 cells expressing p.Q211E mutein exhibited a higher susceptibility to Stx1 and Stx2. The results of assays with untreated cells were similar for both Stx1 and 2; however, the cells with abolished synthesis of globo and neolacto series GSL became refractory to Stx2. Strikingly, while neither Stx1 nor Stx2 was able to kill GSL-deficient cells that overexpressed consensus α-1,4-galactosyltransferase, the cells overexpressing p.Q211E mutein were still partially susceptible to Stx1 despite the depletion of GSLs. Thus, P1 glycoproteins present on the cell surface are sufficient to induce Stx1 cytotoxicity, most likely by acting as functional, internalizing receptors. Presumably, the consensus enzyme produced too little P1 glycotopes on glycoproteins to make the cells vulnerable to Stx1. Collectively, results of this study indicate that Stx1 can recognize and use P1 glycoproteins to enter and kill the cell, while Stx2 can use GSL receptors only.

Recently, (Morimoto *et al.*, 2020) showed that glycoproteins carrying the P1 glycotope synthesized by the pigeon homolog of human α-1,4-galactosyltransferase may serve as functional receptors for Stx1. The authors expressed this enzyme in HeLa cells after knock out of the genes encoding glucosylceramide and galactosylceramide synthases. Similarly, the authors obtained P1 glycoprotein production by human consensus α-1,4-galactosyltransferase, albeit at levels too low to induce Stx1 cytotoxicity. Moreover, disruption of the gene encoding α1,3-mannosyl-glycoprotein 2-β-*N*-acetylglucosaminyltransferase (but not glycoprotein-*N*-acetylgalactosamine 3-β-galactosyltransferase 1) caused a decrease in Stx1B binding to HeLa cells expressing the pigeon homolog of human α-1,4-galactosyltransferase. Thus, it may be argued that P1 glycotopes on glycoproteins are synthesized in HeLa cells only on N-glycans, which is in accordance with this study. The unmodified HeLa cells produce P^k antigen (Gb3), but not P1 glycoproteins. Interestingly, when Morimoto et al. expressed the pigeon homolog of human α-1,4-galactosyltransferase in unmodified HeLa and obtained cells producing both P^k antigen (Gb3) and P1 glycoproteins, they were less sensitive to Stx1 than the unmodified cells.

The authors postulated that P1 glycoproteins served as decoy receptors for the toxin, but it should be noted that HeLa cells expressing the pigeon homolog produced less P^k antigen (Gb3) than unmodified cells, so it could be that the P1 glycoproteins were not able to compensate for the loss of P^k (Gb3), the more potent receptor. In turn, the design of this study prevented potential misinterpretations of cytotoxicity patterns. Interestingly, cytotoxicity assays showed comparable sensitivity of cells producing both P^k antigen (Gb3) and P1 glycoproteins for both Stx1 and Stx2. Since P1 glycoproteins are recognized by Stx1, but not Stx2, one could expect a higher sensitivity for Stx1. Thus, the role of P1 glycotopes on glycoproteins as receptors for Stx1 may depend on their proportion to the P^k antigen (Gb3) molecules on the cell surface.

8.5 Future challenges

A question arises, why P1 glycotopes on glycoproteins account for small fraction of total Galα1→4Gal-terminated glycoconjugates, despite α-1,4-galactosyltransferase being active towards all kinds of Gal-terminating acceptors *in vitro*? In other words, there is an issue whether human α-1,4-galactosyltransferase favors GSL substrates over glycoproteins, or if it can use either of them and shows no clear preference to GSLs or glycoproteins. It can be estimated that the rate of transfer to glycoprotein acceptors in comparison with GSLs measured *in vivo* is less than 5%. On the other hand, the rate *in vitro* (*i.e.*, against purified N-glycans or purified proteins) may well approach 100%, as it was shown with saposin D. In the opinion of the author, the difference in α-1,4-galactosyltransferase activity toward GSLs and glycoproteins *in vivo* is most probably caused by the morphology of the Golgi compartment, where glycosyltransferases may form complexes, which act as conveyor belts for their substrates. For example, human β-1,4-galactosyltransferase 1 (*B4GALT1*) and β-galactoside α-2,6-sialyltransferase (*ST6GAL1*) form heterodimers in the Golgi using lateral interactions by highly charged surface domains (Khoder-Agha *et al.*, 2019). Recently, a Golgi phosphoprotein 3 (GOLPH3) has been shown to specifically recognize LXXR motif present in the cytoplasmic N-terminal domain of human α-1,4-galactosyltransferase and β-1,4-galactosyltransferase 5 (*B4GALT5*), which is responsible for lactosylceramide biosynthesis (Rizzo *et al.*, 2021). The interaction with GOLPH3 is necessary for localization of these enzymes in Golgi. Presumably, GOLPH3 may form tetramers similarly as its yeast homolog (Schmitz *et al.*, 2008), with each monomer possibly interacting with different glycosyltransferase and hence closing them to each other. This is an idea calling for further research and our laboratory already embarked on a series of studies designed to determine if this is indeed the case.

Another idea worth consideration is potential role of O-glycans in Stx binding and internalization. The preliminary study performed in our laboratory by Anna Bereźnicka suggested that α-1,4-galactosyltransferase can add terminal galactose to Galβ1→3GalNac-terminated O-glycans, which opens question whether such structures are present on the surface of the cells and what is the role of such structures is binding of Shiga toxins. In the opinion of the author, the number of such structures is rather low, because sialyltransfrease preferably utilizes O-glycans by adding a terminal Neu5Ac, thus preventing the elongation by α-1,4-galactosyltransferase.

The results of this study have several broader implications. The current understanding of Stx pathology in humans is based on the long-established view that the toxins can use only GSLs to enter and kill the cells. For the time being, the difference between Stx1 and Stx2 receptor preferences found in this study may be considered to be related to the difference in virulence between Stx1 and Stx2-producing STEC strains. The latter strains are more virulent in humans, but evaluation of that link will require further investigation. In a STEC infection progressing into hemolytic uremic syndrome, extracellular vesicles act as a Stx cargoes (Karpman and Tontanahal, 2021). A question arises, whether such vesicles contain P1 glycoproteins and what may be their role in inciting hemolytic uremic syndrome. Finally, the findings presented in the study militate against the potential to use soluble P1-carrying protein decoys as Shiga toxin blocking agents in therapy for STEC infection, at least in the case of Stx1-producing strains. Uptake of toxin-decoy complexes could potentially lead to activation of ribotoxic stress response in antigen presenting cells and exacerbate the dysregulation of immune response seen in severe STEC infections, should the toxin be able to escape degradation. Overall, the results of the study may indicate the need to shift focus from designing efficient Galα1→4Gal-decorated binders to inventing agents that would irreversibly sequestrate the toxins.

9. Conclusions

1. The rs5751348 SNP shows the highest correlation with the P_1/P_2 phenotype in the tested individuals.

2. The recombinant human α-1,4-galactosyltransferase, both consensus and p.Q211E mutein, catalyzes the transfer of galactose residue to the synthetic oligosaccharide. Moreover, the p.Q211E mutein was shown to add a terminal galactose to the N-glycan chain of human recombinant saposin D.

3. The CHO-Lec2 cells transduced with lentiviral vector encoding either consensus α-1,4-galactosyltransferase or p.Q211E mutein express P1 glycotopes on N-glycoproteins. In addition, the p.Q211E mutein expressed in CHO-Lec2 cells is more active toward glycosphingolipid and glycoprotein acceptors in comparison with the consensus α-1,4-galactosyltransferase.

4. The B subunit of Stx1 recognizes glycoproteins carrying P1 glycotopes, which act as functional receptors for Stx1 holotoxins. In contrast, Stx2 and its B subunit do not interact with P1 glycotopes on N-glycoproteins, suggesting that Stx2 cannot utilize such kind of glycans as receptors.

10. References

Albesa-Jové D, Giganti D, Jackson M, Alzari PM and Guerin ME (2014). Structure-function relationships of membrane-associated GT-B glycosyltransferases. *Glycobiology*, 24(2), pp. 108–124. doi: 10.1093/glycob/cwt101.

Albesa-Jové D and Guerin ME (2016). The conformational plasticity of glycosyltransferases. *Current Opinion in Structural Biology*, 40, pp. 23–32. doi: 10.1016/j.sbi.2016.07.007.

Albesa-Jové D, Sainz-Polo MÁ, Marina A and Guerin ME (2017). Structural Snapshots of α-1,3-Galactosyltransferase with Native Substrates: Insight into the Catalytic Mechanism of Retaining Glycosyltransferases. *Angewandte Chemie - International Edition*, 56(47), pp. 14853–14857. doi: 10.1002/anie.201707922.

Albuquerque-Wendt A, Hütte HJ, Buettner FFR, Routier FH and Bakker H (2019). Membrane Topological Model of Glycosyltransferases of the GT-C Superfamily. *International Journal of Molecular Sciences*, 20(19), p. 4842. doi: 10.3390/ijms20194842.

Alperi A and Figueras MJ (2010). Human isolates of *Aeromonas* possess Shiga toxin genes (*stx1* and *stx2*) highly similar to the most virulent gene variants of *Escherichia coli*. *Clinical Microbiology and Infection*, 16(10), pp. 1563–1567. doi: 10.1111/j.1469-0691.2010.03203.x.

Amado M, Almeida R, Carneiro F, Levery SB, Holmes EH, Nomoto M, Hollingsworth MA, Hassan H, Schwientek T, Nielsen PA, Bennett EP and Clausen H (1998). A Family of Human β3-Galactosyltransferases. *Journal of Biological Chemistry*, 273(21), pp. 12770–12778. doi: 10.1074/jbc.273.21.12770.

Ardèvol A and Rovira C (2015). Reaction Mechanisms in Carbohydrate-Active Enzymes: Glycoside Hydrolases and Glycosyltransferases. Insights from *ab Initio* Quantum Mechanics/Molecular Mechanics Dynamic Simulations. *Journal of the American Chemical Society*, 137(24), pp. 7528–7547. doi: 10.1021/jacs.5b01156.

Arvidsson I, Ståhl A, Manea Hedström M, Kristoffersson A-C, Rylander C, Westman JS, Storry JR, Olsson ML and Karpman D (2015). Shiga Toxin–Induced Complement-Mediated Hemolysis and Release of Complement-Coated Red Blood Cell–Derived Microvesicles in Hemolytic Uremic Syndrome. *The Journal of Immunology*, 194(5), pp. 2309–2318. doi: 10.4049/jimmunol.1402470.

Bai X, Fu S, Zhang J, Fan R, Xu Y, Sun H, He X, Xu J and Xiong Y (2018). Identification and pathogenomic analysis of an *Escherichia coli* strain producing a novel Shiga toxin 2 subtype. *Scientific Reports*, 8(1), p. 6756. doi: 10.1038/s41598-018-25233-x.

Beddoe T, Paton AW, Le Nours J, Rossjohn J and Paton JC (2010). Structure, biological functions and applications of the AB5 toxins. *Trends in Biochemical Sciences*, 35(7), pp. 411–418. doi: 10.1016/j.tibs.2010.02.003.

Bergan J, Dyve Lingelem AB, Simm R, Skotland T and Sandvig K (2012). Shiga toxins. *Toxicon*, 60(6), pp. 1085–1107. doi: 10.1016/j.toxicon.2012.07.016.

Bitzan M, Richardson S, Huang C, Boyd B, Petric M and Karmali MA (1994). Evidence that verotoxins (Shiga-like toxins) from *Escherichia coli* bind to P blood group antigens of human erythrocytes in vitro. *Infection and Immunity*, 62(8), pp. 3337–3347. doi: 10.1128/iai.62.8.3337-3347.1994.

Breton C, Fournel-Gigleux S and Palcic MM (2012). Recent structures, evolution and mechanisms of glycosyltransferases. *Current Opinion in Structural Biology*, 22(5), pp. 540–549. doi: 10.1016/j.sbi.2012.06.007.

Breton C, Šnajdrová L, Jeanneau C, Koča J and Imberty A (2006). Structures and mechanisms of glycosyltransferases. *Glycobiology*, 16(2), pp. 29R-37R. doi: 10.1093/glycob/cwj016.

Brigotti M, Carnicelli D, Arfilli V, Porcellini E, Galassi E, Valerii MC and Spisni E (2018). Human monocytes stimulated by Shiga toxin 1a via globotriaosylceramide release proinflammatory molecules associated with hemolytic uremic syndrome. *International Journal of Medical Microbiology*, 308(7), pp. 940–946. doi: 10.1016/j.ijmm.2018.06.013.

Brigotti M, Carnicelli D, Ravanelli E, Barbieri S, Ricci F, Bontadini A, Tozzi AE, Scavia G, Caprioli A and Tazzari PL (2008). Interactions between Shiga toxins and human polymorphonuclear leukocytes. *Journal of leukocyte biology*, 84(4), pp. 1019–1027. doi: 10.1189/jlb.0308157.

Brigotti M, Carnicelli D, Ravanelli E, Vara AG, Martinelli C, Alfieri RR, Petronini PG and Sestili P (2007). Molecular Damage and Induction of Proinflammatory Cytokines in Human Endothelial Cells Exposed to Shiga Toxin 1, Shiga Toxin 2, and α-Sarcin. *Infection and Immunity*, 75(5), pp. 2201–2207. doi: 10.1128/IAI.01707-06.

Bruyand M, Mariani-Kurkdjian P, Gouali M, de Valk H, King LA, Le Hello S, Bonacorsi S and Loirat C (2018). Hemolytic uremic syndrome due to Shiga toxin-producing *Escherichia coli* infection. *Médecine et Maladies Infectieuses*, 48(3), pp. 167–174. doi: 10.1016/j.medmal.2017.09.012.

Burk C, Dietrich R, Acar G, Moravek M, Bulte M and Martlbauer E (2003). Identification and Characterization of a New Variant of Shiga Toxin 1 in *Escherichia coli* ONT:H19 of Bovine Origin. *Journal of Clinical Microbiology*, 41(5), pp. 2106–2112. doi: 10.1128/JCM.41.5.2106-2112.2003.

Cardini CE, Paladini AC, Caputto R and Leloir LF (1950). Uridine Diphosphate Glucose: the Coenzyme of the Galactose–Glucose Phosphate Isomerization. *Nature*, 165(4188), pp. 191–192. doi: 10.1038/165191a0.

Cha HJ, He C, Zhao H, Dong Y, An I-S and An S (2016). Intercellular and intracellular functions of ceramides and their metabolites in skin (Review). *International Journal of Molecular Medicine*, 38(1), pp. 16–22. doi: 10.3892/ijmm.2016.2600.

Chen H-Y and Li X (2017). Identification of a residue responsible for UDP-sugar donor selectivity of a dihydroxybenzoic acid glycosyltransferase from *Arabidopsis* natural accessions. *The Plant Journal*, 89(2), pp. 195–203. doi: 10.1111/tpj.13271.

Cody EM and Dixon BP (2019). Hemolytic Uremic Syndrome. *Pediatric Clinics of North America*, 66(1), pp. 235–246. doi: 10.1016/j.pcl.2018.09.011.

Cooling L (2015). Blood Groups in Infection and Host Susceptibility. *Clinical Microbiology Reviews*, 28(3), pp. 801–870. doi: 10.1128/CMR.00109-14.

Cooling LLW, Kelly K, Barton J, Hwang D, Koerner TAW and Olson JD (2005). Determinants of ABH expression on human blood platelets. *Blood*, 105(8), pp. 3356–64. doi: 10.1182/blood-2004-08-3080.

Coutinho PM, Deleury E, Davies GJ and Henrissat B (2003). An Evolving Hierarchical Family Classification for Glycosyltransferases. *Journal of Molecular Biology*, 328(2), pp. 307–317. doi: 10.1016/S0022-2836(03)00307-3.

D'Angelo G, Capasso S, Sticco L and Russo D (2013). Glycosphingolipids: Synthesis and functions. *FEBS Journal*, 280(24), pp. 6338–6353. doi: 10.1111/febs.12559.

Daniels G (2013). *Human Blood Groups*. 3rd edn. Oxford, UK: Wiley-Blackwell. doi: 10.1002/9781118493595.

DeGrandis S, Law H, Brunton J, Gyles C and Lingwood CA (1989). Globotetraosylceramide Is Recognized by the Pig Edema Disease Toxin. *Journal of Biological Chemistry*, 264(21), pp. 12520–12525. doi: 10.1016/S0021-9258(18)63888-8.

Detzner J, Pohlentz G and Müthing J (2020). Valid Presumption of Shiga Toxin-Mediated Damage of Developing Erythrocytes in EHEC-Associated Hemolytic Uremic Syndrome. *Toxins*, 12(6), p. 373. doi: 10.3390/toxins12060373.

Devenish J, Gyles C and LaMarre J (1998). Binding of *Escherichia coli* verotoxins to cell surface protein on wild-type and globotriaosylceramide-deficient Vero cells. *Canadian Journal of Microbiology*, 44(1), pp. 28–34. doi: 10.1139/w97-123.

Van Die I, Van Tetering A, Schiphorst WECM, Sato T, Furukawa K and Van Den Eijnden DH (1999). The acceptor substrate specificity of human β4-galactosyltransferase V indicates its potential function in O-glycosylation. *FEBS Letters*, 450(1–2), pp. 52–56. doi: 10.1016/S0014-5793(99)00462-7.

Duk M, Kusnierz-Alejska G, Korchagina EY, Bovin N V., Bochenek S and Lisowska E (2005). Anti-α-galactosyl antibodies recognizing epitopes terminating with α1,4-linked galactose: human natural and mouse monoclonal anti-NOR and anti-P1 antibodies. *Glycobiology*, 15(2), pp. 109–118. doi: 10.1093/oxfordjournals.glycob.a034964.

Duk M, Reinhold BB, Reinhold VN, Kusnierz-Alejska G and Lisowska E (2001). Structure of a Neutral Glycosphingolipid Recognized by Human Antibodies in Polyagglutinable Erythrocytes from the Rare NOR Phenotype. *Journal of Biological Chemistry*, 276(44), pp. 40574–40582. doi: 10.1074/jbc.M102711200.

Ferrando ML, Willemse N, Zaccaria E, Pannekoek Y, van der Ende A and Schultsz C (2017). Streptococcal Adhesin P (SadP) contributes to *Streptococcus suis* adhesion to the human intestinal epithelium. *PLOS ONE*. Edited by J. Kreth, 12(4), p. e0175639. doi: 10.1371/journal.pone.0175639.

Gallegos KM, Conrady DG, Karve SS, Gunasekera TS, Herr AB and Weiss A a. (2012). Shiga Toxin Binding to Glycolipids and Glycans. *PLoS ONE*. Edited by A. J. Ratner, 7(2), p. e30368. doi: 10.1371/journal.pone.0030368.

Gannon VPJ and Gyles CL (1990). Characteristics of the Shiga-like toxin produced by *Escherichia coli* associated with porcine edema disease. *Veterinary Microbiology*, 24(1), pp. 89–100. doi: 10.1016/0378-1135(90)90054-Y.

Geyer PE, Maak M, Nitsche U, Perl M, Novotny A, Slotta-Huspenina J, Dransart E, Holtorf A, Johannes L and Janssen K-P (2016). Gastric Adenocarcinomas Express the Glycosphingolipid Gb3/CD77: Targeting of Gastric Cancer Cells with Shiga Toxin B-Subunit. *Molecular Cancer Therapeutics*, 15(5), pp. 1008–1017. doi: 10.1158/1535-7163.MCT-15-0633.

Graf CGF, Schulz C, Schmälzlein M, Heinlein C, Mönnich M, Perkams L, Püttner M, Boos I, Hessefort M, Lombana Sanchez JN, Weyand M, Steegborn C, Breiden B, Ross K, Schwarzmann G, Sandhoff K and Unverzagt C (2017). Synthetic Glycoforms Reveal Carbohydrate-Dependent Bioactivity of Human Saposin D. *Angewandte Chemie - International Edition*, 56(19), pp. 5252–5257. doi: 10.1002/anie.201701362.

Grotiuz G, Sirok A, Gadea P, Varela G and Schelotto F (2006). Shiga Toxin 2-Producing *Acinetobacter haemolyticus* Associated with a Case of Bloody Diarrhea. *Journal of Clinical Microbiology*, 44(10), pp. 3838–3841. doi: 10.1128/JCM.00407-06.

Hagopian A and Eylar EH (1968). Glycoprotein biosynthesis: Studies on the receptor specificity of the polypeptidyl: *N*-acetylgalactosaminyl transferase from bovine submaxillary glands. *Archives of Biochemistry and Biophysics*, 128(2), pp. 422–433. doi: 10.1016/0003-9861(68)90048-9.

Haselberger CG and Schenkel-Brunner H (1982). Evidence for erythrocyte membrane glycoproteins being carriers of blood-group P 1 determinants. *FEBS Letters*, 149(1), pp. 126–128. doi: 10.1016/0014-5793(82)81086-7.

Hellberg Å, Steffensen R, Yahalom V, Sojka BN, Heier HE, Levene C, Poole J and Olsson ML (2003). Additional molecular bases of the clinically important p blood group phenotype. *Transfusion*, 43(7), pp. 899–907. doi: 10.1046/j.1537-2995.2003.00425.x.

Henion TR, Zhou D, Wolfer DP, Jungalwala FB and Hennet T (2001). Cloning of a Mouse β1,3 *N*-Acetylglucosaminyltransferase GlcNAc(β1,3)Gal(β1,4)Glc-ceramide Synthase Gene Encoding the Key Regulator of Lacto-series Glycolipid Biosynthesis. *Journal of Biological Chemistry*, 276(32), pp. 30261–30269. doi: 10.1074/jbc.M102979200.

Heredia N and García S (2018). Animals as sources of food-borne pathogens: A review. *Animal Nutrition*, 4(3), pp. 250–255. doi: 10.1016/j.aninu.2018.04.006.

Hughes AC, Zhang Y, Bai X, Xiong Y, Wang Y, Yang X, Xu Q and He X (2019). Structural and Functional Characterization of Stx2k, a New Subtype of Shiga Toxin 2. *Microorganisms*, 8(1), p. 4. doi: 10.3390/microorganisms8010004.

Iskratsch T, Braun A, Paschinger K and Wilson IBH (2009). Specificity analysis of lectins and antibodies using remodeled glycoproteins. *Analytical Biochemistry*, 386(2), pp. 133–146. doi: 10.1016/j.ab.2008.12.005.

Iwamura K, Furukawa Keiko, Uchikawa M, Sojka BN, Kojima Y, Wiels J, Shiku H, Urano T and Furukawa Koichi (2003). The Blood Group P1 Synthase Gene Is Identical to the Gb3/CD77 Synthase Gene. *Journal of Biological Chemistry*, 278(45), pp. 44429–44438. doi: 10.1074/jbc.M301609200.

Jacob F, Alam S, Konantz M, Liang C, Kohler RS, Everest-Dass A V., Huang Y, Rimmer N, Fedier A, Schötzau A, Lopez MN, Packer NH, Lengerke C and Heinzelmann-Schwarz V (2018). Transition of Mesenchymal and Epithelial Cancer Cells Depends on α1-4 Galactosyltransferase-Mediated Glycosphingolipids. *Cancer Research*, 78(11), pp. 2952–2965. doi: 10.1158/0008-5472.CAN-17-2223.

Jacob F, Anugraham M, Pochechueva T, Tse BWC, Alam S, Guertler R, Bovin N V., Fedier A, Hacker NF, Huflejt ME, Packer N and Heinzelmann-Schwarz VA (2014). The glycosphingolipid P1 is an ovarian cancer-associated carbohydrate antigen involved in migration. *British Journal of Cancer*, 111(8), pp. 1634–1645. doi: 10.1038/bjc.2014.455.

Johannes L and Römer W (2010). Shiga toxins--from cell biology to biomedical applications. *Nature reviews. Microbiology*, 8(2), pp. 105–16. doi: 10.1038/nrmicro2279.

Johansson D, Kosovac E, Moharer J, Ljuslinder I, Brännström T, Johansson A and Behnam-Motlagh P (2009). Expression of verotoxin-1 receptor Gb3 in breast cancer tissue and verotoxin-1 signal transduction to apoptosis. *BMC Cancer*, 9(1), p. 67. doi: 10.1186/1471-2407-9-67.

Kaczmarek R, Buczkowska A, Mikołajewicz K, Krotkiewski H and Czerwinski M (2014). P1PK, GLOB, and FORS Blood Group Systems and GLOB Collection: Biochemical and Clinical Aspects. Do We Understand It All Yet? *Transfusion Medicine Reviews*, 28(3), pp. 126–136. doi: 10.1016/j.tmrv.2014.04.007.

Kaczmarek R, Duk M, Szymczak K, Korchagina E, Tyborowska J, Mikolajczyk K, Bovin N, Szewczyk B, Jaskiewicz E and Czerwinski M (2016). Human Gb3/CD77 synthase reveals specificity toward two or four different acceptors depending on amino acid at position 211, creating P[k], P1 and NOR blood group antigens. *Biochemical and Biophysical Research Communications*, 470(1), pp. 168–174. doi: 10.1016/j.bbrc.2016.01.017.

Kaczmarek R, Mikolajewicz K, Szymczak K, Duk M, Majorczyk E, Krop-Watorek A, Buczkowska A and Czerwinski M (2016). Evaluation of an amino acid residue critical for the specificity and activity of human Gb3/CD77 synthase. *Glycoconjugate Journal*, 33(6), pp. 963–973. doi: 10.1007/s10719-016-9716-9.

Kaczmarek R, Szymczak-Kulus K, Bereźnicka A, Mikołajczyk K, Duk M, Majorczyk E, Krop-Watorek A, Klausa E, Skowrońska J, Michalewska B, Brojer E and Czerwinski M (2018). Single nucleotide polymorphisms in *A4GALT* spur extra products of the human Gb3/CD77 synthase and underlie the P1PK blood group system. *Plos One*, 13(4), p. e0196627. doi: 10.1371/journal.pone.0196627.

Karpman D, Manea M, Vaziri-Sani F, Ståhl A and Kristoffersson A-C (2006). Platelet Activation in Hemolytic Uremic Syndrome. *Seminars in Thrombosis and Hemostasis*, 32(2), pp. 128–145. doi: 10.1055/s-2006-939769.

Karpman D and Tontanahal A (2021). Extracellular vesicles in renal inflammatory and infectious diseases. *Free Radical Biology and Medicine*, 171(April), pp. 42–54. doi: 10.1016/j.freeradbiomed.2021.04.032.

Karve SS and Weiss A a (2014). Glycolipid binding preferences of Shiga toxin variants. *PloS one*, 9(7), p. e101173. doi: 10.1371/journal.pone.0101173.

Kato T, Oizumi T, Ogata M, Murakawa A, Usui T and Park EY (2015). Novel enzymatic synthesis of spacer-linked P[k] trisaccharide targeting for neutralization of Shiga toxin. *Journal of Biotechnology*, 209, pp. 50–57. doi: 10.1016/j.jbiotec.2015.06.403.

Kattke MD, Gosschalk JE, Martinez OE, Kumar G, Gale RT, Cascio D, Sawaya MR, Philips M, Brown ED and Clubb RT (2019). Structure and mechanism of TagA, a novel membrane-associated glycosyltransferase that produces wall teichoic acids in pathogenic bacteria. *PLoS Pathogens*, 15(4), pp. 1–18. doi: 10.1371/journal.ppat.1007723.

Kavaliauskiene S, Dyve Lingelem AB, Skotland T and Sandvig K (2017). Protection against Shiga Toxins. *Toxins*, 9(44). doi: 10.3390/toxins9020044.

Khoder-Agha F, Harrus D, Brysbaert G, Lensink MF, Harduin-Lepers A, Glumoff T and Kellokumpu S (2019). Assembly of B4GALT1/ST6GAL1 heteromers in the Golgi membranes involves lateral interactions via highly charged surface domains. *Journal of Biological Chemistry*, 294(39), pp. 14383–14393. doi: 10.1074/jbc.RA119.009539.

Konowalchuk J, Speirs JI and Stavric S (1977). Vero response to a cytotoxin of *Escherichia coli*. *Infection and Immunity*, 18(3), pp. 775–779. doi: 10.1128/iai.18.3.775-779.1977.

Koutsoumanis K, Allende A, Alvarez-Ordóñez A, Bover-Cid S, Chemaly M, Davies R, De Cesare A, Herman L, Hilbert F, Lindqvist R, Nauta M, Peixe L, Ru G, Simmons M, Skandamis P, Suffredini E, Jenkins C, Monteiro Pires S, Morabito S, Niskanen T, Scheutz F, da Silva Felicio MT, Messens W, Bolton D (2020). Pathogenicity assessment of Shiga toxin-producing *Escherichia coli* (STEC) and the public health risk posed by contamination of food with STEC. *EFSA Journal*, 18(1), pp. 1–105. doi: 10.2903/j.efsa.2020.5967.

Kovbasnjuk O, Mourtazina R, Baibakov B, Wang T, Elowsky C, Choti MA, Kane A and Donowitz M (2005). The glycosphingolipid globotriaosylceramide in the metastatic transformation of colon cancer. *Proceedings of the National Academy of Sciences*, 102(52), pp. 19087–19092. doi: 10.1073/pnas.0506474102.

Lacher DW, Gangiredla J, Patel I, Elkins CA and Feng PCH (2016). Use of the *Escherichia coli* Identification Microarray for Characterizing the Health Risks of Shiga Toxin-Producing Escherichia coli Isolated from Foods. *Journal of Food Protection*, 79(10), pp. 1656–1662. doi: 10.4315/0362-028X.JFP-16-176.

Lai Y-J, Wu W-Y, Yang C-M, Yang L-R, Chu C-C, Chan Y-S, Lin M and Yu L-C (2014). A systematic study of single-nucleotide polymorphisms in the *A4GALT* gene suggests a molecular genetic basis for the P_1/P_2 blood groups. *Transfusion*, 54(12), pp. 3222–3231. doi: 10.1111/trf.12771.

Lairson LL, Henrissat B, Davies GJ and Withers SG (2008). Glycosyltransferases: structures, functions, and mechanisms. *Annual review of biochemistry*, 77(February), pp. 521–555. doi: 10.1146/annurev.biochem.76.061005.092322.

Landsteiner K and Levine P (1927). Further Observations on Individual Differences of Human Blood. *Experimental Biology and Medicine*, 24(9), pp. 941–942. doi: 10.3181/00379727-24-3649.

Lane WJ, Aguad M, Smeland-Wagman R, Vege S, Mah HH, Joseph A, Blout CL, Nguyen TT, Lebo MS, Sidhu M, Lomas-Francis C, Kaufman RM, Green RC and Westhoff CM (2019). A whole genome approach for discovering the genetic basis of blood group antigens: independent confirmation for P1 and Xg[a]. *Transfusion*, 59(3), pp. 908–915. doi: 10.1111/trf.15089.

Lee M-S and Tesh V (2019). Roles of Shiga Toxins in Immunopathology. *Toxins*, 11(4), p. 212. doi: 10.3390/toxins11040212.

Leung PHM, Peiris JSM, Ng WWS, Robins-Browne RM, Bettelheim KA and Yam WC (2003). A Newly Discovered Verotoxin Variant, VT2g, Produced by Bovine Verocytotoxigenic *Escherichia coli*. *Applied and Environmental Microbiology*, 69(12), pp. 7549–7553. doi: 10.1128/AEM.69.12.7549-7553.2003.

Lingwood C (2020). Verotoxin Receptor-Based Pathology and Therapies. *Frontiers in Cellular and Infection Microbiology*, 10(March), pp. 1–10. doi: 10.3389/fcimb.2020.00123.

Liu Y-Y, Hill RA and Li Y-T (2013). Ceramide glycosylation catalyzed by glucosylceramide synthase and cancer drug resistance. *Advances in cancer research*, 117, pp. 59–89. doi: 10.1016/B978-0-12-394274-6.00003-0.

Liu Y, Tian S, Thaker H and Dong M (2021). Shiga Toxins: An Update on Host Factors and Biomedical Applications. *Toxins*, 13(3), p. 222. doi: 10.3390/toxins13030222.

Lombard V, Golaconda Ramulu H, Drula E, Coutinho PM and Henrissat B (2014). The carbohydrate-active enzymes database (CAZy) in 2013. *Nucleic Acids Research*, 42, pp. D490-495. doi: 10.1093/nar/gkt1178.

Łoś JM and Węgrzyn G (2011). Enterokrwotoczne szczepy *Escherichia coli* (EHEC) i bakteriofagi kodujące toksyny Shiga. *Postepy Mikrobiologii*, 50(3), pp. 175–190.

Mahfoud R, Manis A, Binnington B, Ackerley C and Lingwood C a. (2010). A major fraction of glycosphingolipids in model and cellular cholesterol-containing membranes is undetectable by their binding proteins. *Journal of Biological Chemistry*, 285(46), pp. 36049–36059. doi: 10.1074/jbc.M110.110189.

Majowicz SE, Scallan E, Jones-Bitton A, Sargeant JM, Stapleton J, Angulo FJ, Yeung DH and Kirk MD (2014). Global incidence of human Shiga toxin-producing *Escherichia coli* infections and deaths: a systematic review and knowledge synthesis. *Foodborne pathogens and disease*, 11(6), pp. 447–55. doi: 10.1089/fpd.2013.1704.

Marcus DM (1971). Isolation of a Substance with Blood -group P1 Activity from Human Erythrocyte Stroma. *Transfusion*, 11(1), pp. 16–18. doi: 10.1111/j.1537-2995.1971.tb04368.x.

Maria Cherian R, Gaunitz S, Nilsson A, Liu J, Karlsson NG and Holgersson J (2014). Shiga-like toxin binds with high avidity to multivalent O-linked blood group P1 determinants on mucin-type fusion proteins. *Glycobiology*, 24(1), pp. 26–38. doi: 10.1093/glycob/cwt086.

Maszczak-Seneczko D, Olczak T, Jakimowicz P and Olczak M (2011). Overexpression of UDP-GlcNAc transporter partially corrects galactosylation defect caused by UDP-Gal transporter mutation. *FEBS Letters*, 585(19), pp. 3090–3094. doi: 10.1016/j.febslet.2011.08.038.

McArthur JB and Chen X (2016). Glycosyltransferase engineering for carbohydrate synthesis. *Biochemical Society Transactions*, 44(1), pp. 129–142. doi: 10.1042/BST20150200.

Meech R, Rogers A, Zhuang L, Lewis BC, Miners JO and Mackenzie PI (2012). Identification of residues that confer sugar selectivity to UDP-glycosyltransferase 3A (UGT3A) enzymes. *Journal of Biological Chemistry*, 287(29), pp. 24122–24130. doi: 10.1074/jbc.M112.343608.

Melton-Celsa AR (2014). Shiga toxin (Stx) classification, structure, and function. *Microbiol Spectr*, 2(2), pp. 1–21. doi: 10.1128/microbiolspec.EHEC-0024-2013.Shiga.

Mestrom, Przypis, Kowalczykiewicz, Pollender, Kumpf, Marsden, Bento, Jarzębski, Szymańska, Chruściel, Tischler, Schoevaart, Hanefeld and Hagedoorn (2019). Leloir Glycosyltransferases in Applied Biocatalysis: A Multidisciplinary Approach. *International Journal of Molecular Sciences*, 20(21), p. 5263. doi: 10.3390/ijms20215263.

Mikolajczyk K, Bereznicka A, Szymczak-Kulus K, Haczkiewicz-Lesniak K, Szulc B, Olczak M, Rossowska J, Majorczyk E, Kapczynska K, Bovin N, Lisowska M, Kaczmarek R, Miazek A and Czerwinski M (2021). Missing the sweet spot: one of the two N-glycans on human Gb3/CD77 synthase is expendable. *Glycobiology*. doi: 10.1093/glycob/cwab041.

Miller JJ, Kanack AJ and Dahms NM (2019). Progress in the understanding and treatment of Fabry disease. *Biochimica et Biophysica Acta (BBA) - General Subjects*, p. 129437. doi: 10.1016/j.bbagen.2019.129437.

Miyake M, Utsuno E and Noda M (2000). Binding of avian ovomucoid to Shiga-like toxin type 1 and its utilization for receptor analog affinity chromatography. *Analytical Biochemistry*, 281(2), pp. 202–208. doi: 10.1006/abio.2000.4559.

Morimoto K, Suzuki N, Tanida I, Kakuta S, Furuta Y, Uchiyama Y, Hanada K, Suzuki Y and Yamaji T (2020). Blood group P1 antigen–bearing glycoproteins are functional but less efficient receptors of Shiga toxin than conventional glycolipid-based receptors. *Journal of Biological Chemistry*, 2(24), p. jbc.RA120.013926. doi: 10.1074/jbc.ra120.013926.

Müthing J, Meisen I, Zhang W, Bielaszewska M, Mormann M, Bauerfeind R, Schmidt MA, Friedrich AW and Karch H (2012). Promiscuous Shiga toxin 2e and its intimate relationship to Forssman. *Glycobiology*, 22(6), pp. 849–862. doi: 10.1093/glycob/cws009.

Nair PC, Meech R, Mackenzie PI, McKinnon RA and Miners JO (2015). Insights into the UDP-sugar selectivities of human UDP-glycosyltransferases (UGT): A molecular modeling perspective. *Drug Metabolism Reviews*, 47(3), pp. 335–345. doi: 10.3109/03602532.2015.1071835.

O'Brien A, Newland J, Miller S, Holmes R, Smith H and Formal S (1984). Shiga-like toxin-converting phages from *Escherichia coli* strains that cause hemorrhagic colitis or infantile diarrhea. *Science*, 226(4675), pp. 694–696. doi: 10.1126/science.6387911.

Okuda T (2017). PUGNAc treatment provokes globotetraosylceramide accumulation in human umbilical vein endothelial cells. *Biochemical and Biophysical Research Communications*, 487(1), pp. 76–82. doi: 10.1016/j.bbrc.2017.04.019.

Okuda T, Tokuda N, Numata SI, Ito M, Ohta M, Kawamura K, Wiels J, Urano T, Tajima O, Furukawa Keiko and Furukawa Koichi (2006). Targeted disruption of Gb3/CD77 synthase gene resulted in the complete deletion of globo-series glycosphingolipids and loss of sensitivity to verotoxins. *Journal of Biological Chemistry*, 281(15), pp. 10230–10235. doi: 10.1074/jbc.M600057200.

Ooka T, Seto K, Kawano K, Kobayashi H, Etoh Y, Ichihara S, Kaneko A, Isobe J, Yamaguchi K, Horikawa K, Gomes TAT, Linden A, Bardiau M, Mainil JG, Beutin L, Ogura Y and Hayashi T (2012). Clinical Significance of *Escherichia albertii*. *Emerging Infectious Diseases*, 18(3), pp. 488–492. doi: 10.3201/eid1803.111401.

Ouzzine M, Gulberti S, Levoin N, Netter P, Magdalou J and Fournel-Gigleux S (2002). The Donor Substrate Specificity of the Human β1,3-Glucuronosyltransferase I toward UDP-Glucuronic Acid Is Determined by Two Crucial Histidine and Arginine Residues. *Journal of Biological Chemistry*, 277(28), pp. 25439–25445. doi: 10.1074/jbc.M201912200.

Owczarek TB, Suchanski J, Pula B, Kmiecik AM, Chadalski M, Jethon A, Dziegiel P and Ugorski M (2013). Galactosylceramide Affects Tumorigenic and Metastatic Properties of Breast Cancer Cells as an Anti-Apoptotic Molecule. *PLoS ONE*. Edited by A. G. Passi, 8(12), p. e84191. doi: 10.1371/journal.pone.0084191.

Patnaik SK and Stanley P (2006). Lectin-Resistant CHO Glycosylation Mutants. in *Methods in Enzymology*, pp. 159–182. doi: 10.1016/S0076-6879(06)16011-5.

Paton AW and Paton JC (1996). *Enterobacter cloacae* producing a Shiga-like toxin II-related cytotoxin associated with a case of hemolytic-uremic syndrome. *Journal of clinical microbiology*, 34(2), pp. 463–465. doi: 10.1128/JCM.34.2.463-465.1996.

Paton AW, Paton JC, Heuzenroeder MW, Goldwater PN and Manning PA (1992). Cloning and nucleotide sequence of a variant Shiga-like toxin II gene from *Escherichia coli* OX3:H21 isolated from a case of sudden infant death syndrome. *Microbial Pathogenesis*, 13(3), pp. 225–236. doi: 10.1016/0882-4010(92)90023-H.

Pinto G, Sampaio M, Dias O, Almeida C, Azeredo J and Oliveira H (2021). Insights into the genome architecture and evolution of Shiga toxin encoding bacteriophages of *Escherichia coli*. *BMC Genomics*, 22(1), p. 366. doi: 10.1186/s12864-021-07685-0.

Probert WS, McQuaid C and Schrader K (2014). Isolation and identification of an *Enterobacter cloacae* strain producing a novel subtype of Shiga toxin type 1. *Journal of Clinical Microbiology*, 52(7), pp. 2346–2351. doi: 10.1128/JCM.00338-14.

Radosavljević V, Finke EJ and Belojević G (2016). Analysis of *Escherichia coli* O104:H4 outbreak in Germany in 2011 using differentiation method for unusual epidemiological events. *Central European Journal of Public Health*, 24(1), pp. 9–15. doi: 10.21101/cejph.a4255.

Ramakrishnan B and Qasba PK (2002). Structure-based Design of β1,4-Galactosyltransferase I (β4Gal-T1) with Equally Efficient *N*-Acetylgalactosaminyltransferase Activity. *Journal of Biological Chemistry*, 277(23), pp. 20833–20839. doi: 10.1074/jbc.M111183200.

Ramakrishnan B and Qasba PK (2007). Role of a Single Amino Acid in the Evolution of Glycans of Invertebrates and Vertebrates. *Journal of Molecular Biology*, 365(3), pp. 570–576. doi: 10.1016/j.jmb.2006.10.034.

Rizzo R, Russo D, Kurokawa K, Sahu P, Lombardi B, Supino D, Zhukovsky MA, Vocat A, Pothukuchi P, Kunnathully V, Capolupo L, Boncompain G, Vitagliano C, Zito Marino F, Aquino G, Montariello D, Henklein P, Mandrich L, Botti G, Clausen H, Mandel U, Yamaji T, Hanada K, Budillon A, Perez F, Parashuraman S, Hannun YA, Nakano A, Corda D, D'Angelo G and Luini A (2021). Golgi maturation-dependent glycoenzyme recycling controls glycosphingolipid biosynthesis and cell growth via GOLPH3. *The EMBO Journal*, 40(8), pp. 1–21. doi: 10.15252/embj.2020107238.

Roche N, Ilver D, Ångström J, Barone S, Telford JL and Teneberg S (2007). Human gastric glycosphingolipids recognized by *Helicobacter pylori* vacuolating cytotoxin VacA. *Microbes and Infection*, 9(5), pp. 605–614. doi: 10.1016/j.micinf.2007.01.023.

Russmann H, Schmidt H, Heesemann J, Caprioli A and Karch H (1994). Variants of Shiga-like toxin II constitute a major toxin component in *Escherichia coli* O157 strains from patients with haemolytic uraemic syndrome. *Journal of Medical Microbiology*, 40(5), pp. 338–343. doi: 10.1099/00222615-40-5-338.

Samuel JE, Perera LP, Ward S, O'Brien AD, Ginsburg V and Krivan HC (1990). Comparison of the glycolipid receptor specificities of Shiga-like toxin type II and Shiga-like toxin type II variants. *Infection and Immunity*, 58(3), pp. 611–618. doi: 10.1128/IAI.58.3.611-618.1990.

Scheutz F, Teel LD, Beutin L, Pierard D, Buvens G, Karch H, Mellmann A, Caprioli A, Tozzoli R, Morabito S, Strockbine NA, Melton-Celsa AR, Sanchez M, Persson S and O'Brien AD (2012). Multicenter Evaluation of a Sequence-Based Protocol for Subtyping Shiga Toxins and Standardizing Stx Nomenclature. *Journal of Clinical Microbiology*, 50(9), pp. 2951–2963. doi: 10.1128/JCM.00860-12.

Schlager S, Lepuschitz S, Ruppitsch W, Ableitner O, Pietzka A, Neubauer S, Stöger A, Lassnig H, Mikula C, Springer B and Allerberger F (2018). Petting zoos as sources of Shiga toxin-producing *Escherichia coli* (STEC) infections. *International Journal of Medical Microbiology*, (March), pp. 1–6. doi: 10.1016/j.ijmm.2018.06.008.

Schmidt H, Montag M, Bockemühl J, Heesemann J and Karch H (1993). Shiga-like toxin II-related cytotoxins in *Citrobacter freundii* strains from humans and beef samples. *Infection and Immunity*, 61(2), pp. 534–543. doi: 10.1128/IAI.61.2.534-543.1993.

Schmidt H, Scheef J, Morabito S, Caprioli A, Wieler LH and Karch H (2000). A New Shiga Toxin 2 Variant (Stx2f) from *Escherichia coli* Isolated from Pigeons. *Applied and Environmental Microbiology*, 66(3), pp. 1205–1208. doi: 10.1128/AEM.66.3.1205-1208.2000.

Schmitz KR, Liu J, Li S, Setty TG, Wood CS, Burd CG and Ferguson KM (2008). Golgi Localization of Glycosyltransferases Requires a Vps74p Oligomer. *Developmental Cell*, 14(4), pp. 523–534. doi: 10.1016/j.devcel.2008.02.016.

Shiga K (1898). Ueber den Erreger der Dysenterie in Japan, Vorläufige Mitteilung. *Zentralbl Bakteriol Microbiol Hyg*, 23, pp. 599–600.

Ståhl AL, Sartz L, Nelson A, Békássy ZD and Karpman D (2009). Shiga toxin and lipopolysaccharide induce platelet-leukocyte aggregates and tissue factor release, a thrombotic mechanism in hemolytic uremic syndrome. *PLoS ONE*, 4(9). doi: 10.1371/journal.pone.0006990.

Stanley P (1983). Selection of lectin-resistant mutants of animal cells. in *Methods in Enzymology*, pp. 157–184. doi: 10.1016/S0076-6879(83)96015-9.

Steffensen R, Carlier K, Wiels J, Levery SB, Stroud M, Cedergren B, Sojka BN, Bennett EP, Jersild C and Clausen H (2000). Cloning and expression of the histo-blood group P^k UDP-galactose: Galβ1-4Glcβ1-Cer α1,4-galactosyltransferase. Molecular genetic basis of the p phenotype. *Journal of Biological Chemistry*, 275(22), pp. 16723–16729. doi: 10.1074/jbc.M000728200.

Stenfelt L, Westman JS, Hellberg Å and Olsson ML (2019). The P1 histo-blood group antigen is present on human red blood cell glycoproteins. *Transfusion*, 59(3), pp. 1108–1117. doi: 10.1111/trf.15115.

Suchanowska A, Kaczmarek R, Duk M, Lukasiewicz J, Smolarek D, Majorczyk E, Jaskiewicz E, Laskowska A, Wasniowska K, Grodecka M, Lisowska E and Czerwinski M (2012). A single point mutation in the gene encoding Gb3/CD77 synthase causes a rare inherited polyagglutination syndrome. *Journal of Biological Chemistry*, 287(45), pp. 38220–30. doi: 10.1074/jbc.M112.408286.

Suzuki N, Laskowski M and Lee YC (2006). Tracing the history of Galα1–4Gal on glycoproteins in modern birds. *Biochimica et Biophysica Acta (BBA) - General Subjects*, 1760(4), pp. 538–546. doi: 10.1016/j.bbagen.2005.10.005.

Szymczak-Kulus K, Weidler S, Bereznicka A, Mikolajczyk K, Kaczmarek R, Bednarz B, Zhang T, Urbaniak A, Olczak M, Park EY, Majorczyk E, Kapczynska K, Lukasiewicz J, Wuhrer M, Unverzagt C and Czerwinski M (2021). Human Gb3/CD77 synthase produces P1 glycotope-capped N-glycans, which mediate Shiga toxin 1 but not Shiga toxin 2 cell entry. *Journal of Biological Chemistry*, 296(5), p. 100299. doi: 10.1016/j.jbc.2021.100299.

Szymczak K, Kaczmarek R, Duk M, Mikolajczyk K, Zerka A, Bereznicka A, Olczak M and Czerwinski M (2016). Human α1,4-galactosyltransferase (Gb3/CD77 synthase): Expression in insect cells, properties, role of glycans. *New Biotechnology*, 33, p. S123. doi: 10.1016/j.nbt.2016.06.1150.

Takahashi N, Khoo K, Suzuki N, Johnson JR and Lee YC (2001). N -Glycan Structures from the Major Glycoproteins of Pigeon Egg White. *Journal of Biological Chemistry*, 276(26), pp. 23230–23239. doi: 10.1074/jbc.M101380200.

Taniguchi N, Honke K, Fukuda M, Narimatsu H, Yamaguchi Y and Angata T (eds) (2014). *Handbook of Glycosyltransferases and Related Genes*. *Handbook of Glycosyltransferases and Related Genes*. Tokyo: Springer Japan. doi: 10.1007/978-4-431-54240-7.

Tarr PI, Gordon CA and Chandler WL (2005). Shiga-toxin-producing *Escherichia coli* and haemolytic uraemic syndrome. *The Lancet*, 365(9464), pp. 1073–1086. doi: 10.1016/S0140-6736(05)71144-2.

Tatti M, Salvioli R, Ciaffoni F, Pucci P, Andolfo A, Amoresano A and Vaccaro AM (1999). Structural and membrane-binding properties of saposin D. *European Journal of Biochemistry*, 263(2), pp. 486–494. doi: 10.1046/j.1432-1327.1999.00521.x.

Thinley J, Nathalang O, Chidtrakoon S and Intharanut K (2021). Blood group P1 prediction using multiplex PCR genotyping of *A4GALT* among Thai blood donors. *Transfusion medicine (Oxford, England)*, 31(1), pp. 48–54. doi: 10.1111/tme.12749.

Thuresson B, Westman JS and Olsson ML (2011). Identification of a novel *A4GALT* exon reveals the genetic basis of the P_1/P_2 histo-blood groups. *Blood*, 117(2), pp. 678–687. doi: 10.1182/blood-2010-08-301333.

Tian S, Muneeruddin K, Choi MY, Tao L, Bhuiyan RH, Ohmi Y, Furukawa Keiko, Furukawa Koichi, Boland S, Shaffer SA, Adam RM and Dong M (2018). Genome-wide CRISPR screens for Shiga toxins and ricin reveal Golgi proteins critical for glycosylation. *PLoS biology*, 16(11), p. e2006951. doi: 10.1371/journal.pbio.2006951.

Tilley L, Green C and Daniels G (2006). Sequence variation in the 5' untranslated region of the human *A4GALT* gene is associated with, but does not define, the P1 blood-group polymorphism. *Vox Sanguinis*, 90(3), pp. 198–203. doi: 10.1111/j.1423-0410.2006.00746.x.

Ullmann V, Rädisch M, Boos I, Freund J, Pöhner C, Schwarzinger S and Unverzagt C (2012). Convergent Solid-Phase Synthesis of N-Glycopeptides Facilitated by Pseudoprolines at Consensus-Sequence Ser/Thr Residues. *Angewandte Chemie International Edition*, 51(46), pp. 11566–11570. doi: 10.1002/anie.201204272.

Varki A, Cummings RD, Esko JD, Freeze HH, Stanley P, Bertozzi CR, Hart GW and Etzler ME (eds) (2009). *Essentials of Glycobiology*. 2nd edn. Cold Spring Harbor (NY): Cold Spring Harbor Laboratory Press.

Villysson A, Tontanahal A and Karpman D (2017). Microvesicle involvement in Shiga toxin-associated infection. *Toxins*, 9(11). doi: 10.3390/toxins9110376.

Volynsky P, Efremov R, Mikhalev I, Dobrochaeva K, Tuzikov A, Korchagina E, Obukhova P, Rapoport E and Bovin N (2017). Why human anti-Galα1–4Galβ1–4Glc natural antibodies do not recognize the trisaccharide on erythrocyte membrane? Molecular dynamics and immunochemical investigation. *Molecular Immunology*, 90(July), pp. 87–97. doi: 10.1016/j.molimm.2017.06.247.

Watkins WM, Greenwell P, Yates AD and Johnson PH (1988). Regulation of expression of carbohydrate blood group antigens. *Biochimie*, 70(11), pp. 1597–1611. doi: 10.1016/0300-9084(88)90295-7.

Welch LG and Munro S (2019). A tale of short tails, through thick and thin: investigating the sorting mechanisms of Golgi enzymes. *FEBS Letters*, 593(17), pp. 2452–2465. doi: 10.1002/1873-3468.13553.

Westman JS, Stenfelt L, Vidovic K, Möller M, Hellberg Å, Kjellström S and Olsson ML (2018). Allele-selective RUNX1 binding regulates P1 blood group status by transcriptional control of *A4GALT*. *Blood*, p. blood-2017-08-803080. doi: 10.1182/blood-2017-08-803080.

Yamaji T, Sekizuka T, Tachida Y, Sakuma C, Morimoto K, Kuroda M and Hanada K (2019). A CRISPR Screen Identifies LAPTM4A and TM9SF Proteins as Glycolipid-Regulating Factors. *iScience*, 11, pp. 409–424. doi: 10.1016/j.isci.2018.12.039.

Yamamoto F, Cid E, Yamamoto M, Saitou N, Bertranpetit J and Blancher A (2015). An integrative evolution theory of histo-blood group ABO and related genes. *Scientific Reports*, 4(1), p. 6601. doi: 10.1038/srep06601.

Yang Z, Bergström J and Karlsson KA (1994). Glycoproteins with Gal alpha 4Gal are absent from human erythrocyte membranes, indicating that glycolipids are the sole carriers of blood group P activities. *Journal of Biological Chemistry*, 269(20), pp. 14620–14624. doi: 10.1016/S0021-9258(17)36669-3.

Yeh C-C, Chang C-J, Twu Y-C, Hung S-T, Tsai Y-J, Liao J-C, Huang J-T, Kao Y-H, Lin S-W and Yu L-C (2018). The differential expression of the blood group P^1-A4GALT and P^2-A4GALT alleles is stimulated by the transcription factor early growth response 1. *Transfusion*, 58(4), pp. 1054–1064. doi: 10.1111/trf.14515.

Yiu SCK and Lingwood CA (1992). Polyisobutylmethacrylate modifies glycolipid binding specificity of verotoxin 1 in thin-layer chromatogram overlay procedures. *Analytical Biochemistry*, 202(1), pp. 188–192. doi: 10.1016/0003-2697(92)90226-W.

Zhang H, Zhu F, Yang T, Ding L, Zhou M, Li J, Haslam SM, Dell A, Erlandsen H and Wu H (2014). The highly conserved domain of unknown function 1792 has a distinct glycosyltransferase fold. *Nature Communications*, 5(1), p. 4339. doi: 10.1038/ncomms5339.

Zhang W, Bielaszewska M, Kuczius T and Karch H (2002). Identification, Characterization, and Distribution of a Shiga Toxin 1 Gene Variant (stx1c) in *Escherichia coli* Strains Isolated from Humans. *Journal of Clinical Microbiology*, 40(4), pp. 1441–1446. doi: 10.1128/JCM.40.4.1441-1446.2002.

Zhou D, Berger EG and Hennet T (1999). Molecular cloning of a human UDP-galactose:GlcNAcβ1,3GalNAc β1,3 galactosyltransferase gene encoding an O-linked core3-elongation enzyme. *European Journal of Biochemistry*, 263(2), pp. 571–576. doi: 10.1046/j.1432-1327.1999.00541.x.

Zhou D, Henion TR, Jungalwala FB, Berger EG and Hennet T (2000). The β1,3-galactosyltransferase β3GalT-V is a stage-specific embryonic antigen-3 (SSEA-3) synthase. *Journal of Biological Chemistry*, 275(30), pp. 22631–22634. doi: 10.1074/jbc.C000263200.

Zoja C, Buelli S and Morigi M (2010). Shiga toxin-associated hemolytic uremic syndrome: pathophysiology of endothelial dysfunction. *Pediatric Nephrology*, 25(11), pp. 2231–2240. doi: 10.1007/s00467-010-1522-1.

Zumbrun SD, Hanson L, Sinclair JF, Freedy J, Melton-Celsa AR, Rodriguez-Canales J, Hanson JC and O'Brien AD (2010). Human intestinal tissue and cultured colonic cells contain globotriaosylceramide synthase mRNA and the alternate Shiga toxin receptor globotetraosylceramide. *Infection and immunity*, 78(11), pp. 4488–99. doi: 10.1128/IAI.00620-10.

11. Appendix

11.1 Composition of standard buffers and solutions used in the study

Table A1. Bacterial culture media and solutions used in DNA electrophoresis.

Culture medium/buffer	Composition	Manufacturer
E. coli **culture media**		
Super Broth (SB)	30 g/l peptone 20 g/l yeast extract 10 g/l MOPS pH 7.0	Roth Roth Roth
SB agar	30 g/l peptone 20 g/l yeast extract 10 g/l MOPS pH 7.0 15 g/l agar	Roth Roth Roth DIFCO Laboratories, Detroit, MI, USA
Solutions used in DNA electrophoresis		
TAE (Tris-acetate) buffer	40 mM Tris 20 mM glacial acetic acid 1 mM EDTA pH 8.0	Roth POCH Roth
Sample loading buffer	0.03% m/v bromophenol blue 0.03% m/v xylene cyanol FF 60% v/v glycerol 1% m/v SDS 100 mM EDTA pH 7.6	Fermentas, Vilnius, Lithuania
Agarose gel	1% m/v Ultra-pure agarose in TAE 0.5 µg/ml ethidium bromide	Roth Invitrogen

Table A2. Standard buffers and solutions used in protein electrophoresis.

Buffer/solution	Composition	Manufacturer
Standard buffers		
TBS	25 mM Tris-HCl, pH 7.6 140 mM NaCl pH 7.4	POCh
PBS	10 mM Na_2HPO_4, pH 7.2 137 mM NaCl 2 mM KH_2PO_4 2.7 mM KCl 0.5 mM $MgCl_2$ pH 7.2	Laboratory of General Chemistry, IITD PAN, Wroclaw, Poland
Buffers and solutions used in protein electrophoresis		
SDS-PAGE running buffer	25 mM Tris 192 mM glycine 0.1% m/v SDS pH 8.3	Roth POCh Serva
Transfer buffer	25 mM Tris 192 mM glycine 20% v/v methanol pH 8.3	Roth POCh POCh
SDS-PAGE sample loading buffer	62.5 mM Tris-HCl; pH 6.8 2% m/v SDS 10% v/v glycerol 5% v/v β-mercaptoethanol 0.015% m/v bromophenol blue	Serva POCh Bio-Rad POCh
Stacking gel buffer	125 mM Tris 0.1% m/v SDS pH 6.8	Roth Serva
Resolving gel buffer	0.375 mM Tris 0.1% m/v SDS pH 8.8	Roth Serva
3% stacking gel	1.2 ml stacking gel buffer 0.7 ml 30% acrylamide mixture [29.2% m/v acrylamide, 0.8 m/v *N,N'*-methylenebis(acrylamide)] 2.8 ml H_2O 48 µl 10% SDS 29 µl 10% ammonium persulfate (APS) 9.6 µl tetramethylethylenediamine (TEMED)	Bio-Rad Serva Bio-Rad Serva
10% resolving gel	3 ml resolving gel buffer 4 ml 30% acrylamide mixture [29.2% m/v acrylamide, 0.8 m/v *N,N'*-methylenebis(acrylamide)] 4.8 ml H_2O 120 µl 10% SDS 60 µl 10% APS 6 µl TEMED	Bio-Rad Serva Bio-Rad Serva

11.2 DNA vectors used in the study
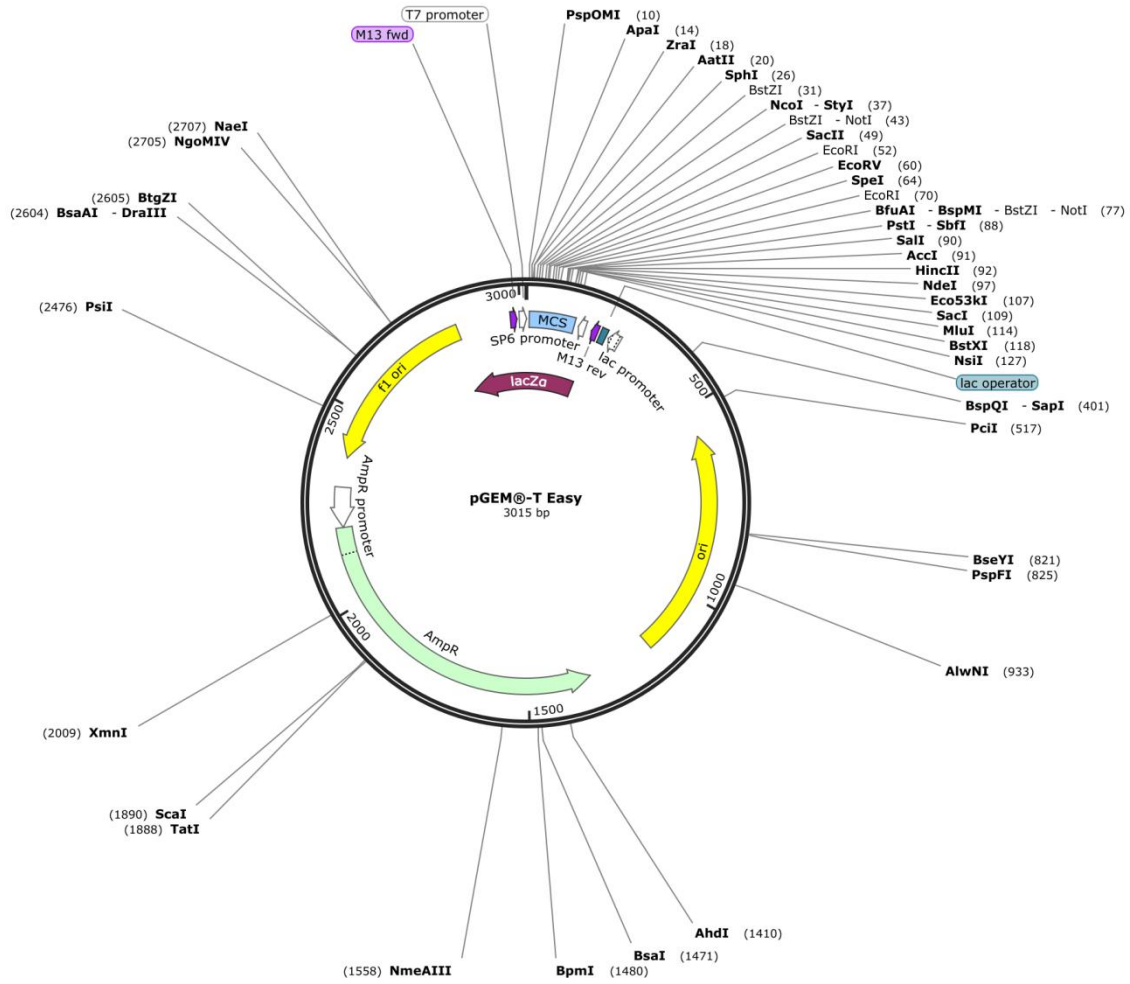
Fig. A1. pGEM-T Easy vector map (https://www.snapgene.com).
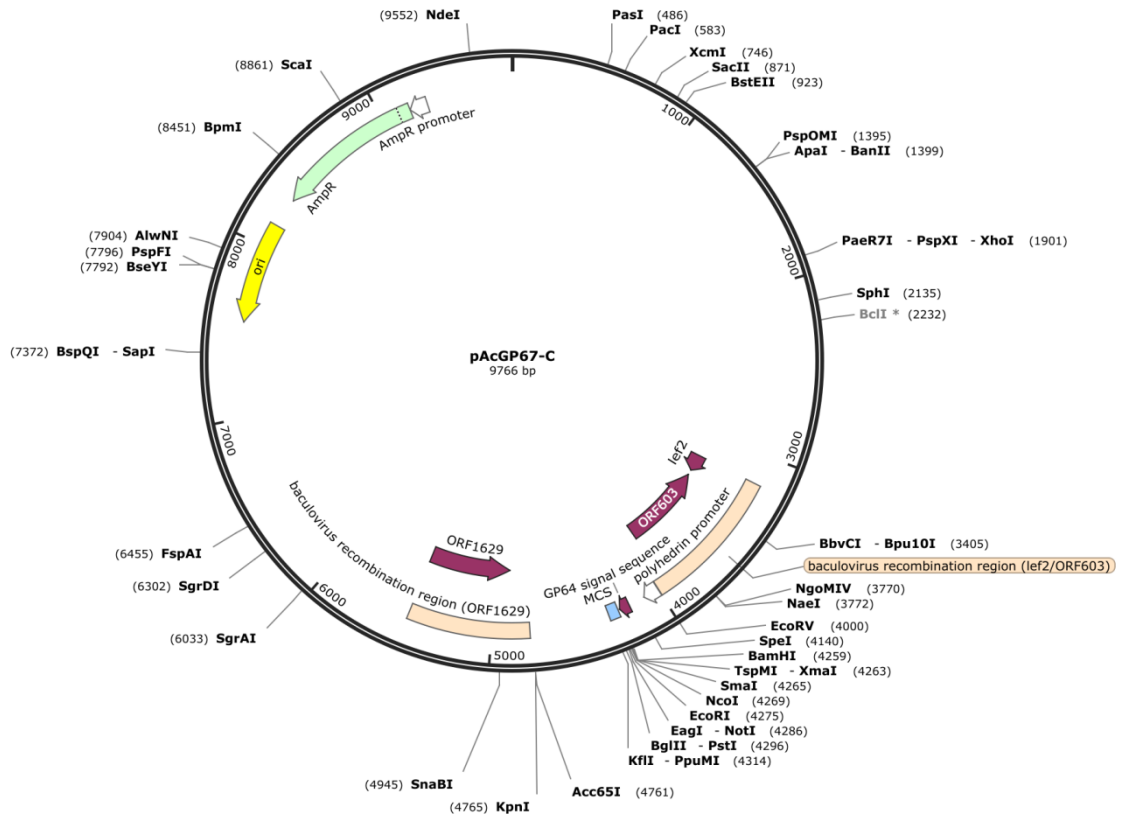
Fig. A2. pAcGP67C vector map (https://www.snapgene.com).
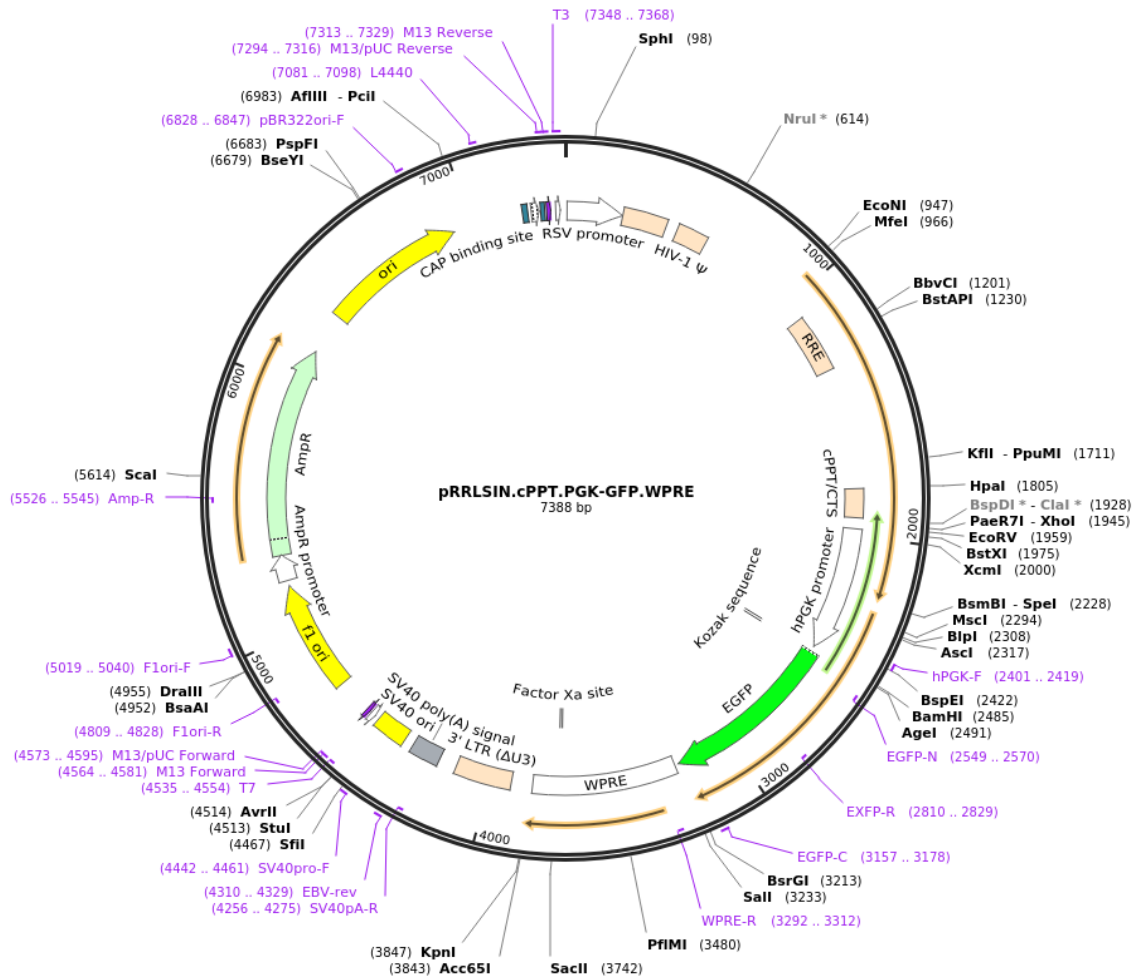
Fig. A3. pRRL-CMV-IRES-PURO vector map (https://www.addgene.org).
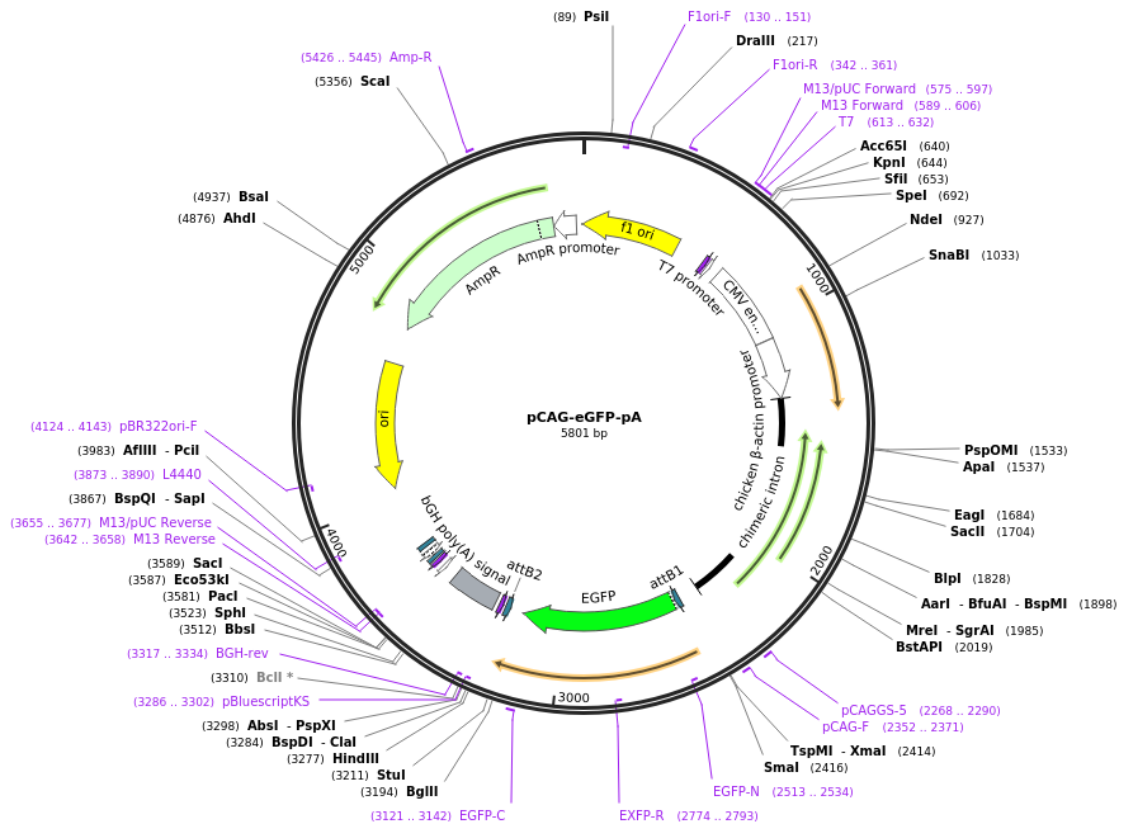
Fig. A4. pCAG vector map (https://www.addgene.org).

11.3 Blood analysis summary

Table A3. Phenotypes, genotypes, RBC antibody and Stx1B binding capacities of blood donors. The colour-coding is explained beneath the table.

Sample	Agglutination				ABC				SNPs correlating with P₁/P₂ status			
	A	B	D	P1	anti-P1 (P3NIL100)	anti-P1 (650)	anti-NOR	Stx1B	rs8138197	rs2143919	rs2143918	rs5751348
15	+	-	+	+	10416	23459		2015	cc	cc	tt	gg
19	+	+	+	+	8387	20511			cc	cg	tt	gg
29	-	-	+	+	14721	17441	0	2011	cc	cg	tt	gg
39	-	-	+	+	6657	13273			cc	cc	tt	gg
41	+	-	+	+	8473	15777			cc	cc	tt	gg
45	-	-	+	+	16880	8038			cc	cg	tt	gg
47	-	+	+	+	7255	8011			cc	cc	tt	gg
52	+	+	+	+	6561	10423		3606	cc	cc	tt	gg
55	+	+	+	+	6168	5847		2420	cc	cc	tt	gg
56	+	-	-	+	10331	23208		2211	cc	cc	tt	gg
75					21226	12055		622	cc	cc	tt	gg
84									cc	cc	tt	gg
89	+	-	+	+					cc	cc	tt	gg
90	-	+	+	+	10186	3913		1326	cc	cc	tt	gg
101	+	-	-	+	316	0			cc	cc	tt	gg
110									cc	cc	tt	gg
111					0	0	0		cc	cc	tt	gg
1	+	-	+	+	9485	11106			ct	cg	tg	gt
4	+	-	+	+	8759	4598			ct	cg	tg	gt
6	-	-	+	+	6761	4936			ct	gg	tg	gt
10	+	-	+	+	6927	6513			ct	cg	tg	gt
11	+	-	+	+	6129	4214			ct	cg	tg	gt
16	+	-	+	+	6769	10299			ct	gg	tg	gt
17	-	+	-	+					ct	cg	tg	gt
18	-	-	+	+	13748	11979		29	ct	cg	tg	gt
20	+	+	+	+	3896	3874			ct	cg	tg	gt
21	+	-	+	+	2448	471			ct	cg	tg	gt
22	+	-	+	+	3626	2505			ct	cg	tg	gt
23	-	-	+	+	4083	3888		3880	ct	cg	tg	gt
24	-	-	+	+	5572	3327			ct	cg	tg	gt
25	+	-	+	+	2815	508			ct	gg	tg	gt
26	+	-	+	+	7143	5991		189	ct	cg	tg	gt
27	+	+	+	+	6071	3976			ct	cg	tg	gt
28	+	-	+	+	5430	2277			ct	cg	tg	gt
30	+	-	+	+	4572	1170			ct	cg	tg	gt
31	-	+	+	+	4630	2548			ct	cg	tg	gt
35	+	+	+	+					ct	cg	tg	gt
36	+	-	+	+	3376	2045		409	ct	gg	tg	gt

42	+	-	+	+	5376	3378			ct	cg	tg	gt
43	+	-	+	+	4600	6159			ct	cg	tg	gt
44	-	-	+	+	14296	15286			ct	cg	tg	gt
46	+	-	+	+	3256	1927			ct	gg	tg	gt
48	+	-	+	+	8133	4887		3619	ct	cg	tg	gt
49	+	-	+	+	5295	1895			ct	cg	tg	gt
50	+	+	+	+	5868	3691		1989	ct	cg	tg	gt
51	+	-	+	+	6565	7916		2057	ct	gg	tg	gt
54	+	+	+	+	6498	7225			ct	cg	tg	gt
57	-	+	+	+	7317	4911			ct	cg	tg	gt
58	+	-	+	+	12338	12389			ct	cg	tg	gt
59	+	-	+	+	6424	3994			ct	cg	tg	gt
60	+	-	+	+	2932	2396			ct	cg	tg	gt
72	-	-	+	+	2507	99			ct	cg	tg	gt
73	-	+	-	+	1761	93			ct	cg	tg	gt
74	+	-	+	+	3103	528			ct	cg	tg	gt
80					7619	2403		194	ct	cg	tg	gt
81							0	1933	ct	gg	tg	tg
85								69	ct	cg	tg	gt
86								85	ct	cg	tg	gt
87	-	+	+	+					ct	cg	tg	gt
88	-	-	+	+					ct	cg	tg	gt
92									ct	cg	tg	gt
95	+	-	+	+	225	156			ct	cg	tg	gt
96	-	-	+	+	1042	228			ct	cg	tg	gt
97	-	-	+	+	554	108			ct	cg	tg	gt
98	-	-	+	+	581	170			ct	cg	tg	gt
99	+	+	-	+	410	84			ct	cg	tg	gt
100	-	-	+	+	1067	286			ct	cg	tg	gt
108									ct	cg	tg	gt
109									ct	cg	tg	gt
2	-	-	+	-	239	25		22	tt	gg	gg	tt
3	+	-	+	-	0	3		46	tt	gg	gg	tt
5	-	-	+	-	585	85		1392	tt	gg	gg	tt
7	-	-	-	-	120	0		226	tt	gg	gg	tt
8	-	-	+	-	97	5			tt	gg	gg	tt
12	+	+	+	-	46	1			tt	gg	gg	tt
32	+	+	-	-	41	1			tt	gg	gg	tt
33	-	-	+	-	36	0			tt	gg	gg	tt
34	+	-	+	-	14	0	0	795	tt	gg	gg	tt
38	+	-	+	+	1236	77		105	tt	gg	gg	tt
40	+	-	+	-	81	0			tt	gg	gg	tt
53	-	-	+	-	468	14			tt	gg	gg	tt
76					267	31		548	tt	gg	gg	tt
77	-	-	+	-	112	5		16	tt	gg	gg	tt

78	+	-	+	-	44	3		21	tt	gg	gg	tt
79	+	+	+	-	30	0		23	tt	gg	gg	tt
82								40	tt	gg	gg	tt
83								258	tt	gg	gg	tt
91									tt	gg	gg	tt
93	-	+	+	-	208	43			tt	gg	gg	tt
94	+	-	+	-	516	153			tt	gg	gg	tt
105									tt	gg	gg	tt
106									tt	gg	gg	tt
107									tt	gg	gg	tt
13	+	-	+	+	14652	18393		197	cc	cg	tg	gt
14	-	+	+	+	6285	14271		341	cc	cg	tg	gt
67					6411	4099	6083	2387	cc	cc	tt	gg
68					6691	6133	2824	4077	cc	cc	tt	gg
69					6134	8567	4071	2583	cc	cg	tt	gg
71					4077	6620	7872	4857	cc	cc	tt	gg
102					7160	4087	922		cc	cc	tt	gg
61	+	-	+	+	4602	1803			ct	cg	tg	gt
62	+	-	+	+	3417	1284			ct	cg	tg	gt
63	-	+	+	+	4191	651			ct	cg	tg	gt
64	-	+	+	+	3432	1465			ct	cg	tg	gt
65	+	+	+	+	3013	376	2922	2241	ct	cg	tg	gt
66					4077	1111	5568	334	ct	cg	tg	gt
70					5517	1722	8425	4960	ct	cg	tg	gt
103					6441	3769	780		ct	cg	tg	gt
104					7177	4491	843		ct	cg	tg	gt

The genotypes are colour-coded as follows:

P^1P^1

P^1P^2

P^2P^2

pp (null)

Unassigned

$P^{1NOR}P^1$

NOR-negative family of NOR-positive individuals

$P^{1NOR}P^2$

12. List of figures

13. List of tables